University of Stavanger

FACULTY OF SCIENCE AND TECHNOLOGY

MASTER'S THESIS

Study programme/specialisation : Petroleum Engineering/Reservoir Engineering	Spring semester, 2018 Open
Author: Faisal Abdulhameed	Faisal Abdulhameed (signature of author)

Programme coordinator: Prof. Aly Anis Hamouda

Supervisor: Prof. Aly Anis Hamouda

Co-supervisor: Rockey Abhishek

Title of master's thesis:

Adsorption of silica nanoparticles in chalk and sandstone and it effect of fluid/rock interactions.

Credits: 30

Keywords: Silica nanoparticles Chalk Berea Adsorption Kinetic models Transport Calcite dissolution Fines migration	Number of pages: 78 + supplemental material/other: …… Stavanger, 15/06/2018 date/year

Adsorption of silica nanoparticles in chalk and sandstone and it effect of fluid/rock interactions.

Written by: **Faisal Abdulhameed**

Supervised by: **Prof. Aly Anis Hamouda**

Co-supervised by: **Rockey Abhishek**

MSc Thesis

Reservoir Engineering

Department of Petroleum Engineering

Faculty of Science and Technology

The University of Stavanger

Norway

2018

The University of Stavanger

June 2018

ACKNOWLEDGMENT

I respect and thank my supervisor, Professor Aly Anis Hamouda for providing me an opportunity to do this master's Thesis in University of Stavanger and giving me all support and guidance, which made me complete the project duly. I am extremely thankful to him for providing such a nice support and guidance.

I owe my deep gratitude to PhD candidate Rockey Abhishek, who took keen interest and made an enormous contribution to this master's Thesis and guided me all along as my co-supervisor, till the completion of my master's Thesis.

I would like to thank the University of Stavanger and the Department of Petroleum Engineering for their help and support.

Faisal Abdulhameed

ABSTRACT

This study addresses the adsorption of Silica nanoparticles (NPs) and its effect on fluid/rock interactions in chalk and sandstone reservoirs. The first part of this thesis addresses the kinetic adsorption behaviour of silica NPs dispersed in three types of waters: deionized water (DIW), low salinity water (LSW) and synthetic seawater (SSW) on calcite and quartz which are the major mineral constituents of chalk and sandstone reservoirs. Kinetic adsorption of NPs was addressed by running a set of static adsorption experiments with increasing mixing time between the mineral and silica nanofluid prepared at three different salinities. Pseudo-first order and Pseudo-second order kinetic models were used to describe to kinetic behaviour of silica NPs on calcite and quartz. Intraparticle diffusion model is used to describe the adsorption mechanism of silica NPs on calcite and quartz. Ion and pH analysis was performed to study the fluid/rock interactions with and without NPs. The second part of the thesis addresses the NPs' transport behaviour, dynamic adsorption/retention and effect on fluid/rock interactions in chalk and sandstone. To address this, single phase core flood experiments were conducted with chalk and Berea sandstone cores at ambient temperature. The effluent produced from these floods was analysed for NP concentration, cations concentration and pH to investigate the fluid/rock interactions.

The kinetic adsorption experiments indicated that the adsorption of NPs on calcite is higher than quartz. It was also shown that the adsorption of NP was enhanced by increasing the salinity. The adsorption of NP on calcite showed best fit with pseudo-second order kinetic model. From this kinetic model, highest adsorption rate of NPs on calcite was in SSW. It was also observed that the estimated adsorption capacity of calcite increased with salinity. Both kinetic models (pseudo-first and second order kinetic model) did not give good fits to describe the adsorption behaviour of NP on quartz. In addition, the kinetic adsorption mechanism of NP on calcite and quartz surfaces was shown to be controlled by intraparticle diffusion and film diffusion mechanisms. The dynamic adsorption experiments in high salinity condition showed strongly irreversible adsorption of NP on Chalk and Berea surfaces. Comparing the results from this thesis to work previously done in our lab showed that: (1) NP adsorption can reduce the calcite dissolution induced by low salinity flooding in chalk reservoirs and (2) NP adsorption can reduced formation damage in sandstone reservoirs. This suggests a synergy between silica nanofluid and low salinity flooding techniques.

TABLE OF CONTENTS

LIST OF FIGURES

LIST OF TABLES

LIST OF ABERAVTIONS

Abs – Absorbance

DIW – Deionized water

DP – Nanofluid “DP 9711”

IC – Ion chromatography

LSW – Low salinity water

NP – Nanoparticles

PV – Pore volume

SSW – Synthetic sea water

UV – Spectrophotometer “UV – 1700”

Conc. – Concentration

K_1 – Pseudo-first order rate constant

K_2 – Pseudo-second order rate constant

q_e (exp) – nanoparticle adsorbed on (mg/g) on mineral at equilibrium in lab experiments

q_e (est) – nanoparticle adsorbed on (mg/g) on mineral at equilibrium obtained from kinetic model.

q_e (t) – nanoparticle adsorbed (mg/g) on mineral at time t.

M – Molar

rpm – rotation per minute

SK – Stevns Klint

1. Introduction

Nanoparticles have been used in different science branches since it is introduced in 1960, for example medical and biological science, environmental, electronics and agriculture. In the past decade, a range of experimental investigation is done by using nanotechnology in petroleum industry. These investigations showed that applying nanotechnology in petroleum industry could solve a range of problems faced in this industry. Nanoparticles have been used in different forms in petroleum industry (Dehghan Monfared et al. 2015). Nanoparticles is used as an additive to improve drilling fluid properties and well completion slurries (William et al. 2014; Li et al. 2004). NP can also be used as an agent for controlling the fines migration and as a sensor for reservoir characterization (Habibi et al. 2012; Prodanovic et al. 2010). In addition, nanoparticles suspension fluid (nanofluid) has been demonstrated to have potential use for EOR in petroleum industry (Suleimanov, Ismailov, and Veliyev 2011). Different EOR mechanisms for nanofluid have been investigated and discussed in the previous studies. These EOR mechanisms are interfacial tension (IFT), disjoining pressure, wettability alteration, emulsification and pore channels plugging (Li and Torsæter 2015). The silica nanoparticle has many advantages as EOR agent and considered as proper candidate for these mentioned mechanisms and applications due to its modification ability by chemical methods, cheap to produce, environmentally friendly and its fluid (nanofluid) has good stability (Metin, Baran, and Nguyen 2012).The interactions of nanofluid with other fluids and reservoir rocks are the key processes here and they playing an important role in the nanofluids performance for EOR. These key processes can be connected to the adsorption and retention and transport of nanoparticles in the reservoir (Abhishek, Bagalkot, and Kumar 2016). So, describing and understanding of these key processes are very important to identify the properties of nanoparticles and its effects of rock minerals. This understanding may help to plan an effective NP-assisted EOR process.

This Master's Thesis consists of two experimental parts. The first part is the kinetic adsorption behaviour of silica nanoparticles prepared in DIW, LSW and SSW on different mineral surfaces (Calcite and quartz). The second part address the nanoparticles transport behaviour in Chalk and sandstone reservoirs by implementation of core flooding experiments on chalk and Berea cores.

2. Literature review

2.1. Introduction

The nanotechnology is the study of engineering, science, medical and technology at Nano-scale. In this study the nanoparticle with size range from 1nm to 100 nm (Nano-scale) is used. The most important problem that facing the oil industry now is to find a new technology to improve oil recovery especially at tertiary level. One of the most promising solution is the application of nanotechnology to improve the oil recovery methods. The most attractive features of nanoparticles are: its size and its large and effective surface area. The nanoparticles is applied in EOR methods because its ability to change the wettability of rock surface(Abhishek, Kumar, and Sapru 2015), reduce adsorption of chemicals injected onto rock surface and reduce interfacial tension between the water and oil (Bera and Belhaj 2016).

2.2. The mechanism of nanofluids to spread on solid surfaces

Nanofluids are used in different technological contexts. The spreading and adhesion behaviour of nanofluid on solid surfaces can yield materials with desirable optical and structural properties. The nanofluids spreading behaviour has implication for EOR, but the concepts of simple liquids spreading and adhesion do not apply to nanofluids (Wasan and Nikolov 2003). (Wasan and Nikolov 2003) studied the effects of the particle structure and structural disjoining pressure on the colloidal fluids spreading on solid surfaces. By looking to Figure 2.1, they explained that when an oil/liquid drop or a gas bubble dispersed in nanofluid approaches solid, smooth, hydrophilic horizontal surface, a microscopic transition occurs between the meniscus and liquid film. The reflected- light digital video microscopy are being used to observe the particle-structuring phenomena. The thickness of nanofluid film is changed in steps. Three-phase (air, liquid and solid) contact region are formed when oil drop is existed on a solid glass surface. Then the pre-wetting aqueous film between solid surface and oil droplet are formed and spread. When the whole area is covered by the pre-wetted film, small water lenses are formed. Finally, the separation of oil droplet from the glass surface are caused by the thick aqueous film with a dimple.

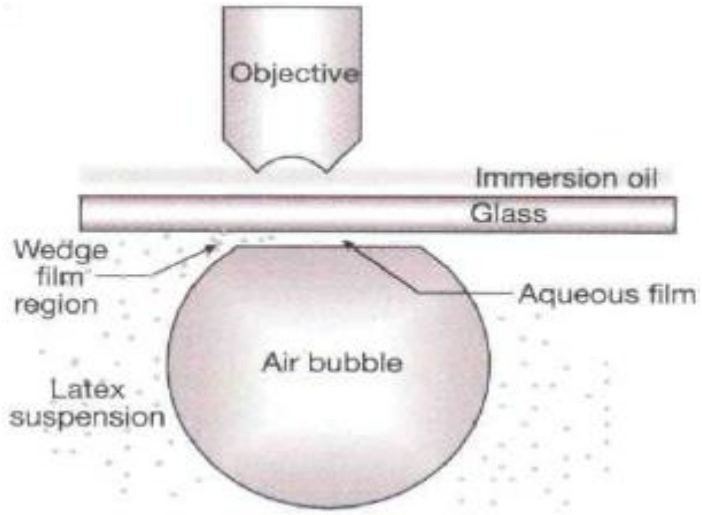

Figure 2.1: Particle structuring in a wedge film (Wasan and Nikolov 2003).

NP structuring phenomena introduce a force normal to interface (structural disjoining pressure) in the wedge film as shown in Figure 2.2.a. By using an analytical expression based on statistical mechanics, the plot of disjoining pressure is obtained. While the spreading coefficient (S) is estimated as a function of the particle layers number in the wedge of the film. By looking to Figure 2.2.a, the structural disjoining pressure is higher near the wedge tip than that in the bulk meniscus. The quantity of this disjoining pressure depends on the particle size and the effective particle volume fraction, charge and polydispersity (Wasan and Nikolov 2003; Zhang, Nikolov, and Wasan 2014).

Figure 2.2.b and the calculation made by (Wasan and Nikolov 2003) shows that the spreading coefficient (S) increases with a decrease in film thickness. Which means that this coefficient is increasing with a decrease of particle layers number inside the film. At the thickness of the wedge film double than the particle diameter, the slope of the curve is changed significantly as shown in Figure 2.2.b. The particle in-layer structure changes to an ordered structure precisely at this film thickness. These results point to that the in-layer particle structuring can improve the nanofluids spreading on solid surfaces.

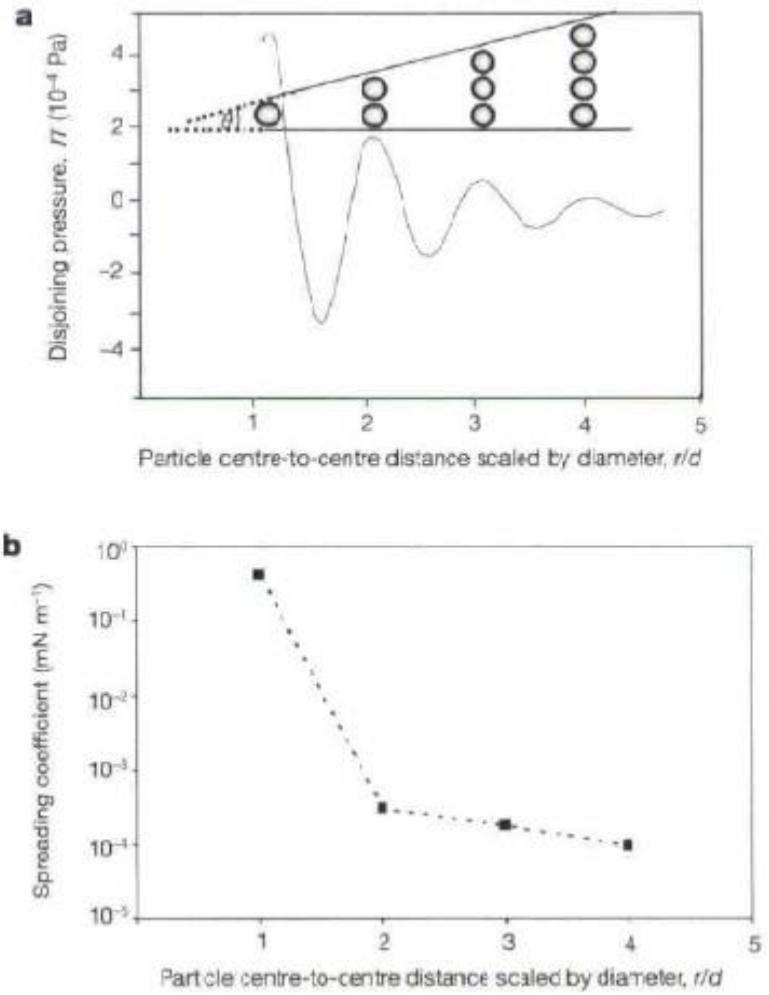

Figure 2.2.(a): Pressure profile as function of film thickness. (b): Pressure profile as function of spreading coefficient (Wasan and Nikolov 2003).

When the nanofluid concentration increase in the film, NPs diffuse more and more into the wedge of the film and interact with film surfaces. The disjoining pressure increase significantly at the wedge thickness of one NPs layer. This leads to move the oil/nanofluid interface forward and spreads the nanofluid over the solid surface and detaching the oil drop as shown in Figure 2.3. This phenomenon describing how an oil drop be detached from a solid surface using a nanofluid. (Wasan and Nikolov 2003; Zhang, Nikolov, and Wasan 2014).

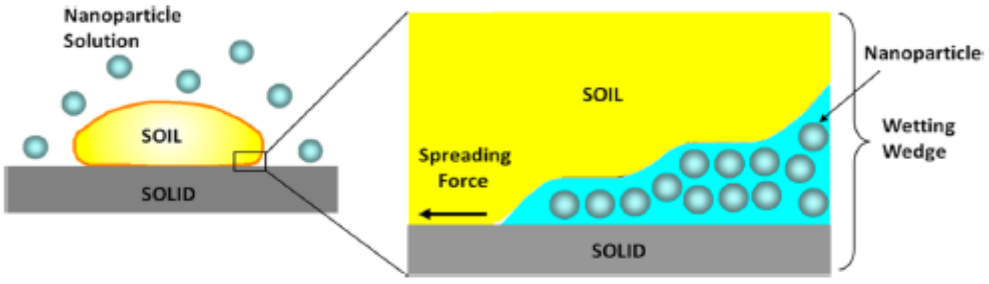

Figure 2.3: oil-solid displacement driven by structural forces and film tension gradient (Zhang, Nikolov, and Wasan 2014).

To investigate more of the nanofluid mechanism to detach oil drop from solid surfaces and its effect to enhance oil recovery, (Zhang, Nikolov, and Wasan 2014) did a series of imbibition experiments using . In these experiments they used a reservoir crude oil and a solution of reservoir brine with high salinity and a suitable nanofluid to displace the crude oil from single-glass capillaries and water-wet Berea sandstone. Two types of nanofluids are used in this experimental work: IIT nanofluid and silica nanofluid. The Illinois Institute of Technology (IIT) nanofluid was created to survive in a high-salinity environment without agglomeration.
The aim their work was to develop the NP formulation to survive in a high salinity environment (containing Ca^{2+} and Mg^{2+}). Then they investigated the underlying mechanism based on structural disjoining pressure concept. The nanofluid should have low polydispersity, small nanoparticles, high osmatic pressure and small solid/nanofluid/oil three-phase contact angle to optimize nanofluid formulation and enhance the effect of structural disjoining pressure. The calculation of interfacial tension between oil/nanofluid and oil/brine and the solid-nanofluid-oil three phase contact angle are done by using the classical method of oil drop-shape analysis. Reflected-light interference microscopy are used to monitor the movement of three-phase contact lines for nanofluid. The crude oil pre-saturated Berea sandstone is used in imbibition tests to test performance of the IIT nanofluid and brine, silica nanofluid and pH 9.7 DI water. Due to the suspension of silica nanofluid is unstable in harsh reservoir environment. Single glass capillaries are used in imbibition experiments to visualize the crude oil displacement process from the solid surface.
The results of single glass capillaries imbibition experiments confirms the structural disjoining mechanism which reported previously by (Wasan and Nikolov 2003) due to the wedge film surface confinement.
The results of the crude oil displacement from rock samples by using the silica nanofluids shows that 55% crude oil was recovered by silica nanofluid and only 2% recovered by pH 9.7 DI water at room temperature as shown in Figure 2.4. Then the results of using the IIT nanofluid to displace the crude oil from rock samples shows that 50% of crude oil can be recovered by IIT nanofluid and only 17% recovered by brine solution alone as shown in Figure 2.5. These results conclude that the IIT nanofluid had a good performance and can survive in a harsh saline environment (Zhang, Nikolov, and Wasan 2014).

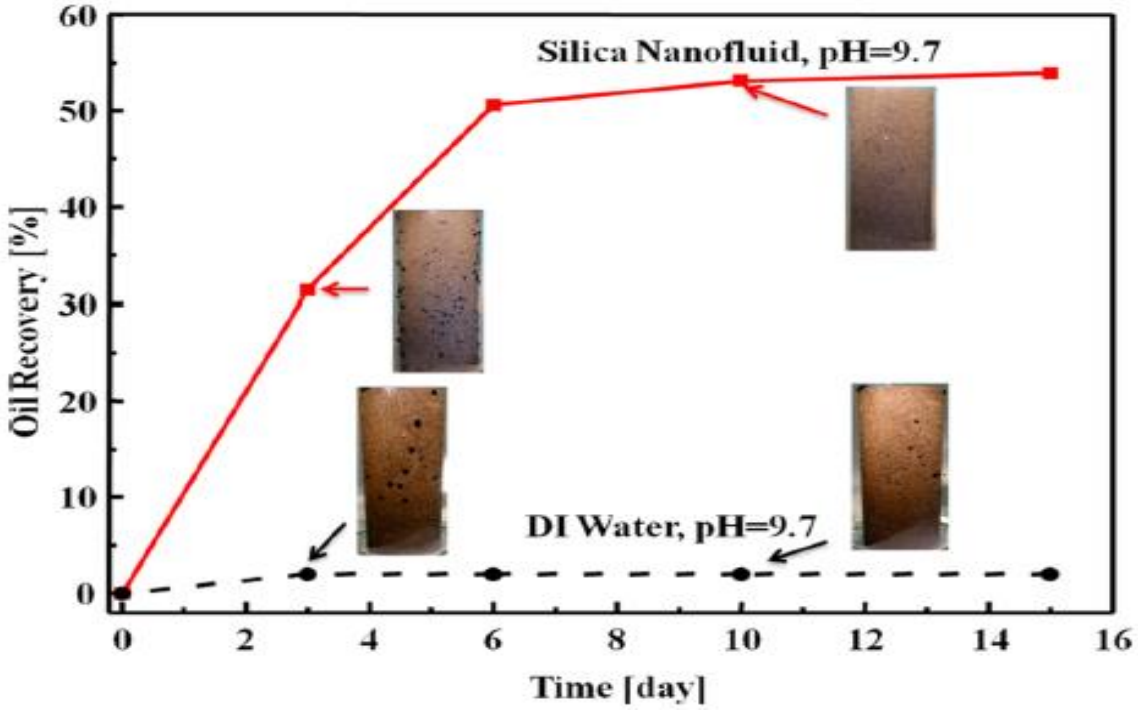

Figure 2.4: The results of oil recovery from the imbibition of silica nanofluid and pH 9.7 DI water into crude-oil-pre-saturated Berea sandstone at 25 °C (Zhang, Nikolov, and Wasan 2014).

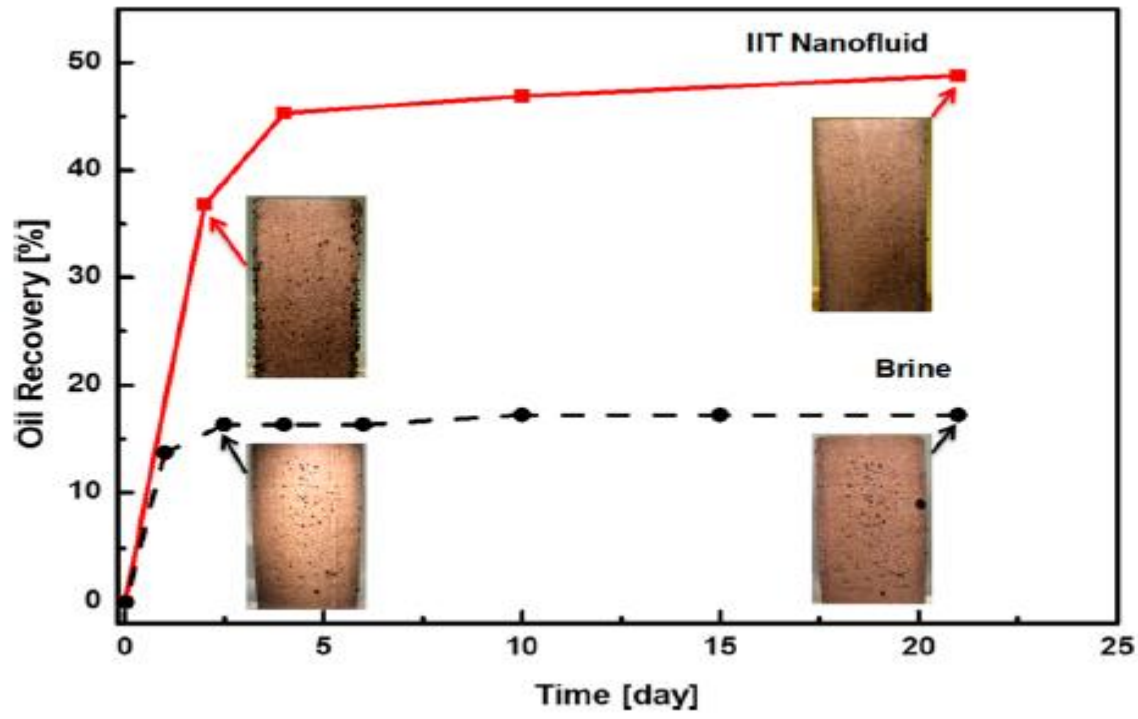

Figure 2.5: The results of oil recovery from Imbibition of IIT nanofluid and brine solution into crude-oil-pre-saturated Berea sandstone at 55 °C (Zhang, Nikolov, and Wasan 2014).

2.3. NP adsorption and its effect to mitigate Fines Migration

(Yuan, Moghanloo, and Zheng 2016) studied the effect of nanoparticles to mitigate fines migration in porous media by an application of the method of characteristic (MOE). This mitigation is characterised by retention concentration of fines particles on the grain of the rock. They described the effect of nanoparticles to mitigate fines migration by two reactions: nanoparticles adsorption onto grain/fines surface and increased retention of fines attachment on pore surface because of reducing surface potential between fines and grains. For this purpose, they developed a semi analytical MOC solutions for two scenarios. The first scenario is that the co-injection of nanoparticles with fines suspension into permeable medium. The second scenario is that the porous medium coated with nanoparticles before fines injection. The major contribution of this study is that to provide semi analytical solutions (mathematical structures) for two-phase (stationary and flowing) three- component (water, nanoparticles and fines) flow in 1D permeable porous medium to study the application of nanoparticles to control fines migration in two different scenarios. The most important conclusions of this study are:

1- Increasing the concentration of adsorbed nanoparticles leads to enhance fines particles attached on the rock surface.
2- The fines migration can be controlled even with small amount of injected nanoparticle.
3- Their results show that the precoating of the porous medium with nanoparticles before the injection of fines (second scenario) reduce the fines migration by 89.9% and the co-injection of nanoparticles with fines (first scenario) reduce the fines migration by 36.91%. By these results the precoating of the porous medium with nanoparticles before the injection of fines (second scenario) is best scenario (Yuan, Moghanloo, and Zheng 2016).

(Wang et al. 2016) studied nanoparticles dynamic adsorption, detachment and straining behaviours and its effects on Berea Cores permeability. They did both the lab and theoretical investigations. The associated formation damage is studied too in this paper.

By using the method of characteristics (MOC), an analytical model is derived to quantify NP straining, adsorption and detachment behaviour and associated effect on fluid flow. The maximum adsorption concentration model and coupled classical filtration theory are used to describe the interplay between rocks and NP.

For the experimental method (core-flooding), three different concentrations of Nano-structure particles (NSP) are used (0.05 wt.%, 0,2 wt.% and 0.5 wt.%). 2 ml/min is the flow rate in all the experiments and a confining pressure of 20 bar is used.

The major assumption used for the mathematical model and analytical solution are:

1- 1D, homogenous and uniform porous medium.
2- Two components (NP and water).
3- Two-phase (flowing and stagnant).

The major contributions of this paper are:

1- Using lab experiments to study the effect of NP adsorption, detachment and straining behaviours on the formation damage.

2- Using the analytical solutions to optimize the application of nanofluid and quantify the flow performance of nanofluid.

The main conclusions of this paper are:

1- Increasing the concentration of injected nanoparticles leads to delay the breakthrough time of Nano structure particles (NSP) nanofluid.
2- Increasing the concentration of injected nanoparticles leads to increase the amount of adsorption of reversible nanoparticles and the amount of maximum adsorption as shown in Figure 2.6.
3- The adsorption rates are larger than straining rates.
4- Increasing the NP injected concentration leads to increase the formation damage coefficients related to straining and adsorption behaviours of nanoparticles as shown in Figure 2.7 (Wang et al. 2016).

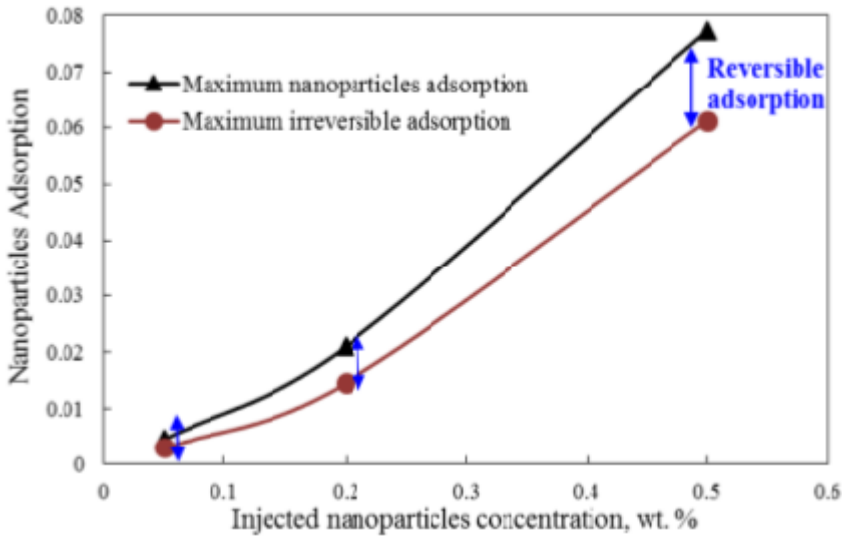

Figure 2.6: The injected NP concentration effects on the maximum reversible/ irreversible NP adsorption and maximum NP adsorption concentration (Wang et al. 2016).

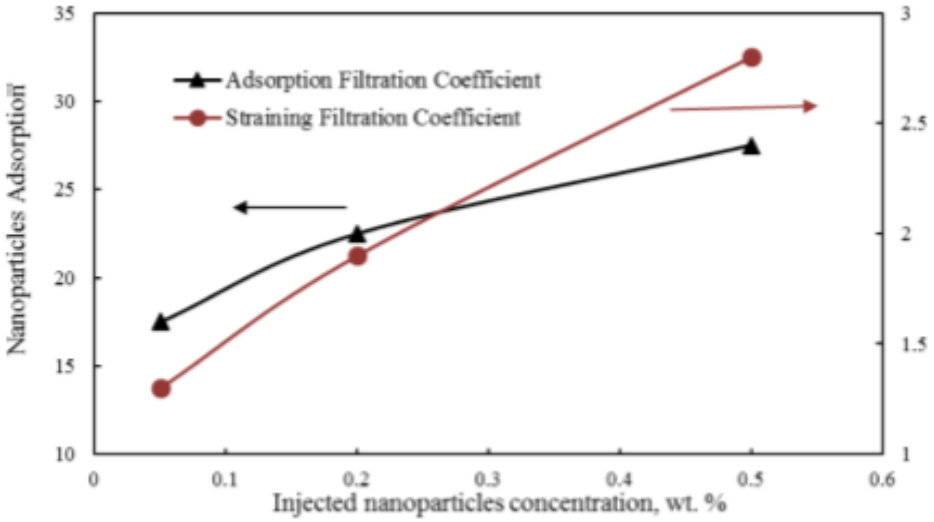

Figure 2.7: The injected NP concentration effects on the adsorption rates and straining rates (Wang et al. 2016).

Another group at University Of Texas (Zhang et al.) investigated the adsorption of nanoparticles during transport in of a single phase porous media under different flow conditions. In this study a series of transport experiments of nanoparticles in columns packed with crushed sedimentary rocks and core plugs are done. Different type of nanoparticles, flow rats, sizes and number of dispersion slugs, dispersion concentrations and size of column grain are used in these experiments. Two different type of nanoparticles are used in this study. One is silica nanoparticles with different types of surface coating and the other one is DP nanoparticles. The injected concentrations of nanoparticles in column flood experiments are: 5 wt.%.1 wt.% and 0.01wt.%. The brine salinity used in these experiments were 3wt.% of NaCl. For core flood experiments the brine salinity and pH same as the nanoparticle dispersion and some of the experiments were conducted with 18.64wt.% concentration of silica nanoparticles dispersion. The concentration history of effluent nanoparticles (breakthrough curve) for every experiment was recorded and the adsorption of each particle was calculated during the injection and after post flush. NP can be adsorbed by physicochemical interactions during its transport in porous media. The physicochemical interactions are including thermodynamic force, hydrodynamic force, particle-surface static interaction and particle-media collision. Van der Waals attraction and double layer repulsion are included in nanoparticle-surface interactions, based on Derjaguin-Landau-Verwey-Overbeek (DLVO) theory.

The result of this experimental work showed that both the irreversible and reversible NP adsorption occur during transport through water-saturated sand packs. The adsorption capacities are depending on concentrations, flow rates, type of nanoparticle, coating and specific surface area of porous media. So, the adsorption capacity is not an intrinsic property for nanoparticles or porous medium. This behaviour is not same as classical filtration behaviour and typical solute adsorption behaviour. The irreversible adsorption of nanoparticles increases as the specific surface area of the porous medium decreases, as flow rate decreases and as injection concentration increases. The interactions between grain surfaces and nanoparticles in porous medium does not fit with classical adsorption theory and classical filtration theory (Zhang et al.).

2.4. Enhanced Oil Recovery by Low Salinity Water (LSW)

The low salinity water (LSW) flooding is one of the enhanced oil recovery (EOR) techniques. Many of studies has confirmed that this EOR method is an excellent method to increase oil recovery.
(Hamouda et al. 2014) studied the mechanisms of oil recovery from sandstone and chalk rocks during LSW flooding. In this study they tried to classify the oil/brine/rock (COBR) interaction and the possible thermodynamically product of this interaction.
The LSW is used as a secondary recovery method following the synthetic seawater (SSW) in most of the designed experiments of this study. They did both the core flooding and spontaneous imbibition experiments to study the different effect and mechanism of LSW to enhance oil recovery.
The main conclusions and results of this study for Sandstone (SS) experiments are:

1- Primary flooding with SSW give higher oil recovery than the primary flooding with LSW. Secondary flooding of LSW following primary flooding of SSW give no increasing in oil recovery.
2- LSW flooding increase the pH, mineral dissolution and pressure drop across the cores compared to SSW flooding.
3- The mechanism of LSW to enhance oil recovery is based on mineral dissolution which leads to fine detachment and migration and double layer expansion.

The conclusions made by Chalk experiments are:

1- 1% additional oil recovery by switching from SSW to LSW flooding.
2- Imbibition of previously flooded cores give less oil recovery than the imbibition of unflooded cores.
3- Double layer expansion and mineral dissolution/precipitation are the main mechanism of LSW to enhance oil recovery in chalk reservoirs.

2.5. Application of nanofluid to improve the performance low salinity and alkaline flooding

LSW flooding:

Low salinity water flooding is one of the EOR methods. The problem with this EOR method is fines migration which leads to formation damage. A number studies done to investigate to ability of nanofluids to reduce fines migration and hence formation damage during LSW flooding.
(Arab and Pourafshary 2013) investigated the application of NP treatment of low salinity water (LSW) to reduce the induced migration of colloidal particles in the porous medium. In this study two set of core flood experiments are applied. The first set is done by using engineered cores as a porous media and in the second one Brea cores are used. In these experiments (both set 1 and 2) five different types of metal oxides NP (γ -Al2O3, CuO, MgO, SiO2, and ZnO)

are used to treat the porous medium. The first set of experiment are used to find the best nanoparticles for adsorbing the fine particles. The second set of experiments are used to study the nanoparticles treatment of permeability impairment caused by low salinity flooding. For the first set of experiments they applied an overburden pressure of 700 psia, 4 ml/min as a flow rate and 0.03 wt.% as NPs concentration for different scenarios. For the second set of experiments the overburden pressure is changed to 1400 psia, flow rate at 4 ml/min and the core was saturated with LSW-based γ-Al2O3 nanofluid (0.03 wt.% NP concentration). The salinity of LSW is 0.003M NaCl. Zeta potential and dynamic light scattering analysis are used to compare different scenarios.

The major contribution of this study is that the porous medium soaked with nanofluid slug before the injection of LSW leads to remediation of formation damage that subsequently induced by LSW flooding. So, it is possible to get the features of LSW flooding and avoid formation damage induced by fines migration which induced by LSW flooding.

The most important outcomes of this paper are:

1- Using LSW as EOR method can increase the oil recovery but can also cause a formation damage by increasing fines migration.
2- Using nanoparticles can reduce the fines migration problems by alteration of zeta potential of the beads surface. Zeta potential is the main parameter that affect the interactions between fine particles and rock surface.
3- γ-Al_2O_3 nanoparticle dispersed in LSW is the best adsorbent of the tiny particles existing in the flow as shown in Figure 2.8.
4- The ionic strength of nanoparticles dispersing fluid is another important parameter that effect the treatment efficiency.
5- Better dispersing of nanoparticles in solution leads to greater alteration in the surface properties.
6- γ-Al_2O_3 nanoparticle is used to treat the permeability impairment induced by LSW flooding into Berea core. γ-Al_2O_3 nanoparticles can increase the surface charge of Bear core to 33.2 mV. This leads to reduce the fines migration by 70% compared with blank test (without nanofluid) as shown in Figure 2.9. The same conclusion have made by (Abhishek and Hamouda 2017) by using the silica nanoparticles with LSW flood.

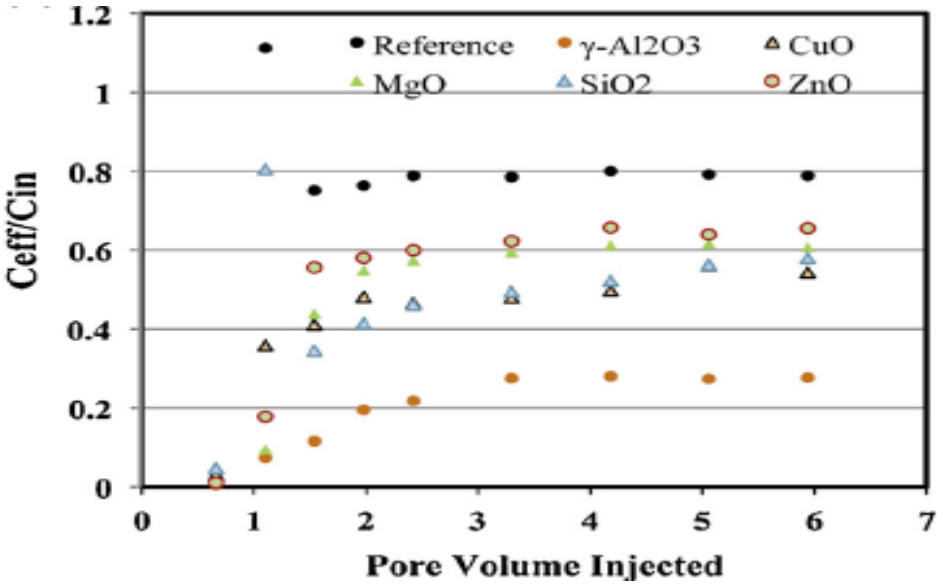

Figure 2.8: Dimensionless form of particle concentration breakthrough profile for the tests in which the medium was treated with NPs dispersed in LSW (Arab and Pourafshary 2013).

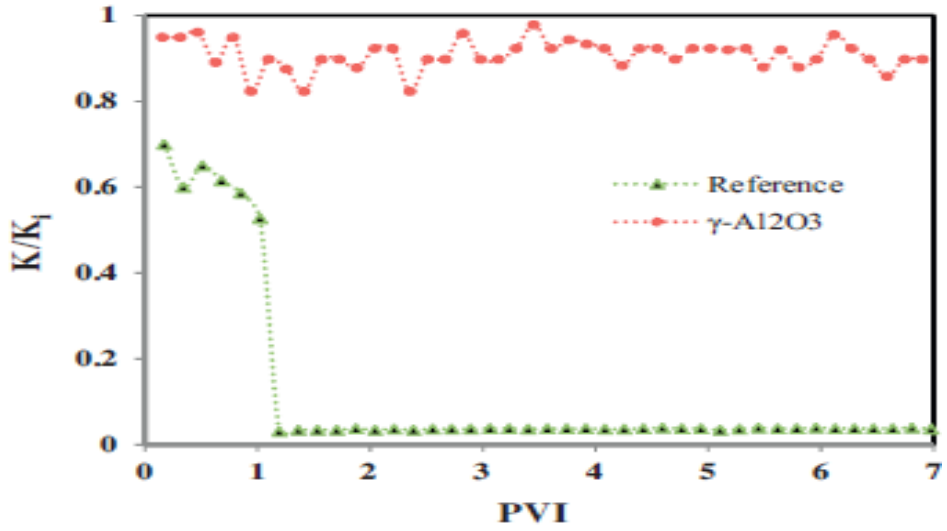

Figure 2.9: Permeability change during LSW flooding (Arab and Pourafshary 2013).

Alkaline flooding:

Alkaline flooding is one of the efficient techniques to improve oil recovery. This method is improved by increasing the pH of the injected slug during the alkaline flooding. The high pH value of the alkaline flooding leads to fines migration and then formation damage.

(Assef, Arab, and Pourafshary 2014) studied nanoparticles treatment of colloidal particles migration during alkaline flooding. In this experimental work MgO NP at different concentrations are used to modify the surface charge of the beds. The turbidity and zeta potential analysis are used to study the effect of MgO NPs on the interactions between medium surface and colloidal particles. In these experiments glass beads are used to mimic sandstone reservoirs. The effect of MgO NP to modify the point of zero charge (PZC) was also

investigated in this study. To study these effects, different values of pH are used in several experiments. The experiments done with MgO NP, the porous medium is saturated with solution containing 0.0075 wt.% of MgO NP.

The results of this experimental study show that, increasing the pH of injected fluid leads to alter the zeta potential of medium surface to more negative values as shown in Figure 2.10. This leads to increase the number of particles released from medium surface (as shown in Figure 2.10) because of the increment of the double layer repulsion between medium surface and a fine. When surface medium treated with MgO NP, the zeta potential of the surface is modified toward more positive values as shown in Figure 2.11.a. This modification of zeta potential leads to retain the negatively charged fines particles during the alkaline flooding as shown in Figure 2.11.b. At very alkaline conditions, 97% of in-situ fine particles are retained on the MgO NP treated medium as shown in Figure 2.11.b. The MgO NP can increase the PCZ of beads surface from 3 to 9 which leads to justify the retention of fines particles in wide range of alkaline conditions.

The main conclusion of this paper is that pre-flush of the medium with MgO NP fluid slug before the injection of alkaline fluid can do a promising remedy to reduce colloidal particles migration. By using this method, one can get the benefits of alkaline flooding into reservoir without fines migration problems.

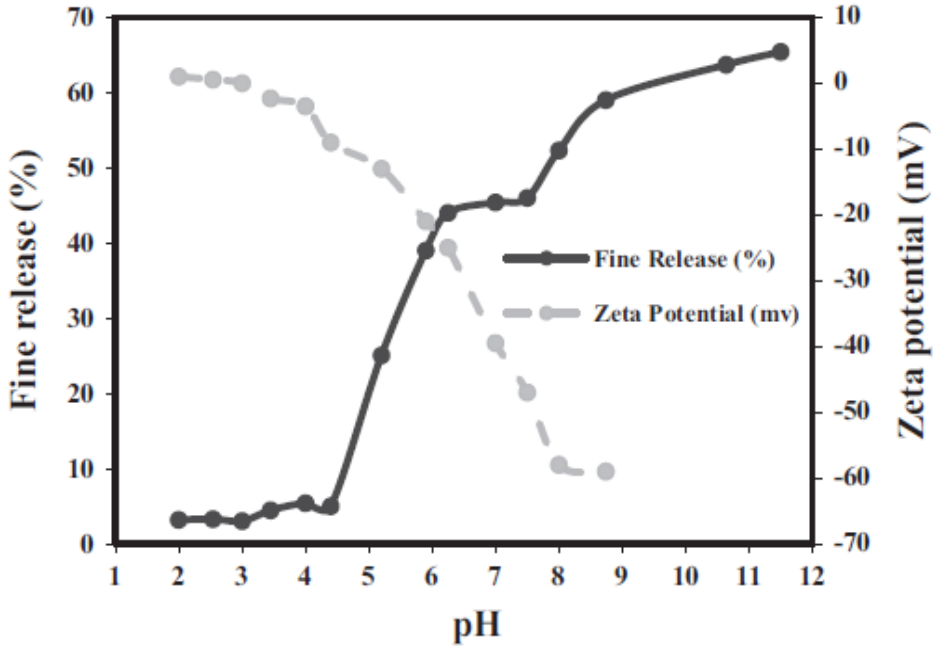

Figure 2.10: Zeta potential of the beads and percentage of particle release at different pH (Assef, Arab, and Pourafshary 2014).

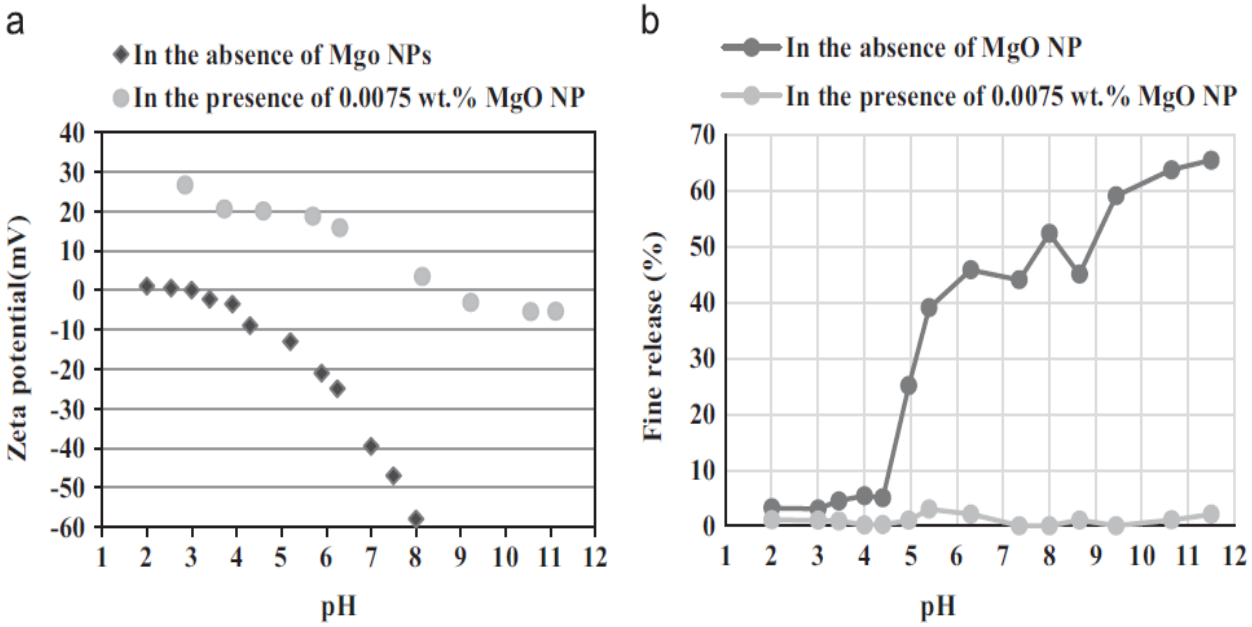

Figure 2.11. (a): Zeta potential of the medium surface at different pH. (b): percentage of particle release at different pH (Assef, Arab, and Pourafshary 2014).

2.6. Enhanced Oil recovery by nanofluids

Most of the researches have indicated that the injection of nanofluid in the lab experiments can give promising results in case of increasing oil recovery. Many researchers studied the effect of nanoparticles to improve oil recovery and investigated the possible working mechanisms behind this effect.

(Hendraningrat, Li, and Torsæter 2013) studied the possibility of nanofluid to enhance oil recovery in low (9 md) to high (400 md) permeability sandstone rocks. The suitable concentration was also investigated. The interfacial tension and wettability alteration which are involved in the structural disjoining mechanism were studied too in this study.

In this experimental work, water-wet Berea SS cores with different permeabilities from 4mD to 400md are used. The core flood experiments were performed by using three different concentrations of nanofluids (0.01wt.%, 0.05wt.%, 0.1wt.%). Lipophobic and hydrophilic nanoparticles (LHP) used in this study, consists around 99.8% of silicon dioxide (SiO_2). The brine is injected at constant rate 0.2 cm^3/min as a first imbibition process. Then the nanofluid is injected at constant rate 0.2 cm^3/min as tertiary recovery mode.

The results of this experimental study show that the contact angle of aqueous phase and the interfacial tension (IFT) between oil and aqueous are reduced by introducing LHP nanoparticles. The reduction of IFT and contact angel is increased by increasing the concentration of nanofluid. The porosity and permeability impairment in this study are caused by the retention of nanoparticles inside the core plug and the interaction between clay and nanofluid/brine had no effect on the impairment of porosity and permeability of the cores. Their results showed that there is no extra oil recovery obtained in low permeability cores during the

injection of high nanofluid concentration (0.1wt.% or more) as shown in Figure 2.12. High concentration leads to block the pore network in low permeability cores. Higher additional oil recovery is obtained by nanofluid in high permeability cores than the cores with low permeability as shown in Figure 2.12 and 2.13. Based on these results, the best silica nanofluids concentration is 0.05 wt.% for both low and high permeability water wet Berea SS in terms of oil recovery.

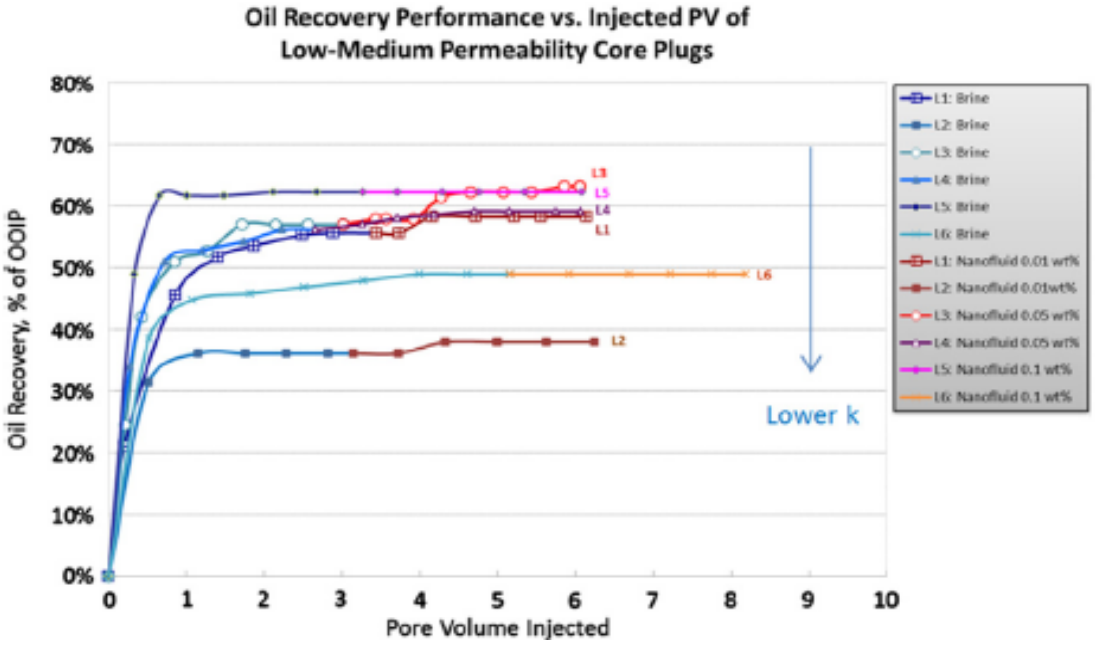

Figure 2.12: Oil recovery performance vs. injected PV for low–medium permeability core plugs with various nanofluid concentrations (Hendraningrat, Li, and Torsæter 2013).

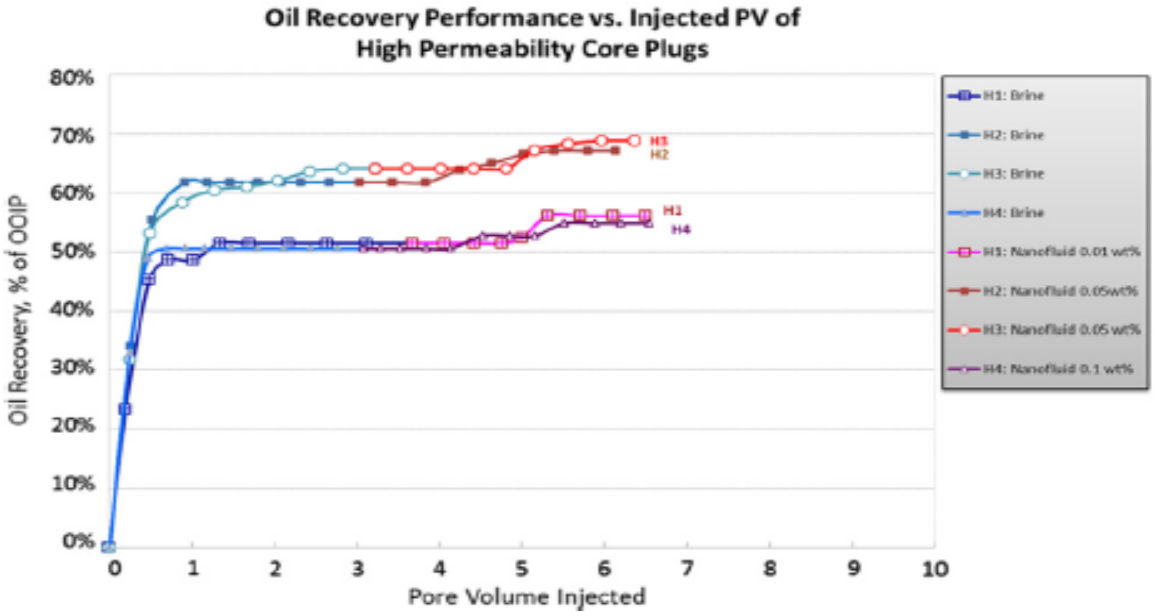

Figure 2.13: Oil recovery performance vs. injected PV for high-permeability core plugs with various nanofluid concentrations (Hendraningrat, Li, and Torsæter 2013).

The next study of (Hendraningrat and Torsæter 2014) is done to study hydrophilic metal oxide NPs. In this study they studied the potential of hydrophilic metal oxide NPs dispersed in brine to enhance oil recovery at different wettability of Berea sandstone cores. Different wettability is used in this paper to identify the most suitable conditions for each type of nanoparticles. In this way the relationship between initial rock wettability, metal oxide nanoparticles and oil recovery could be identified. To figure out the possible oil displacement mechanisms, an analysis of rock-fluid and fluid-fluid interactions is done via effluent analysis, IFT measurement and contact angle measurement. The stability of nanofluid was also investigated in this study to avoid the agglomeration of nanoparticles. The main factor that effect the stability of nanofluid is the ratio of surface area to volume. The large and effective surface area of nanoparticles implies better reactivity and tendency to agglomerate. So, the nanoparticles should maintain their small size to be able to easily flow through reservoir pore throat. That means the stability of nanofluids is very important parameter when nanoparticles are applied to enhance oil recovery. In this study, three coupled methods are used for nanofluid stability (Surface conductivity, particle size measurements and direct visual observation). PVP dispersant at three different concentrations are used (0.1 wt.%, 0.5wt.%, 1wt.%). The Investigation of using dispersant in metal oxide NPs are done at different temperatures and concentrations. Three different hydrophilic oxide nanoparticles are used in this experimental work (aluminium (Al_2O_3), titanium (TiO_2), and silica (SiO_2)).

The results of this study show that adding PVP at concentration 1 wt.% improving the stability of metal oxide-based nanofluids. Higher oil recovery is obtained by combinations of metal oxide nanofluids and PVP than the silica-based nanofluid and dispersant alone. Changing the wettability from water wet to oil wet leads to decrease the extra oil recovery obtained by metal oxide-based nanofluids. All nanofluids alter the wettability of quartz plate toward more water-wet system. TiO_2-based nanofluid noticed to be the most effective wettability-altering fluid. This result is proportional to the extra oil recovery from the core flood experiments. The lowest IFT between oil phase and aqueous is reached by metal oxide nanoparticles, but the IFT reduction degree is not proportional to the results of extra oil recovery. This observation indicates that the wettability alteration is the dominant parameter in the mechanism of oil displacement using Nano-EOR (Hendraningrat and Torsæter 2014).

3. Methodology

3.1. The experimental study

This chapter includes the experimental part of the investigation. First, it begins with describing the fluids, minerals and chemicals used in the experimental part of this master's thesis. After that, a brief explanation of the laboratory equipment used during this study. Finally, a detailed description of the experimental procedures is listed at the end of this part.

3.1.1. The experimental fluids and materials

3.1.1.1. Deionized water (DIW)

DIW was used for preparation of brines and some samples for adsorption experiments. The properties of this DIW was measured previously at ambient condition. Its pH is equal to 6.54 and density equal to 0.997 g/cm^3. The DIW used during this study was provided with "Milli-Q® Integral 5 Water Purification System" supplied by "Merck KGaA"

3.1.1.2. Nanofluid (DP)

The nanofluid suspension "DP9711" used during this study was produced by "NYACOL® Nano Technologies Inc." This nanofluid is a surface modified colloidal silica nanoparticle and stable against agglomeration in the harsh conditions (high salinity brine solutions, temperature and pressure) and over a wide range of pH values (NYACOL ; Murzin 2017). The typical properties of the nanofluid ''DP9711'' produced by ''NYACOL'' are summarized in table 3.1.

Table 3.1: Nanofluid ''DP9711'' properties (NYACOL)

Property	Value
Silica, weight %	30
Nominal Particle Size, nm	20
pH @ 25º C	3
Viscosity @ 25º C, cP	5
Specific Gravity	1.2

3.1.1.3. Brines

Synthetic sew water (SSW) and low salinity water (LSW) are the brine solutions used during throughout the laboratory experiments. SSW are prepared by adding different type of minerals (salts) to the DIW. The minerals are dissolved in DIW by stirring them with a magnetic bar. After the salts dissolution into DIW, the brine is filtered through a 0.22 μm filter by using a filtration setup. This filtration is necessary to remove the undissolved impurities in the brine solution (SSW). SSW are diluted by 10 times with DIW to prepare the LSW. Table 3.2 presents the salts composition of 1 litre SSW.

Table 3.2: Salts composition for 1 litre SSW.

Mineral	Amount (g)
NaCl	23.38
$NaHCO_3$	0.17
Na_2SO_4	3.41
KCl	0.75
$MgCl_2.6H_2O$	9.05
$CaCl_2.2H_2O$	1.91

3.1.1.4. Mineral powders

Calcite ($CaCO_3$), Kaolinite ($Al_2Si_2O_5(OH)_4$) and Quartz (SiO_2) are the mineral powders used in the kinetic adsorption experiments. These minerals were produced by ‘‘Fluka® Analytical” (Germany).

3.1.1.5. Porous Media

One outcrop chalk cylindrical core (Stevns Klint (SK) core) and one cylindrical Berea sandstone core are used for the core flooding experiments. Both cores are saturated with brine (SSW) and used for the core flood experiments. The cores are of the same type that used during previous experimental work. Chalk core is 99% pure biogenic chalk and with high porosity of 51% and the mineral analysis of Berea sandstone core are presented in Table 3.4 (Hamouda et al. 2014). The pore volume (PV) of the cores are calculated by using Equation 3.10 and Table 3.3 lists the main properties of the chalk and Berea cores.

Table 3.3:Chalk and Berea cores properties.

Core Type	Core Name	Length (mm)	Diameter (mm)	Dry weight (g)	Saturated weight (g)	Porosity (%)	PV (ml)
Chalk	FSK-1	39	37.78	58.92	81.01	51.68	22.61
Berea	FBR-1	90	37.78	211.42	232.26	21.17	21.34

Table 3.4: Mineral analysis of Berea sandstone (Hamouda et al. 2014).

Mineral Name	Chemical Formula	Semi-quantitative (%)
Quartz	SiO_2	94
Kaolinite	$Al_2Si_2O_5(OH)_4$	1
Muscovite	$(K, Na)\ (Al, Mg, Fe)_2(Si_3{\cdot}Al, O_{10})O_{10}(F, OH)_2$	1
Microcline	$KAlSi_3O_8$	1

3.1.2. Laboratory equipment

3.1.2.1. S220 SevenCompact^{TM}pH/ion meter

(S220 SevenCompactTM pH/ion meter) is used to measure the pH of samples during the kinetic adsorption experiments and the of effluents produced from the core flood experiments. This machine has an accuracy of ±0.002.

3.1.2.2. Reax Top Vortex Mixer

(Reax Top Vortex Mixer) is used to shake the prepared solutions before putting it in rotation. The step is done for all the samples used during the kinetic adsorption experiments.

3.1.2.3. Rotator Stuart SB-3

(Rotator Stuart SB-3) is used for rotating and mixing the prepared solutions for the kinetic adsorption experiments.

3.1.2.4. Analytical balance (MS104-S)

Analytical balance (MS104-S) is used to during the experiments to weight mineral powders and nanofluid. It has a weight range from 0.1 mg to 120 g.

3.1.2.5 Precision balance (Mettler PM 4600)

Precision balance “Mettler PM 4600” is used to measure the dry and saturated weights of cores for core flooding experiments. It has a weight range from 0 to 4100 g.

3.1.2.6. Magnetic stirrer (VWR VMS-C10)

Magnetic stirrer (VWR VMS-C10) is used to mix the fluids during brines preparation and nanofluid dilution. The flask with fluid and magnetic bar is placed on the magnetic stirrer for mixing.

3.1.2.7. Centrifuge 5804

Centrifuge 5804 is used to centrifuge the samples to separate mineral sediments from fluid in the samples before the UV abs and Ions concentration measurements. This machine has a spin range from 200 rpm to 10000 rpm and can centrifuge six samples simultaneously.

3.1.2.8. UV-1700 spectrophotometer

UV - 1700 spectrophotometer is used to analyse the kinetic adsorption of nanoparticles (DP) on minerals in the samples. This analysis is done by measuring the change in concentration of nanoparticles in the samples.

The principal of the machine work is that when a light beam is induced from this machine and passed through two transparent rectangular quartz cuvettes (cells used to keep the samples in

the UV-machine), the intensities of the light beam I_0 and I_t are measured. Equation 3.1 is used to calculate the transmittance (T).

$$T = \frac{I_t}{I_0} \tag{3.1}$$

Where the I_o is the light beam intensity measured after the light beam passes through the cuvette containing a solvent only(reference) and I_t is the light beam intensity measured after the light beam passes through cuvette containing a solution (produced by dissolving the sample in the solvent).

Equation 3.2 is used to calculate the absorbance (Abs) which is used often for the solution samples (Shimadzu 2018).

$$Abs = Log\frac{1}{T} \tag{3.2}$$

This machine is used for the wavelength range between 190 and 1100 nm and photometric range (Abs) from -0.5 to + 3.0 (Coletti 2007).

3.1.2.9. Ion Chromatograph (Dionex Ics-5000$^+$ DP)

Ion Chromatograph (IC) machine is used to measure and analyse the ions concentration in the solutions samples from the kinetic adsorption experiments and in the effluent samples from the core flood experiments. All the samples are diluted by 1000 times and filtered with 0.2 μm micron filter (to remove the impurities and the residual of mineral particles) before the ion chromatography (IC) analysis is done. This dilution is done by using "GX-271 Liquid handler"

3.1.2.10. Core flooding equipment

The core flooding experiments were performed using a special experimental setup. This setup comprises an injection pump, confinement pump, fluid cylinders, core holder, inlet pressure gauge, differential pressure gauge, confinement pressure gauge, back pressure valve, N_2 tank, burettes to collect the samples and laboratory oven. To reach and maintain the required temperature for the core flood experiments, the fluid cylinders and the core holder are placed inside the laboratory oven during the execution of the core flood experiments. The nitrogen in the N_2 tank is used to build the back pressure of the system.

3.1.3. Kinetic Adsorption experiment procedure

In this part a set of static experiments is done to study the kinetic adsorption behaviour of nanoparticles on Calcite and quartz. To do this study 6 different types of fluids are used (DIW, DIW+DP, SSW, SSW+DP, LSW and LSW+DP) and these fluids are kept in the plastic tubes. The concentration of nanofluid (DP) added to the fluids are diluted with DIW, LSW or SSW to 1 g/l. Then, 5 grams of each mineral are added to 30 ml of each fluid in these plastic tubes individually. After the addition of mineral to fluid, they are mixed intensively together by using the "Reax Top Vortex Mixer" for a couple of minutes and then they are placed in "Rotator Stuart SB-3" for further mixing at 40 rpm for a range of time between 2 to 75 hours.

After mixing for the specified time, the samples are collected from the rotator and placed in "Centrifuge 5804" for centrifuging. The samples are centrifuged for 10 minutes with speed of 10000 rpm and this led to separate mineral sediments from fluid in the samples. After that, 5 ml of the fluid of each sample are taken by a 5 ml syringe. Some of the 5 ml of fluid is poured into transparent rectangular quartz cuvette and placed in the "UV - 1700 spectrophotometer" to measure the nanoparticle adsorption on mineral surface by absorbance (Abs) calculation. Then, the rest of the 5 ml fluid is poured in to very small plastic tubes and placed in Ion Chromatograph (IC) machine to do the Ions concentration analysis. All the fluid samples should be filtered by 0.2 μm micron filter before placed into The UV and IC machine. Finally, the remaining of samples (fluid and mineral sediment) in the plastic tube are remixed by "Reax Top Vortex Mixer" and their pH are measured using (S220 SevenCompactTM pH/ion meter). The machine is calibrated using fluids with pH values of 7 and 10 before starting the pH measurement of the samples.

"UV - 1700 spectrophotometer" is used to investigate the nanoparticles adsorption on mineral surfaces by measuring the absorbance (Abs). This investigation is based on ''Lambert-Beer law'', which is express a proportional relationship between the absorbance and the concentration of the sample as shown in Equation 3.3 (Shimadzu 2018).

$$Abs = \varepsilon * C * L \tag{3.3}$$

Here, Abs is the absorbance, ε is the absorption coefficient of the sample, C is sample concentration and L is the optical path length of the cell (Shimadzu 2018).

Based on Equation 3.3, the (Abs) measurement from the UV-machine leads to estimate the concentration of nanoparticles in the sample and the amount of nanoparticle adsorbed on the surface of minerals. Increasing of the Abs value means more transmission of light beam through the cuvette which is filled with a sample. This means a decreasing of the nanoparticles amount in the sample or in the other words the adsorption of nanoparticles on mineral surface during the mixing/rotating stage is increased and less number of nanoparticles is left in the sample which is in the cuvette.

To find out the correct nanoparticle concentration in the sample and the amount adsorbed on the mineral surface, a calibration curves for DP in DIW, DP in LSW and DP in SSW are used as shown in Figure 3.1. These calibration curves are demonstrating the relation between the absorbance (Abs) and the nanofluid concentration (DP9711) in DIW, LSW and SSW respectively. High sensitivity between the nanofluid concentration and absorbance are represented by a straight line as shown in the Figure 3.1.

These three calibration curves were made by preparation of three known different nanofluid concentrations (0.33 g/l, 0.5 g/l and 1 g/l) for each type of the fluids (DP in DIW, DP in LSW and DP in SSW). Then they are placed in UV-machine and their Abs are measured. After the Abs measurement, it would be able to plot the calibration curves for the three fluids. By applying the trend line option in Excel for these curves, the trend line equations could be used to calculate the nanoparticle concentration from the Abs values for all the samples.

The samples that prepared without nanofluid (only 5 g of mineral powder + 30 ml of fluid) are used to consider the effect of mineral on Abs value or in other words to do a baseline correction for the corresponding samples. The correct Abs values for the nanoparticles are calculated by subtraction of the Abs values of samples without NP (baseline) from the Abs values for the samples with NP (the corresponding samples) as shown in Equation 3.4.

The following equations show the calculation method for the nanoparticles adsorption in mg on per gram of mineral powder:

$$Correct\ Abs\ for\ NP = Abs\ for\ samples\ with\ NP - Abs\ for\ the\ baseline \quad (3.4)$$

Using the trendline's equation in this case for DIW as shown in Figure 3.1, to find NP concentration

$$NP\ concentration\ (\frac{g}{l}) = \frac{Correct\ Abs\ for\ NP}{0.1663} \quad (3.5)$$

Where (x) corresponding to NP concentration and (y) corresponding to correct Abs for NP.

$$Mass\ of\ NP\ left\ in\ a\ sample\ (g) = NP\ concntration\ \left(\frac{g}{l}\right) * \frac{30\ (ml)}{1000} \quad (3.6)$$

$$Mass\ of\ NP\ added\ to\ a\ sample\ (g) = \frac{30\ (ml)}{1000} * 1\ (\frac{g}{l}) \quad (3.7)$$

$$\longrightarrow\ Mass\ of\ NP\ added\ to\ a\ sample = 0.03\ gram\ (applied\ for\ all\ the\ samples).$$

$$Mass\ of\ NP\ adsorbed\ on\ mineral(g) = 0.03(g) - mass\ of\ NP\ left\ in\ the\ sample(g) \quad (3.8)$$

$$Mass\ of\ NP\ adorbed\ on\ per\ gram\ mineral\ \left(\frac{mg}{g}\right) = \frac{mass\ of\ NP\ adsorbed\ on\ mineral(g)*1000}{5\ (g)\ (mass\ of\ mineral\ in\ a\ sample)} \quad (3.9)$$

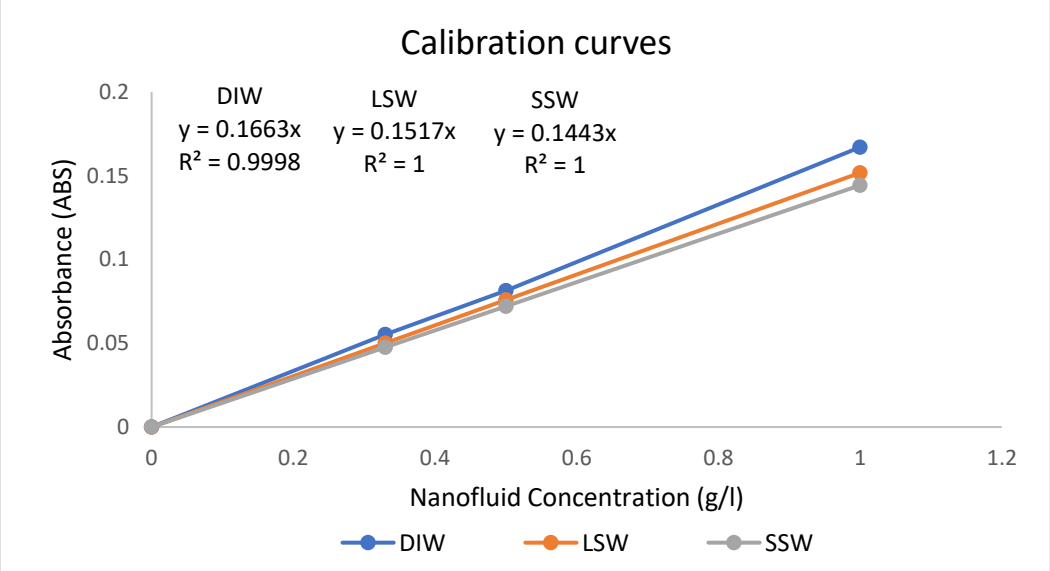

Figure 3.1 : Calibration curves for nanofluid (DP9711) in DIW, LSW and SSW.

3.1.4. Core flood experiment procedure

In this part two experiments/floods are run using chalk core (SK-core) and Berea sandstone core, and the general aim of these experiments are to investigate the transport behaviour of NPs in chalk and sandstone rock.

First, the core dimensions and weight (dry) are measured before the experiment is run. After that, the core saturated with SSW using the vacuum saturation setup and then its weight (wet) is measured again. Equation (3.10) is used to calculate the pore volume (PV) of the cores.

$$PV = \frac{weight\ after\ saturation\ (g) - Dry\ weight(g)}{density\ of\ SSW\ (\frac{g}{ml})} \quad (3.10)$$

Where the density of SSW is (1.024 g/ml) and the detailed information of the cores is presented previously in Table 3.3.

PV is needed to determine the injection rate of the injection pump. Then the core is placed inside the core holder. The injection fluids are placed in the fluid cylinders and connection lines of the core flooding equipment are cleaned with DIW before the flooding starts.

Two types of fluids used during the core flooding experiments, brine (SSW) and nanofluid prepared in SSW (SSW + 1(g/l) DP + 0.1M LiCl). Where LiCl is a tracer added to the nanofluid prepared in SSW. Both cores are saturated with SSW before flooding and the SSW is used as an injection fluid during the Pre-Flush and Post-Flush stages. These two experiments are flooded at constant injection flow rate of 10 (PV/Day) or 0.16 (ml/min) and against constant confinement pressure of 25 bar and constant back pressure of 10 bar.

After each quarter PV which means around 35 min, the sample effluents are collected in small glass flasks automatically using Auto sampler as shown in Figure 3.2. After all the samples are collected, its pH values are measured by using (S220 SevenCompactTM pH/ion meter). The machine is calibrated with two fluids with pH values of 7 and 10 before the pH measurement of the samples starts. After that, the absorbance (Abs) values of the sample effluents are measured by using (UV-1700 spectrophotometer). Some of each sample are taken by a 5 ml syringe. Some of the 5 ml of fluid and poured into transparent rectangular quartz cuvette and placed in the "UV - 1700 spectrophotometer" to measure the nanoparticle adsorption on mineral surface by absorbance (Abs) calculation. The Abs measurement of the effluent samples followed the same procedure that done during the kinetic adsorption experiments and all the samples are measured against DIW which is used as a refence fluid. Finally, the ion chromatography (IC) is done for the sample effluents by using (Dionex Ics-5000+ DP) machine. Before The sample effluents are putted inside the IC machine, the effluents are diluted with DIW at a ratio of 1:1000 by using (GX-271 Liquid handler) and filtered by 0.2 μm micron filter. The DIW is used as a reference fluid for the IC measurements. The analysis of IC data of the effluents is very important to find out the different types of ions present in the effluents. By this analysis, the change in the nanofluid slug concentration could be detected and the ion exchange chemistry in the cores during the core flooding could be understood.

To find out the correct nanoparticle concentration in the effluent samples and the amount adsorbed on the Chalk and Berea surfaces, a calibration curve (SSW + DP + 0.1M LiCl) is used as shown in Figure 3.3. The calibration curve is prepared in the same way as done during the kinetic adsorption experiments and its Abs values are measured against DIW. By applying the trend line option in Excel for this curve, the trend line equation could be used to calculate the nanoparticle concentration from the Abs values for all the effluents samples. The effluent samples produced without NP, which means before and after the NPs production period are used as a baseline. The correct Abs values for the nanoparticles are calculated by subtraction of the Abs values of samples without NP (baseline) from the Abs values for the effluent samples with NP produced during the NP production stage as shown in Equation 3.11.

The following equations show the calculation method for the nanoparticle concentration (g/l) in the produced effluents, total NP produced and injected in gram and the amount of NP adsorbed (%) on Chalk or Berea surfaces during the flood:

$$Correct\ Abs\ for\ NP = Abs\ for\ samples\ with\ NP - Abs\ for\ the\ baseline \quad (3.11)$$

Using the trendline's equation shown in Figure 3.3, to find NP concentration:

$$NP\ concentration\ (\frac{g}{l}) = \frac{Correct\ Abs\ for\ NP}{0.1101} \quad (3.12)$$

Where (x) corresponding to NP concentration and (y) corresponding to correct Abs for NP.

$$Volume\ of\ produced\ \ effluent\ for\ each\ \ sample\ (l) = \frac{Pore\ volume\ (PV)}{4} \quad (3.13)$$

$$NP\ produced\ for\ each\ sample\ (g) = \frac{Volume\ of\ produced\ \ effluent\ for\ each\ \ sample\ (l)}{NP\ concentration\ (g/l)} \quad (3.14)$$

$$NP\ adsorbed(\%) = \frac{\left(NP\ injected\ conc\ \left(\frac{g}{l}\right) * slug\ volume(l)\right) - \Sigma(NP\ produced\ for\ each\ sample(g))}{NP\ injected\ conc\ (g/l)\ \ * slug\ volume\ (l)}\% \quad (3.15)$$

Table 3.5 and 3.6 summarize the core flooding experiments scheme for Chalk and Berea sandstone cores respectively. Figure 3.2 shows the schematic illustration of the core flooding setup.

Table 3.5: Flood scheme for Chalk core.

Stage	Injected fluid	Injection rate (PV/Day)	PV injected
Pre-Flush	SSW	10	7
Slug	SSW + 1(g/l) DP + 0.1M LiCl	10	1.5
Post-Flush	SSW	10	7

Table 3.6: Flood scheme for Berea Sandstone core.

Stage	Injected Fluid	Injection rate (PV/Day)	PV injected
Pre-Flush	SSW	10	7.75
Slug	SSW + 1(g/l) DP + 0.1M LiCl	10	1.5
Post-Flush	SSW	10	5.75

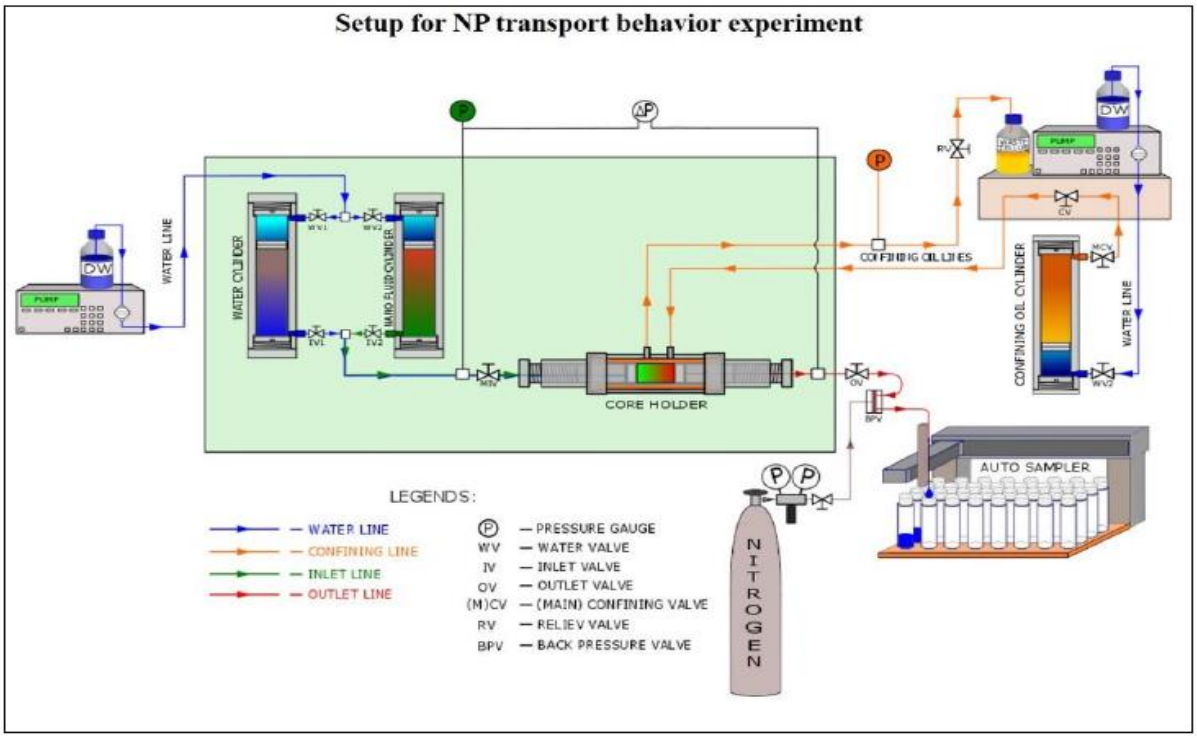

Figure 3.2: Schematic illustration of Core flooding setup

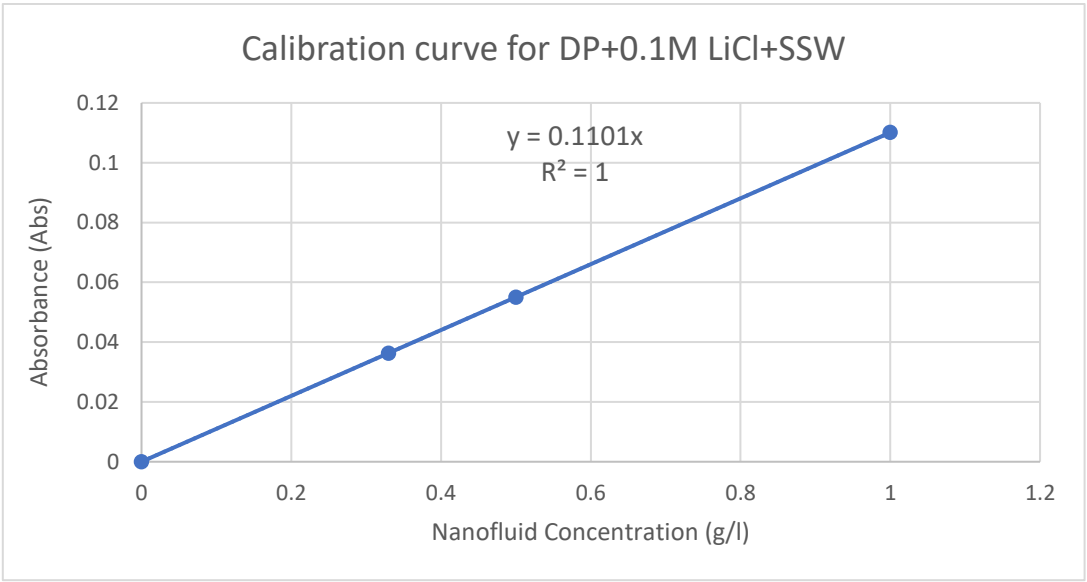

Figure 3.3: Calibration curve for nanofluid (DP9711) in SSW+ 0.1M LiCl.

4. Results and Discussion

4.1. Kinetic Adsorption

In this part of this chapter, the kinetic adsorption of nanoparticles on Calcite and quartz surfaces are investigated by running a set of Isothermal adsorption experiments. A comparison on NPs adsorption on mineral surfaces is done by using three fluids (DIW, LSW and SSW). Then a kinetic model is chosen to describe the kinetic adsorption behaviour of NPs on mineral surfaces. The adsorption of the NPs is studied on Calcite and quartz mineral which are the major minerals present in Chalk and sandstone reservoirs respectively. Further, IC and pH measurements are made for NP adsorption on calcite to address the effect of NP on fluid mineral interaction.

4.1.1. Calcite

4.1.1.1. NPs adsorption on Calcite

The nanoparticles (NPs) kinetic adsorption on calcite is investigated by adding 5 grams of Calcite to 30 ml of three different fluids with nanoparticles (DP in DIW, DP in LSW and DP in SSW). After the specified mixing time for each sample, their Abs values are measured and their adsorption on Calcite surface are calculated by using the calibration curves (Figure 3.1), the Abs readings and the equations (3.4 - 3.9). The Abs correction for the NPs samples (the baseline correction) is done by preparing the same samples in similar manner, but without NPs and their Abs values are measured and subtracted from the Abs values for NPs samples.

The results of the adsorption of NPs on Calcite (mg of NP /g of Calcite) in DIW are plotted against the specified mixing time for the samples (interaction time between nanofluid and calcite) in hours (Figure 4.1). From Figure 4.1, the adsorption of NPs on Calcite in DIW is increasing with the mixing time. The equilibrium (maximum adsorption of NPs on Calcite) is reached after about 49.5 hours of interaction between the nanoparticles and Calcite and its value was about 2.4 (mg/g).

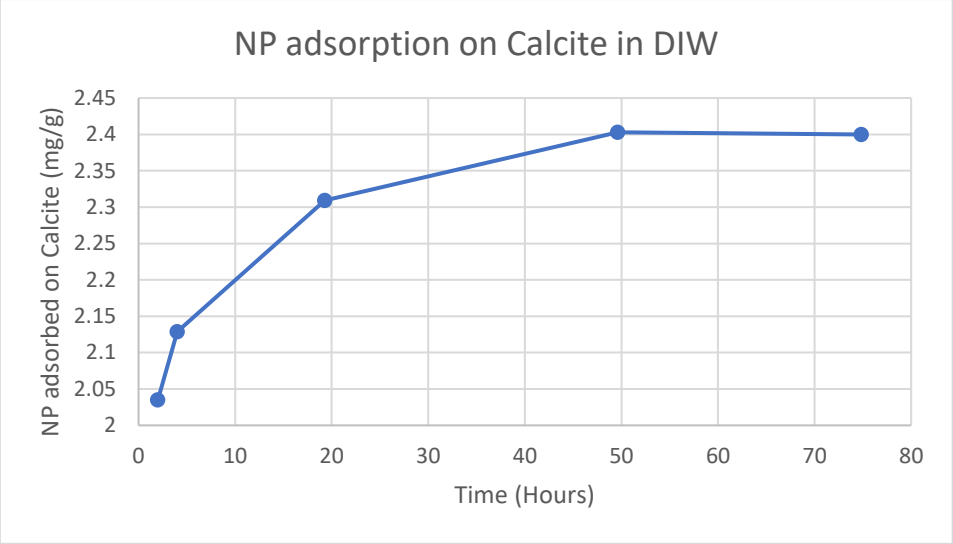

Figure 4.1: NPs kinetic adsorption on Calcite in DIW.

Figure 4.2 shows the results of the adsorption of NPs on Calcite in LSW. By looking to this figure, the adsorption of NP is increased with time and did not reach the equilibrium. The slope of the adsorption curve starts to decrease after about 10 hours. The maximum adsorption of NP on Calcite in LSW was about 4.4 (mg/g) after 49 hours.

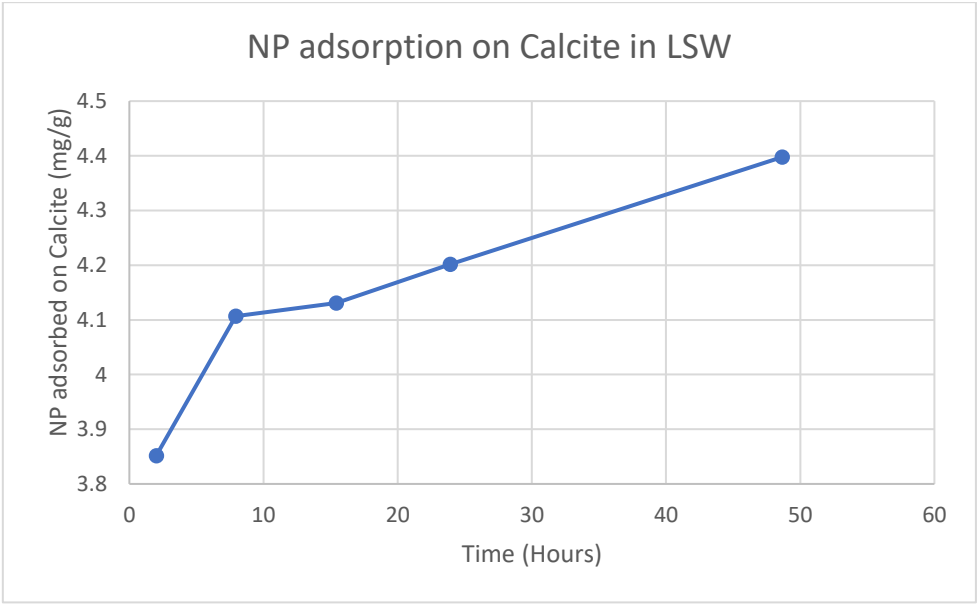

Figure 4.2: NPs kinetic adsorption on Calcite in LSW.

The results of NP adsorption on Calcite in SSW are shown in Figure 4.3. The adsorption of NP on Calcite is increased with time and reached the equilibrium after around 13 hours. The maximum amount of NP adsorbed on Calcite in SSW after 24 hours was about 4.75 (mg/g).

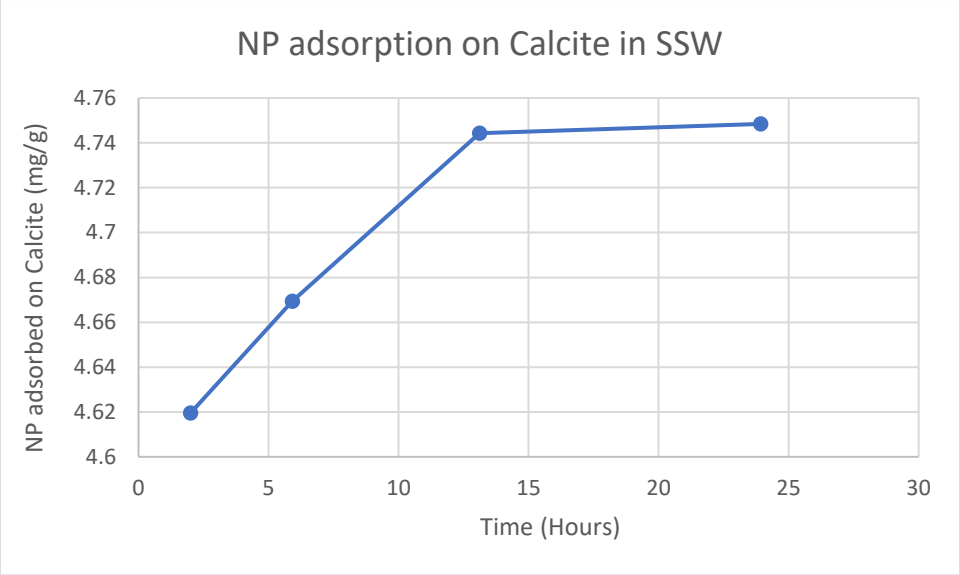

Figure 4.3: NPs kinetic adsorption on Calcite in SSW.

For comparison, the results of NP adsorption on Calcite in DIW, LSW and SSW are plotted together against the mixing time in Figure 4.4. This figure show that the highest adsorption of NP on calcite is reached in SSW and the lowest in the DIW. This indicates that increasing the salinity (ionic strength) of the fluid leads to increase the adsorption of nanoparticles on Calcite. Increasing the ionic strength of the solution leads to reduction of absolute value of zeta potential for NP and Calcite. This happens because increasing the ionic strength leads to compression of the double layer and this leads to reduction of the electrostatic repulsion between the Calcite and NP which means that the adsorption of NP on calcite surface is enhanced as shown in Figure 4.4 (Dehghan Monfared et al. 2015; Abdelfatah et al. 2017; Mondragon et al. 2012) have made similar conclusions. In table 4.1, the detailed information of NPs adsorption on Calcite in DIW, LSW and SSW is presented.

Table 4.1: NPs adsorption on calcite in DIW, LSW and SSW

DIW		LSW		SSW	
Time (Hours)	Adsorption (mg/g)	Time (Hours)	Adsorption (mg/g)	Time (Hours)	Adsorption (mg/g)
2	2.03	2	3.85	2	4.62
4	2.13	7.92	4.11	5.92	4.67
19.3	2.31	15.42	4.131	13.12	4.74
49.63	2.4	23.92	4.2	23.92	4.75
74.85	2.4	48.65	4.4		

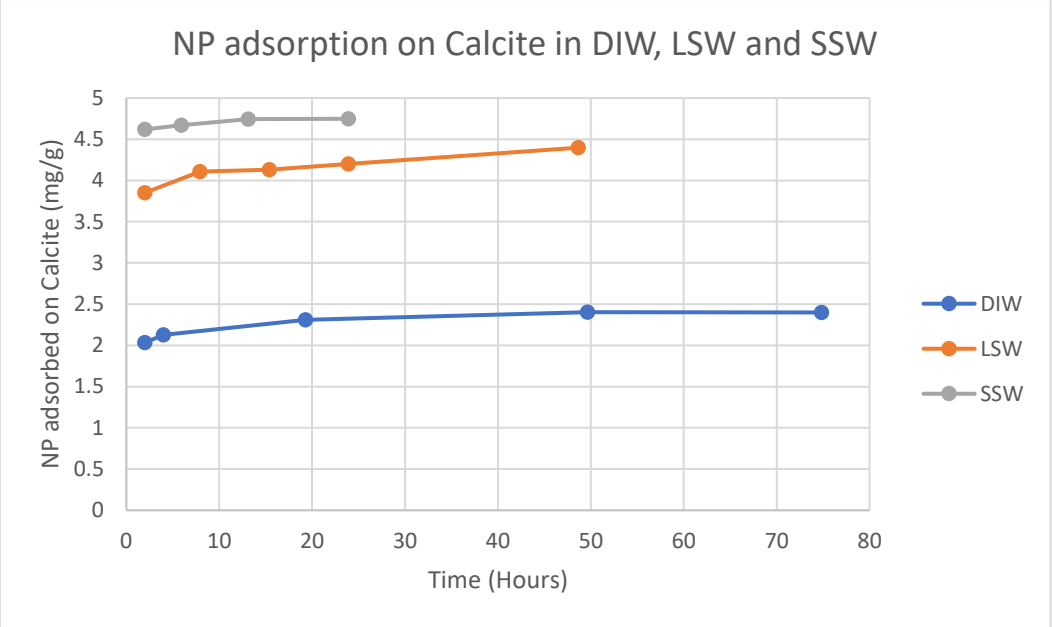

Figure 4.4: NPs kinetic adsorption on Calcite in DIW, LSW and SSW.

To analyse the kinetic adsorption behaviour of nanoparticles on Calcite in DIW, LSW and SSW and its adsorption mechanism, three common kinetic models are investigated. This investigation is done by fitting the adsorption data to kinetics models and to find the best kinetic model that can describe the adsorption process presented in this thesis. These kinetics models are: pseudo-first order model, pseudo-second order model and Intraparticle diffusion model.

The first model was investigated to fit the adsorption model presented here is the pseudo-first order model. Equation 4.1 present the linear formulation of this model.

$$\ln\big(q_e(exp) - q(t)\big) = \ln q_e(est) - k_1 * t \qquad (4.1)$$

Here, the q(t) is the amount of nanoparticle adsorbed (mg/g) on Calcite at time t, q_e(exp) (mg/g) is the amount of nanoparticles adsorbed on Calcite when the equilibrium is reached, q_e (est) is estimated from the kinetic model and K_1 is the pseudo-first order rate constant (1/h) (Yuh-Shan 2004; Dehghan Monfared et al. 2015).

Figure 4.5 shows the description of kinetic adsorption of NPs onto calcite in DIW, LSW and SSW using the pseudo-first order kinetic model. $\ln\big(q_e(\exp) - q(t)\big)$ is plotted against time for all the three fluids. The q_e (exp) for DIW, LSW and SSW are 2.4 ,4.4 and 4.75 (mg/g) respectively as shown in Table 4.2. The trendline's equations in Figure 4.5 are used to obtain the K_1 and the q_e (est) as shown in Table 4.2. For q_e (est) values, equation 4.2 is also needed to use

$$q_e(est) = e^c \qquad (4.2)$$

Where (c) is equal to -0.9206,0.0891 and -0.0293 for DIW, LSW and SSW respectively as shown in Figure 4.5.

R^2 is the correlation coefficient used to determine the fit quality for each case. By looking to Figure 4.5 and Table 4.2, the R^2 values for pseudo first order is relatively high for all the three types of fluids. The best fit is reported for the adsorption of NPs onto Calcite in DIW. The constant rate (K_1) show much faster adsorption of NPs on calcite surface in SSW followed by LSW and DIW.

Table 4.2: Estimated parameters of Pseudo-first order kinetic model for Calcite.

DIW			LSW			SSW		
K_1 (1/h)	q_e(est) (mg/g)	R^2	K_1 (1/h)	qe(est) (mg/g)	R^2	K_1 (1/h)	q_e(est) (mg/g)	R^2
0.077	0.398	0.9904	0.1149	1.093	0.9025	0.2136	0.971	0.9365

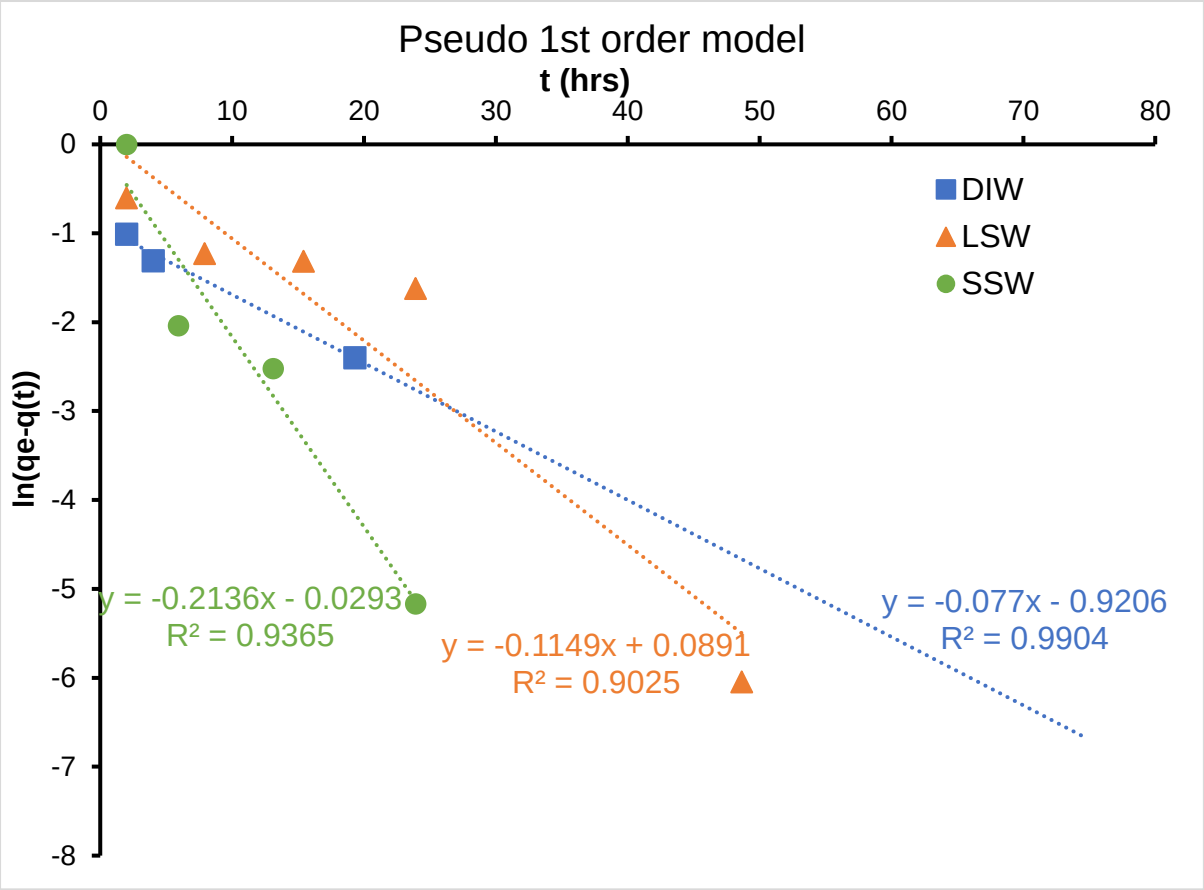

Figure 4.5:Pseudo-first order kinetic model for the adsorption experiments of NPs on Calcite in DIW, LSW and SSW.

Pseudo-second order model is the second model investigated to fit the adsorption model of this study. Equation 4.3 expresses the linear formulation of pseudo-second order model.

$$\frac{t}{q(t)} = \frac{1}{k_2 * q_e^2(est)} + \frac{t}{q_e(est)} \qquad (4.3)$$

In this equation, k_2 is the pseudo-second order rate constant (g/mg*h) (Ho and McKay 1999; Dehghan Monfared et al. 2015).

To determine the pseudo-second order model's parameters (k_2 and q_e (est)) for DIW, LSW and SSW, t/q(t) is plotted against time (t) for all these three types of fluids as shown in Figure 4.6. the trendline's equations shown in Figure 4.6 and equations 4.4 and 4.5 are used to calculate k_2 and q_e (est).

$$q_e(est) = \frac{1}{m} \tag{4.4}$$

Where, (m) is equal to 0.4133, 0.2255 and 0.2098 for DIW, LSW and SSW respectively as shown in Figure 5.6.

$$k_2 = \frac{1}{C * q_e^2} \tag{4.5}$$

Where, (c) is equal to 0.233, 0.1708 and 0.0176 for DIW, LSW and SSW respectively as shown in Figure 4.6.

By looking to Figure 4.6 and Table 4.3, the R^2 values for pseudo second order is higher than the pseudo first order for all the three types of fluids. Which means that pseudo-second order is more appropriate to describe the kinetic adsorption process than the pseudo first order. The best fit is reported for the adsorption of NPs onto Calcite in SSW. The constant rate (K_2) show much faster adsorption of NPs on calcite surface in SSW followed by DIW and LSW.

Table 4.3 presents the values of estimated parameters and correlation coefficient (R^2) for pseudo second order model.

Table 4.3: Estimated parameters of Pseudo-second order kinetic model for Calcite.

DIW			LSW			SSW		
K_2 (g/mg*h)	q_e(est) (mg/g)	R^2	K_2 (g/mg*h)	q_e(est) (mg/g)	R^2	K_2 (g/mg*h)	q_e(est) (mg/g)	R^2
0.733	2.419	0.9999	0.297	4.434	0.9994	2.500	4.766	1

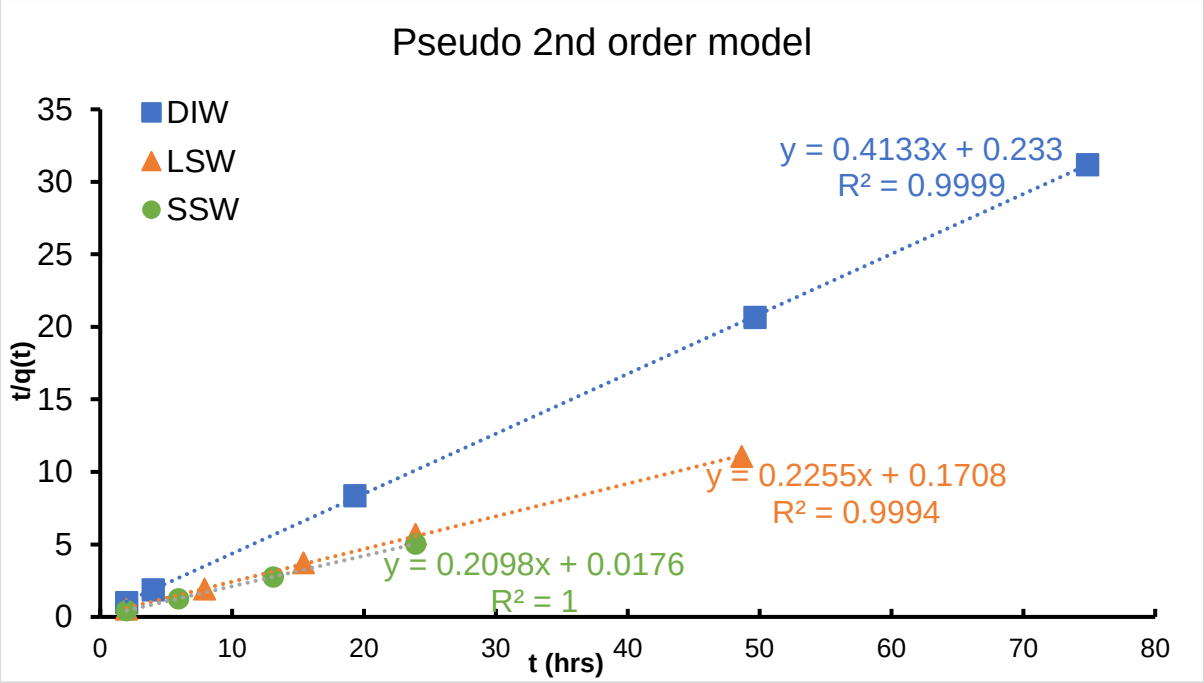

Figure 4.6: Pseudo-second order kinetic model for the adsorption experiments of NPs on Calcite in DIW, LSW and SSW.

The correlation coefficient (R^2) and the difference between experimental and estimated equilibrium adsorption (q_e (exp) – q_e(est)) are used as criterions to choose the most appropriate kinetic model that can describe the NPs adsorption on Calcite.

Table 4.4 shows a comparison between the pseudo first and second order model. This table shows that the R^2 values are highest and the difference between experimental and estimated equilibrium adsorption is smallest for pseudo-second order model. This may indicate the Pseudo-second order model best describes the adsorption behaviour of the used NPs on the calcite surface.

Table 4.4: A comparison between Pseudo first and second order model for Calcite.

Pseudo-first order						Pseudo-second order					
DIW		LSW		SSW		DIW		LSW		SSW	
R^2	q_e(exp) - q_e(est) (mg/g)	R^2	qe(exp) - qe(est) (mg/g)	R^2	qe(exp) - qe(est) (mg/g)	R^2	qe(exp) - qe(est) (mg/g)	R^2	qe(exp) - qe(est) (mg/g)	R^2	qe(exp) - qe(est) (mg/g)
0.9904	2.002	0.9025	3.307	0.9365	3.779	0.9999	-0.019	0.9994	-0.034	1	-0.016

According to the pseudo-second order model, the adsorption capacity of calcite or in other word the amount of nanoparticle adsorbed at equilibrium estimated from the model (qe (est)) is highest for the SSW samples followed by LSW and DIW as showing in Table 4.3. Pseudo-second order rate constant (K_2) is highest for SSW (2.500 (g/mg*h)) as shown in Table 4.3. Pseudo-second order rate constant (K_2) is proportionally related to adsorption rate. Which means that the highest adsorption rate of NPs onto calcite surface was in SSW.

Finally, the intraparticle diffusion model is used to understand the adsorption mechanism. Equation 4.6 is used to describe this model.

$$q(t) = k_i t^{0.5} + C_i \quad (4.6)$$

Where C_i (mg/g) present the boundary layer effect and K_i is the intraparticle diffusion rate constant (mg/g*$h^{0.5}$) (Dehghan Monfared et al. 2015; Suriyanon, Punyapalakul, and Ngamcharussrivichai 2013).

To determine the intraparticle diffusion model's parameters (k_i and C_i) for DIW, LSW and SSW, q(t) is plotted against time ($t^{0.5}$) for all these three types of fluids as shown in Figure 4.7. the trendline's equations shown in Figure 4.7 is used to determine the parameters k_i and C_i.

By looking to Figure 4.7 and Table 4.5, the R^2 values for intraparticle diffusion model are relatively low compared to pseudo first and second order models (except LSW). The best fit is reported for the adsorption of NPs onto Calcite in LSW. Table 4.5 shows the values of these parameters and the values of correlation coefficient (R^2).

Three steps are commonly used to describe the adsorption mechanisms. These steps are: film diffusion, Intraparticle diffusion and the adsorbate adsorbed at a site on the adsorbent external/internal surface. The last step is relatively fast, and the adsorption rate is controlled by the slowest step. So clearly, the last step is not the rate controlling mechanism (Suriyanon, Punyapalakul, and Ngamcharussrivichai 2013; Dehghan Monfared et al. 2015). The Intraparticle diffusion model in Figure 4.7 is used to find the rate controlling mechanism for the adsorption process of NPs onto calcite surface in DIW, LSW and SSW. When the plot is linear and passes through the origin, the intraparticle diffusion is the sole rate controlling mechanism (Ho 2003) . If the plot was only linear and didn't pass through origin, means that the mechanism of intraparticle diffusion has contributed in the adsorption process, but it was not the only the mechanism that contributed in the adsorption process (Dehghan Monfared et al. 2015).

From Figure 4.7, the three plots for DIW, LSW and SSW were linear and didn't pass through the origin. This means that the intraparticle diffusion was not the only rate controlling mechanism and the film (boundary layer) diffusion mechanism had some effect on the adsorption process of NPs onto calcite surface in DIW, LSW and SSW.

Table 4.5: Estimated parameters and correlation coefficient (R^2) of intraparticle diffusion model for Calcite.

DIW			LSW			SSW		
K_i (mg/g*$h^{0.5}$)	Ci (mg/g)	R^2	K_i (mg/g*$h^{0.5}$)	Ci (mg/g)	R^2	K_i (mg/g*$h^{0.5}$)	Ci (mg/g)	R^2
0.0501	2.0197	0.8937	0.0978	3.7294	0.9955	0.0393	4.5741	0.8971

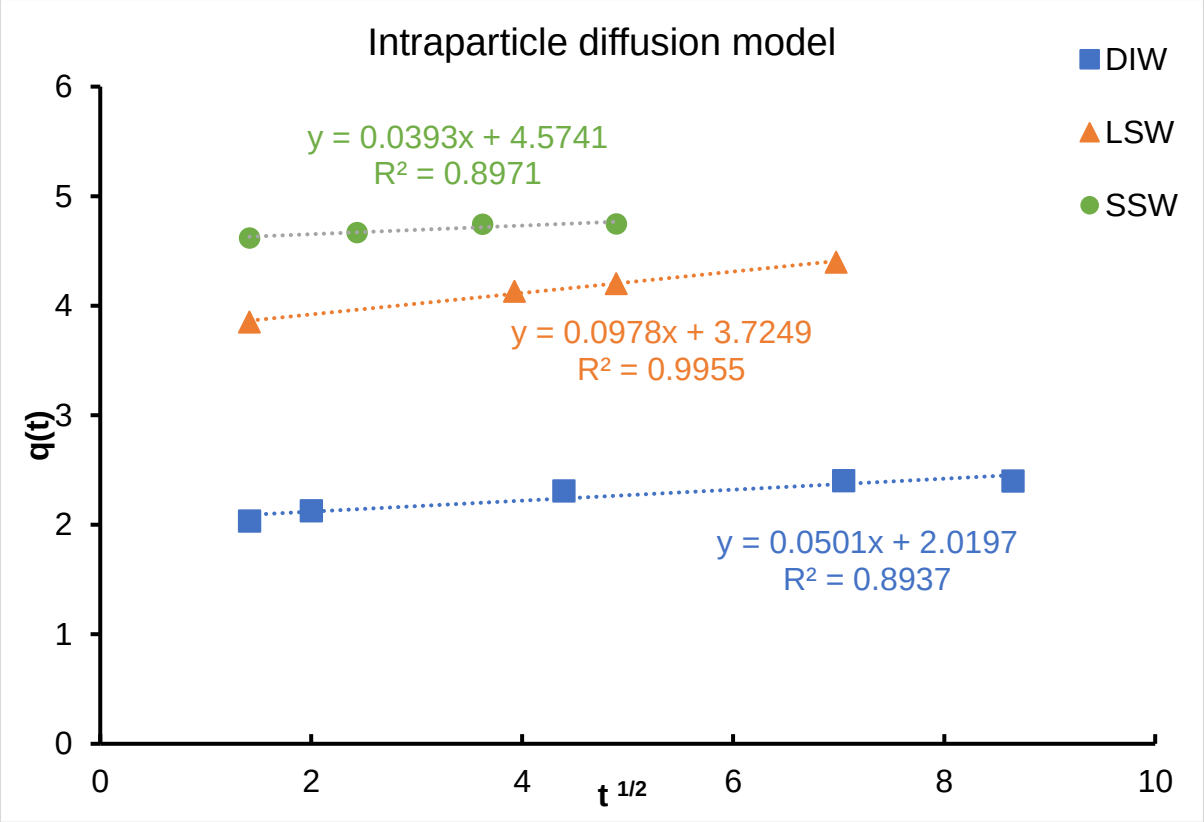

Figure 4.7: Intraparticle diffusion model for the adsorption experiments of NPs on Calcite in DIW, LSW and SSW.

4.1.1.2. PH measurement

First, the pH is measured for selected samples without NPs (Calcite + DIW, Calcite + LSW and Calcite + SSW) and plotted against mixing time of the sample as shown in Figure 4.8 and then the pH of the corresponding samples with NPs is measured (NP+ Calcite + DIW, NP + Calcite + LSW and NP+ Calcite + SSW) and plotted against mixing time as shown in Figure 4.9.

By looking to Figure 4.8, the pH values of DIW samples without NP are highest (about 9.6) and lowest for SSW samples without NP (about 7.5). The pH values for LSW samples without NP are between them and they are around 8.9. So, the pH value is decreased as the salinity (ionic strength) of the samples increased. Equation 4.7 presents the dissolution of Calcite. According to this equation, the dissolution of Calcite could increase the pH value of the samples.

$$CaCO_3(calcite) + H_2O \rightarrow Ca^{2+} + HCO_3^- + OH^- \quad (4.7)$$

Lower pH for SSW samples means that the dissolution of calcite in these samples are lower than LSW and DIW samples. The low dissolution of calcite in caused by the common ion effect. As mentioned previously the SSW brine includes originally some ions of Ca^{2+} and HCO_3^-. That's why the dissolution of calcite in SSW is lowest and this leads to increase the pH value just a little bit to around 7.5. On the other side, the dissolution of calcite is highest in

DIW because there are no common ions, and this leads to increase the pH to value of about 9.6. A small amount of Ca^{2+} and HCO_3^- ions in LSW samples leads to higher calcite dissolution in LSW samples than the SSW samples. This leads to increase pH values (to around 8.9) above the SSW and keep it below the DIW at the same time.

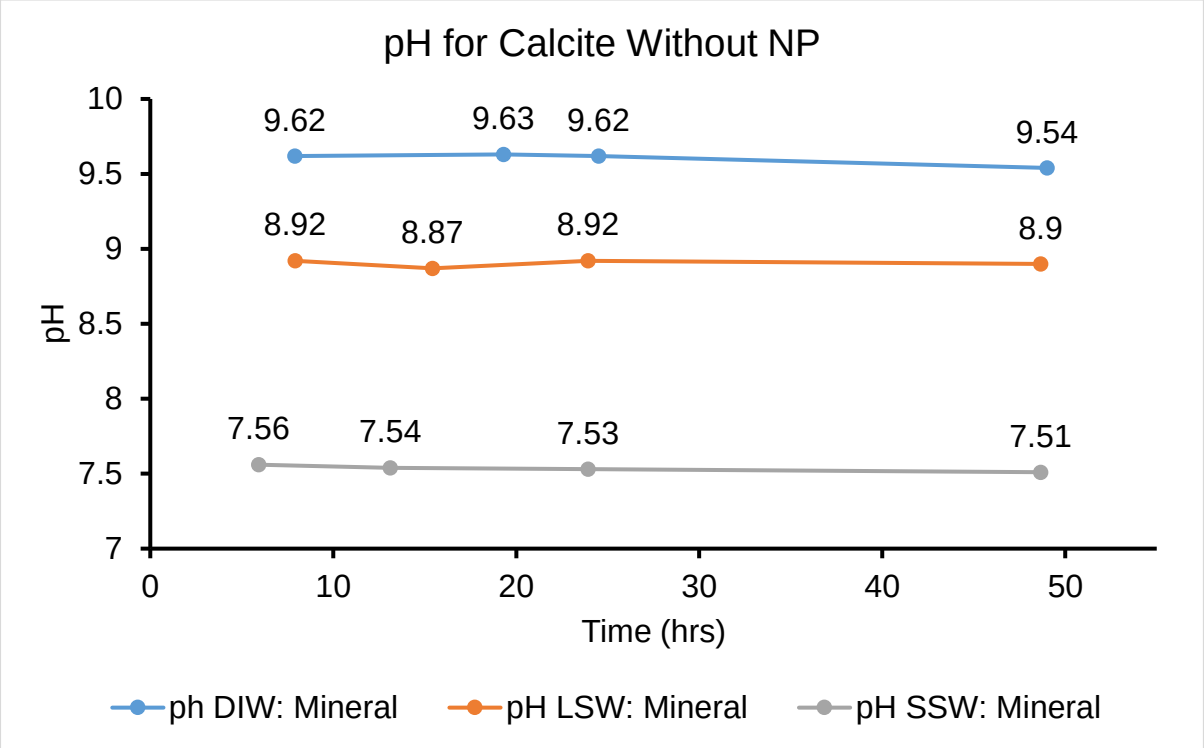

Figure 4.8: The pH measurements for the samples without NPs (Calcite in DIW, LSW and SSW).

Adding NPs to the samples reduce the pH values for all the samples as shown in Figure 4.9. The pH values of the corresponding samples with NPs in DIW is reduced from around 9.6 to around 9.15, but still shows the higher pH values compared to the samples with NP in LSW and SSW. The LSW samples is reduced from around 8.9 to around 8.77 and for SSW the reduction in pH value is not significant. The reduction in pH values may be explained by the ability of NPs to adsorb onto calcite surface and mitigate the calcite dissolution which leads to reduce the production of OH^- ions and reduce the pH.

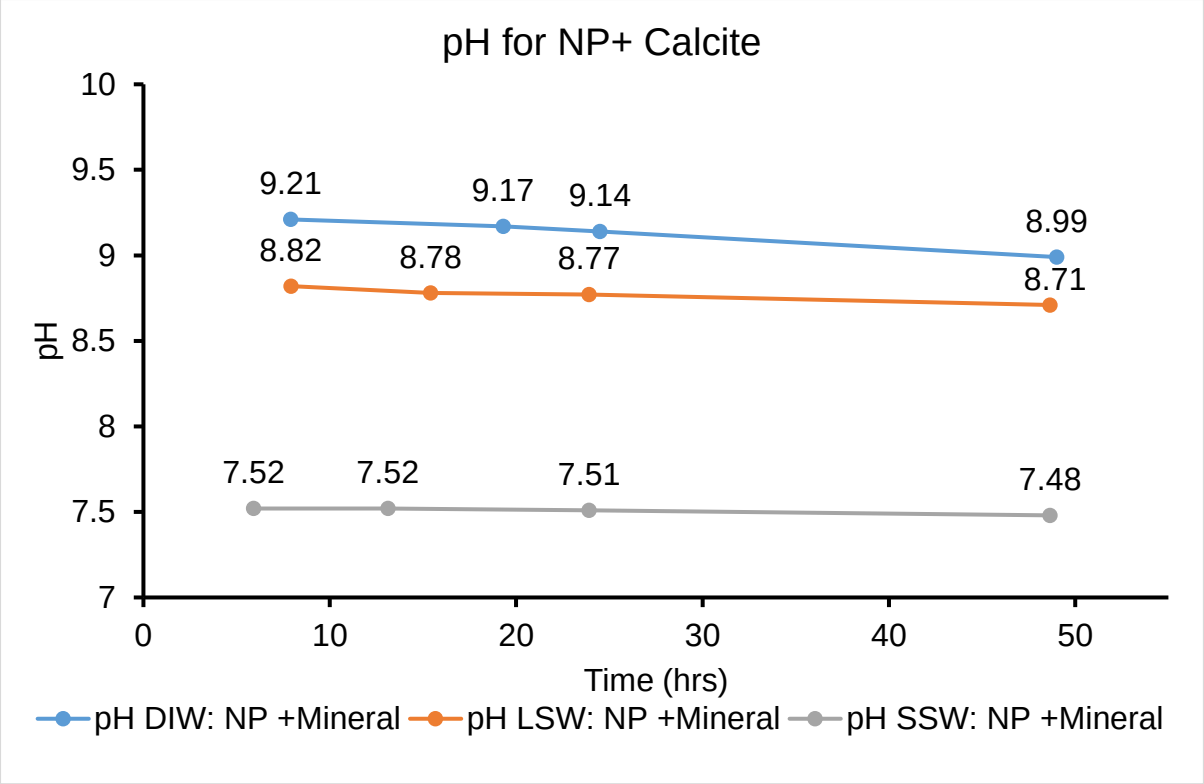

Figure 4.9: The pH measurements for the samples with NPs (Calcite + NP in DIW, LSW and SSW).

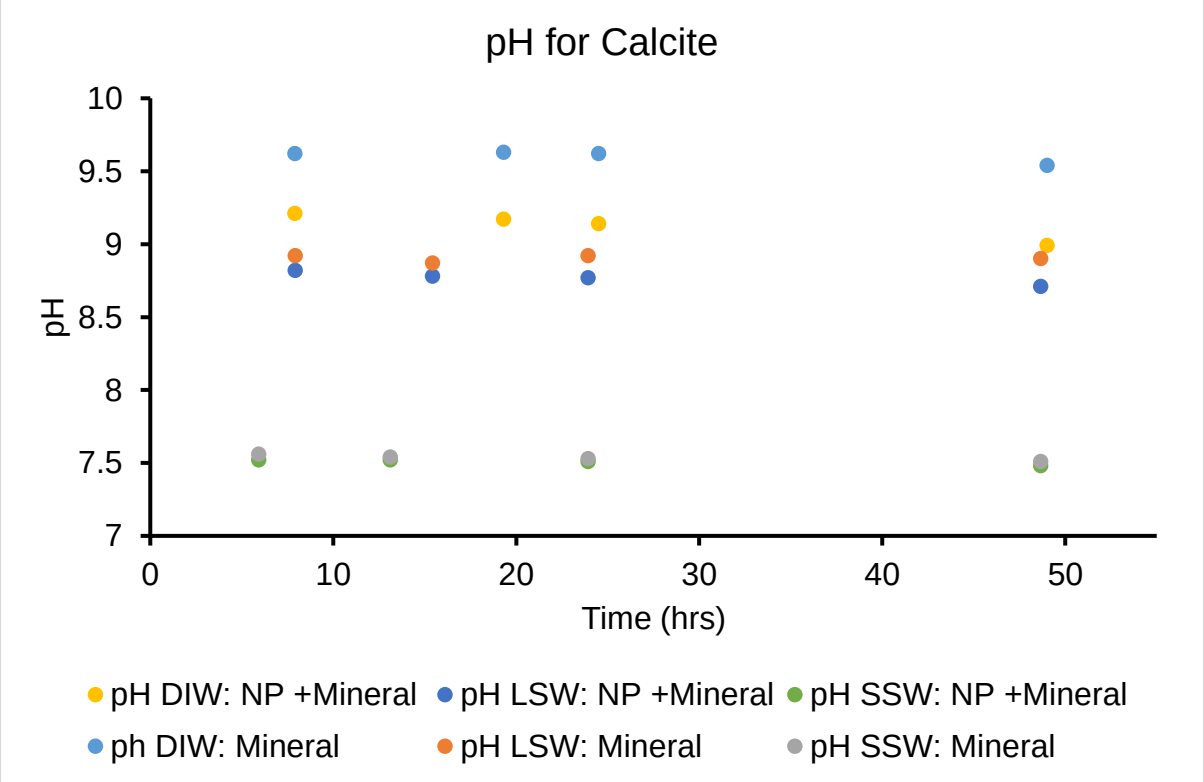

Figure 4.10: A comparison of pH values for the samples with and without NP for Calcite in DIW, LSW and SSW.

In Figure 4.10 the pH values for all the samples with and without NP are plotted together against mixing time to compare the difference in pH between them. Adding NPs to the DIW, prepared in LSW and SSW samples reduce their pH values. The highest reduction in pH values was observed for samples prepared in DIW, followed by LSW and SSW. This indicates that the reduction in pH increased with reduced salinity. In low salinity environments the dissolution of Calcite is increased which leads to increase the pH as mentioned before. The greatest effect of NP on Calcite dissolution is only observed in DIW and LSW (low salinity water). Adding NP could mitigate the calcite dissolution induced by low salinity water.

4.1.1.3. Ion chromatography (IC) measurement

The ion chromatography (IC) is measured for all the calcite samples with and without NP. This measurement is done to investigate the ions presented in the samples, their concentrations and the chemistry of ion exchange that happen in the samples. The most important ion to be investigated here is Ca^{2+} to study the dissolution of Calcite in these samples with and without NP in DIW, LSW and SSW. The chalk reservoirs consist mostly of Calcite and the dissolution of calcite may affect the rock integrity and reservoir subsidence in chalk reservoirs.

Figure 4.11 shows the result of IC measurement of Calcite in DIW, where a comparison between the Ca^{2+} concentration in the calcite samples with and without NP in DIW is presented. The Ca^{2+} concentration (mol/l) in the sample is plotted against mixing time for each sample. This figure shows that Ca^{2+} concentration in the samples with NPs are lower than samples without NPs. The Ca^{2+} concentration in the samples with NPs increased at the start and then the concentration is started to stabilize after 30 hours of mixing time. While the Ca^{2+} concentration in the samples without NPs is keep increasing with mixing time. This indicates that adding silica NPs to the samples reduces the dissolution of calcite. This observation may have implications for low salinity flooding. The effect of NPs on fluid mineral in saline environments is discussed in the following section.

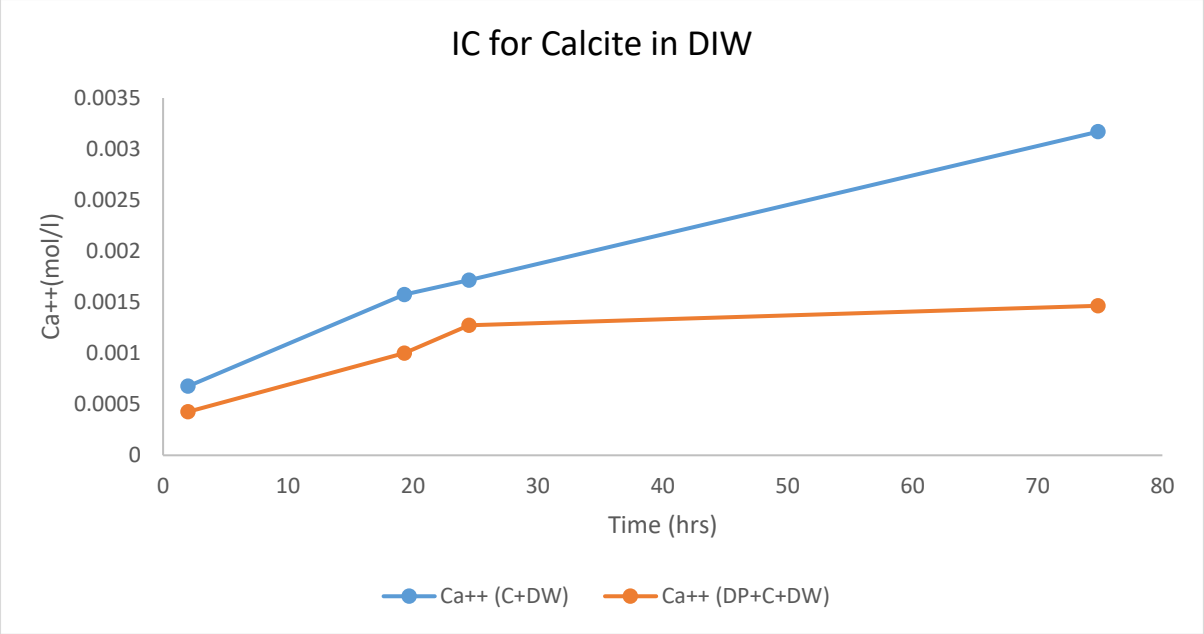

Figure 4.11:A comparison between the Ca^{2+}concentration (Mol/litre) in the calcite samples with and without NP in DIW.

The analysis of the IC measurement for the calcite samples prepared in LSW and SSW brines are more difficult than the samples prepared in DIW because of the presence of the Ca^{2+} ion and other ions initially in the brines. That is why the ions concentrations (Co) was normalized with respect to the initial ions concentrations in the brines (Ci).

Figures 4.12 and 4.13 show the result of IC measurement of Calcite in LSW, where comparisons of the Ca^{2+} and Mg^{2+} concentrations in the calcite samples with and without NP in LSW are presented. The Ca^{2+} concentration (Co/Ci) in the sample is plotted against mixing time for each selected sample (Figure 4.12). This figure shows that Ca^{2+} ion in the samples with NPs are lower than samples without NPs. This indicates that adding silica NPs to the samples prepared in LSW reduces the dissolution of calcite and this observation is supported also by lower pH values measured for the calcite samples with NPs prepared in LSW as shown in Figure 4.10.

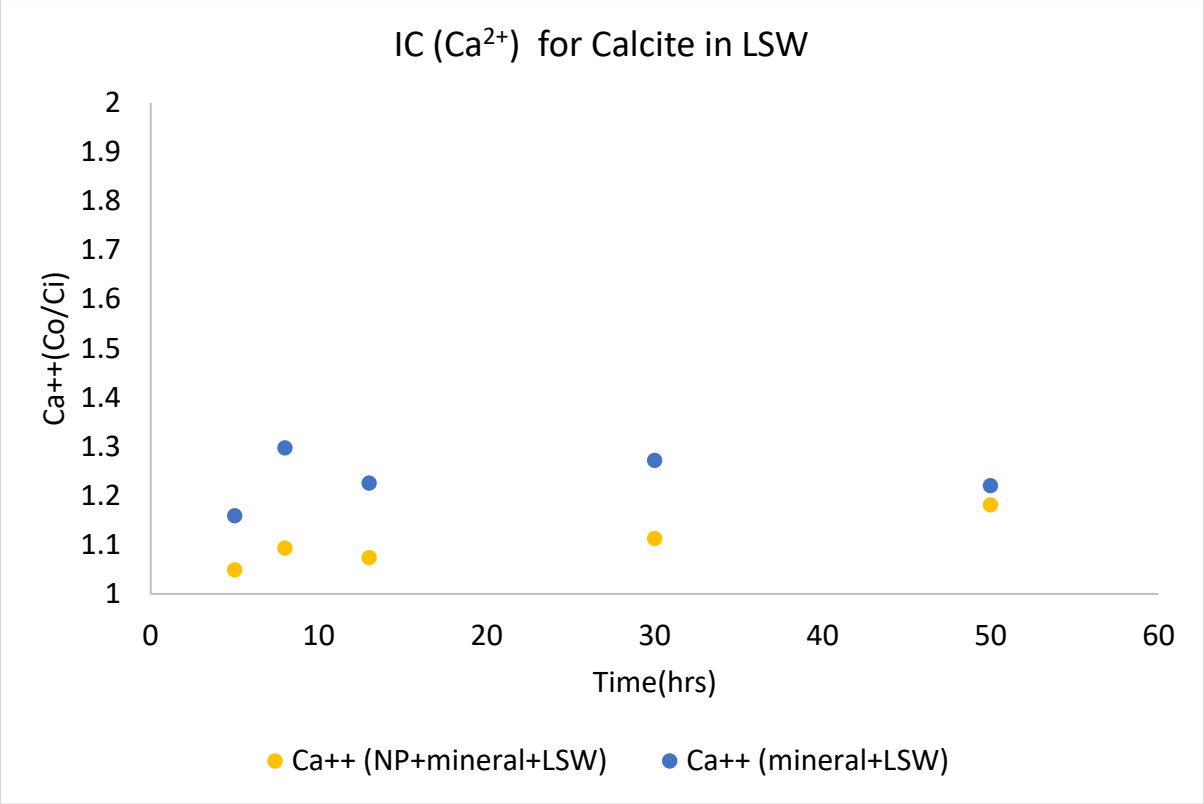

Figure 4.12: A comparison between the Ca^{2+} concentration (Co/Ci) in the calcite samples with and without NP in LSW.

In Figure 4.13 the Mg^{2+} concentration (Co/Ci) and sample is plotted against mixing time for each selected sample. This figure shows that Mg^{2+} ion concentration in the samples with NPs are higher than samples without NPs (except the last reading). This could be explained by comparing the Ca^{2+} and Mg^{2+} ions concentrations in Figure 4.12 and 4.13. These figures show that the increase of Ca^{2+} concentration in the samples without NPs corresponds to a reduction in Mg^{2+} concentration (lower than its initial concentration in LSW) in these samples. Which means that there is an ion exchange between calcite (Ca^{2+} ions) and magnesium ions (Mg^{2+}) initially in LSW. So, the Calcite tends to accommodate the Mg^{2+} ions instead for Ca^{2+} ions in its structure, (Stumm et al. 1970; Hamouda, Abhishek, and Ayoub 2018) have made the same conclusions. This exchange could lead to the formation of Dolomite as shown in Equation 4.8 (Hamouda, Abhishek, and Ayoub 2018; Petrovich and Hamouda 1998).

$$2CaCO_{3(s)} + Mg^{2+} \rightarrow CaMg(CO_3)_2 + Ca^{2+} \quad (4.8)$$

So, adding NPs to the samples reduce the dissolution of calcite (lower Ca^{2+}) according to Figure 4.12 and Equation 4.8. This leads to reduce the ion exchange between Ca^{2+} and Mg^{2+} and keep the amount of Mg^{2+} ion almost same as its initially amount in LSW brine as shown in Figure 4.13.

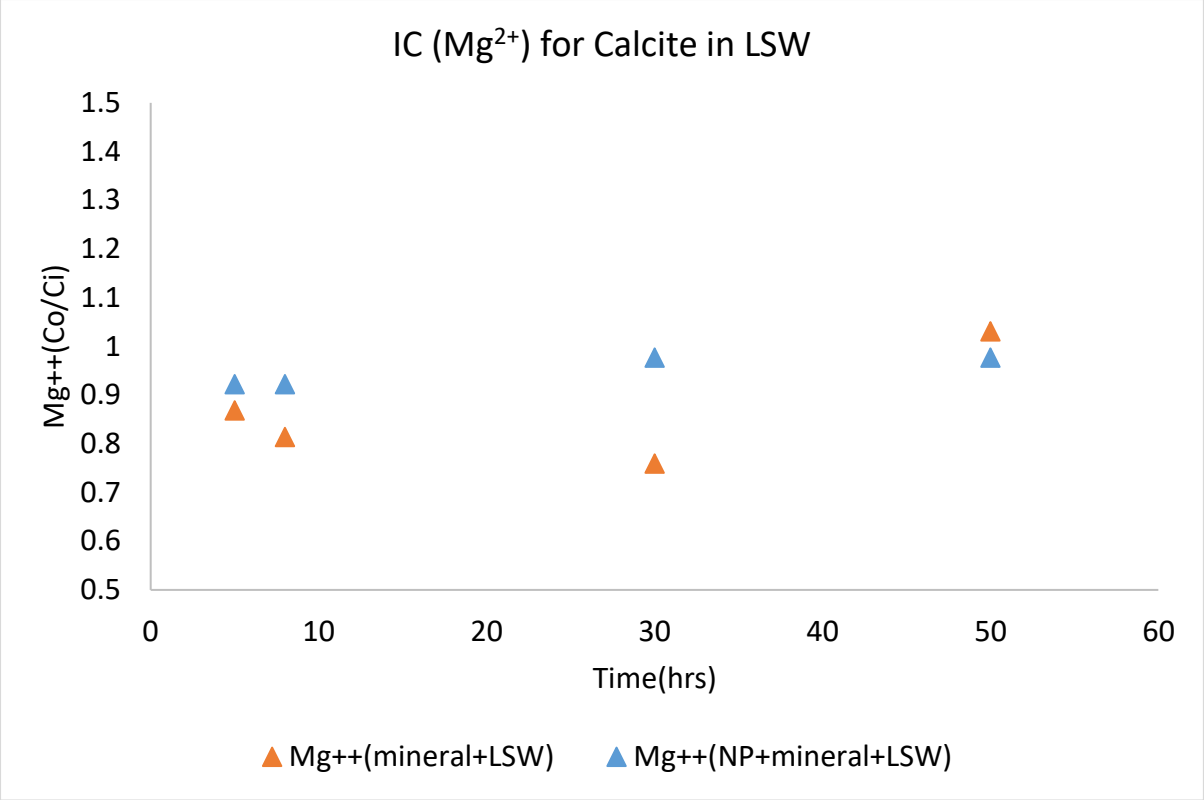

Figure 4.13: A comparison between the Mg^{2+}concentration (Co/Ci) in the calcite samples with and without NP in LSW.

Figures 4.14 and 4.15 show the result of IC measurement of Calcite in SSW, where comparisons of the Ca^{2+} and Mg^{2+} concentrations in the calcite samples with and without NP in SSW are presented. The Ca^{2+} concentration (Co/Ci) in the sample is plotted against mixing time for each selected sample (Figure 4.14). This figure shows that the concentration of Ca^{2+} in the samples with and without NPs is same for 0 to 8 hours of mixing. After 8 hours of mixing for both types of samples, the concentration of Ca^{2+} in the samples with NPs start to be lower than the samples without NPs. This may indicate that adding silica NPs to the samples prepared in SSW reduces the dissolution of calcite and this is the same observation made previously for samples prepared in LSW and DIW. The difference in SSW samples that the dissolution of Calcite is relatively lower than in LSW and DIW as mentioned previously and the Ca^{2+} concentration for all the samples are lower than its initial concentration in SSW brine. This indicates that the Ca^{2+} ions participate in some others chemical reactions more work is ongoing to better analyse this behaviour.

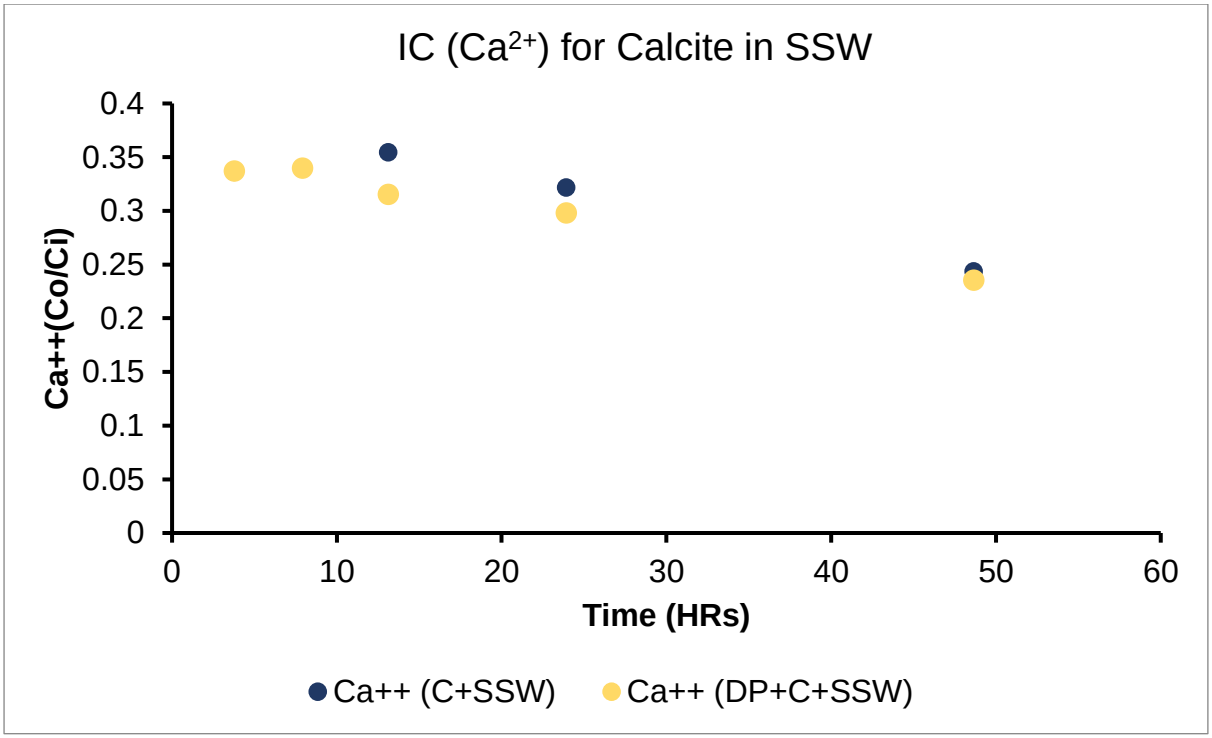

Figure 4.14: A comparison between the Ca^{2+}concentration (Co/Ci) in the calcite samples with and without NP in SSW.

In Figure 4.15 the Mg^{2+} concentration (Co/Ci) and in the sample is plotted against mixing time for each selected sample. From the start of mixing until 15 hours Figure 4.15 shows that Mg^{2+} ion concentration in the samples without NPs are higher than samples with NPs. After about 15 hours of mixing the Mg^{2+} ion concentration in all the samples is reduced, but the samples with NPs at this time has a little bit higher Mg^{2+} ion concentration than samples without NPs. Notice that the concentration Mg^{2+} during whole the adsorption process in SSW is higher than its initial value in SSW brine. Comparing Figure 4.14 and 4.15 show that there is a significant reduction in Ca^{2+} and increase in Mg^{2+} concentration. Which indicates that the dissolution of Calcite in SSW is low, and this observation is also supported by the pH values presented in Figure 4.10. In addition, e that the Ca^{2+} and Mg^{2+} ions participate in some others chemical reactions that release more Mg^{2+} ions and capture Ca^{2+} ions simultaneously and these reactions had the significance effect on the IC results for the SSW samples. This part needs further investigation.

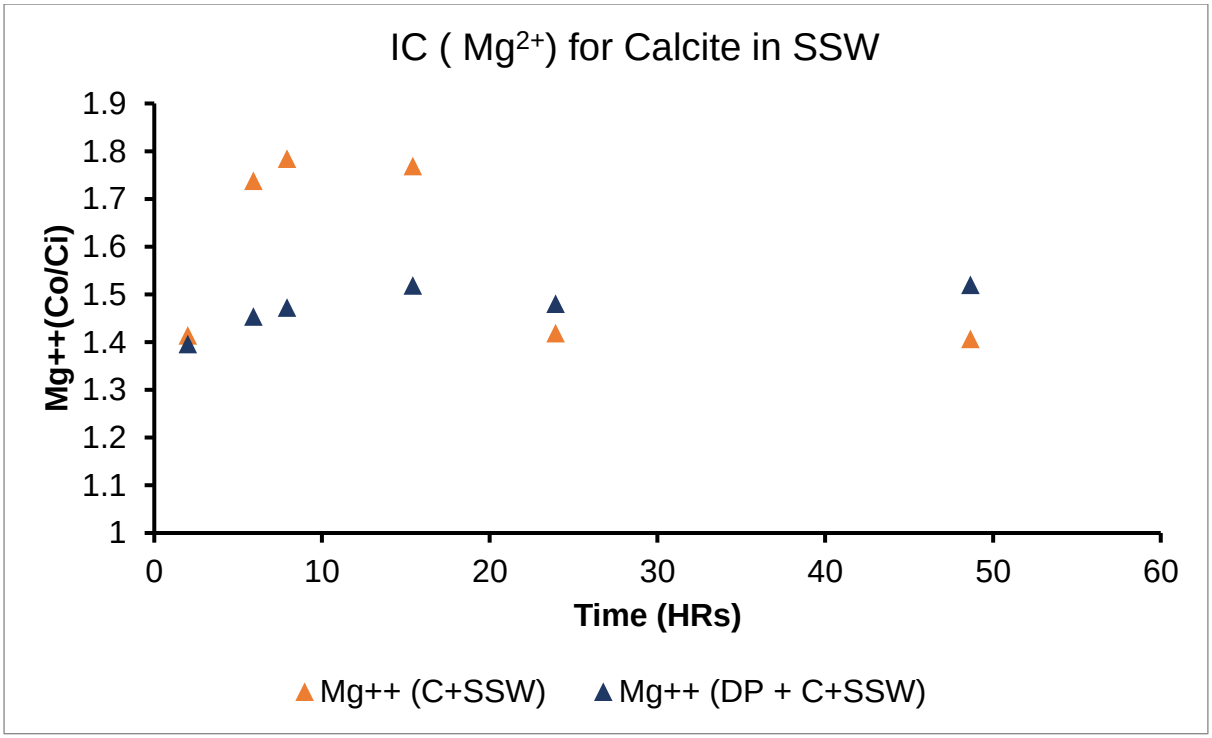

Figure 4.15: A comparison between the Mg^{2+}concentration (Co/Ci) in the calcite samples with and without NP in SSW.

4.1.2. Quartz

4.1.2.1. NPs adsorption on quartz

The nanoparticles (NPs) kinetic adsorption on quartz is investigated by adding 5 grams of quartz to 30 ml of three different fluids with nanoparticles (DP in DIW, DP in LSW and DP in SSW). After the specified mixing time for each sample, their Abs values are measured and their adsorption on quartz surface are calculated by using the calibration curves (Figure 3.1), the Abs readings and the equations (3.4 - 3.9). The Abs correction for the NPs samples (the baseline correction) is done by preparing the same samples in similar manner, but without NPs and their Abs values are measured and subtracted from the Abs values for NPs samples.

The results of the adsorption of NPs on Calcite (mg of NP /g of quartz) in DIW are plotted against the specified mixing time for the samples (interaction time between nanofluid and quartz) in hours (Figure 4.16). From Figure 4.16, the adsorption of NPs on quartz in DIW is increasing with the mixing time. As shown in this Figure, the NPs adsorption process did not reach the equilibrium (maximum adsorption of NPs on quartz). The slope of the adsorption curve starts to decrease after about 20 hours of mixing or in other words 20 hours of interaction between the nanoparticles and quartz in DIW. The maximum adsorption amount of NP on quartz in DIW was about 1.53 (mg/g) and reached after about 72 hours of mixing.

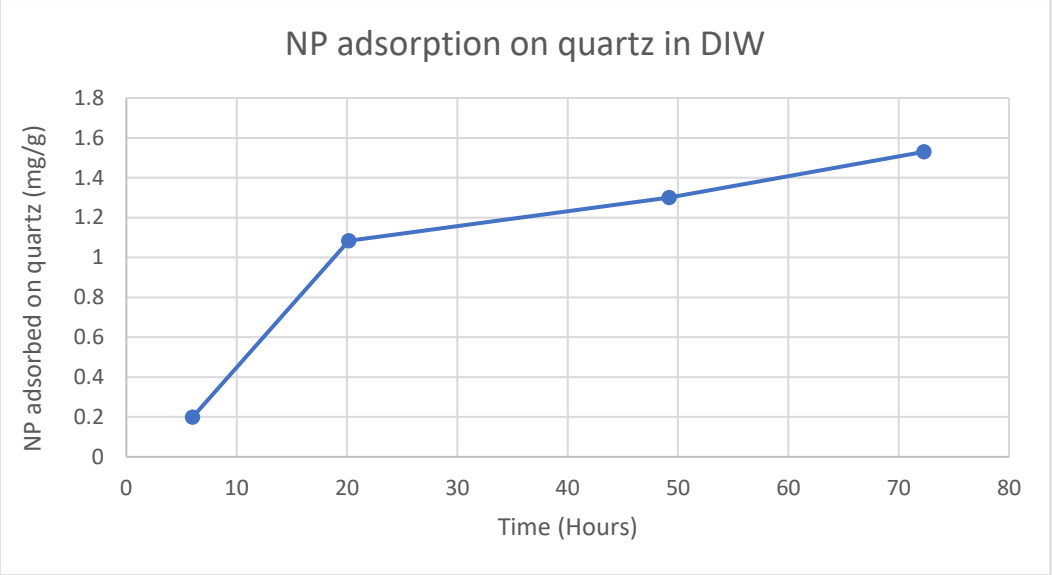

Figure 4.16: NPs adsorption on quartz in DIW.

Figure 4.17 shows the results of the adsorption of NPs on quartz in LSW. By looking to this figure, the adsorption of NP is increased with time and did not reach the equilibrium. The slope of the adsorption curve starts to decrease after about 24 hours of mixing and starts to increase again after about 41 hours. The maximum adsorption amount of NP on quartz in LSW was about 1.47 (mg/g) and reached after about 49 hours of mixing.

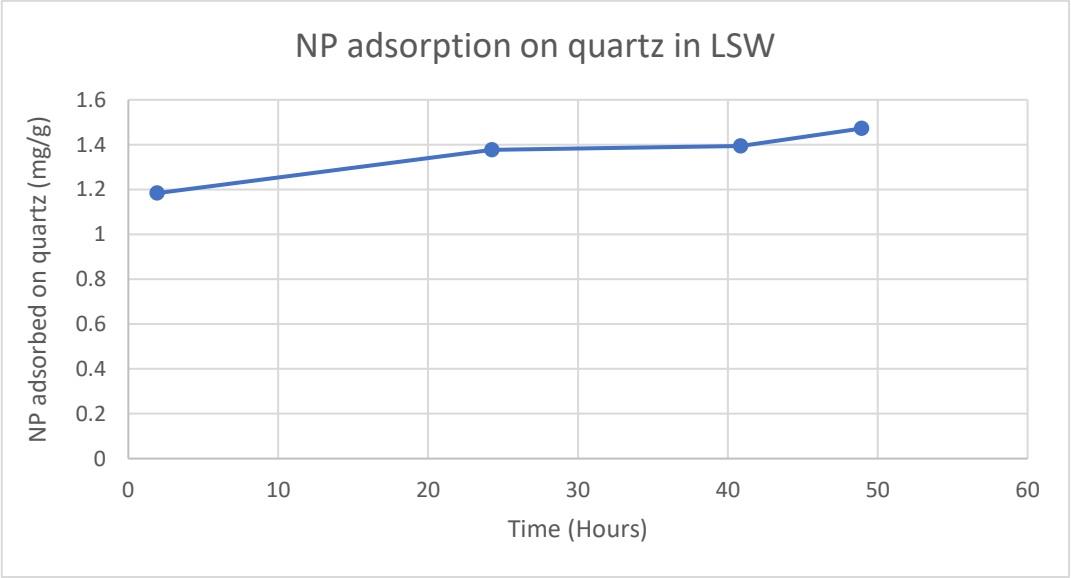

Figure 4.17: NPs adsorption on quartz in LSW.

The results of NP adsorption on Calcite in SSW are shown in Figure 4.18. The adsorption of NP on quartz is increased with time and reached the equilibrium after around 48 hours. The maximum amount of NP adsorbed on quartz in SSW after 72 hours was about 1.73 (mg/g).

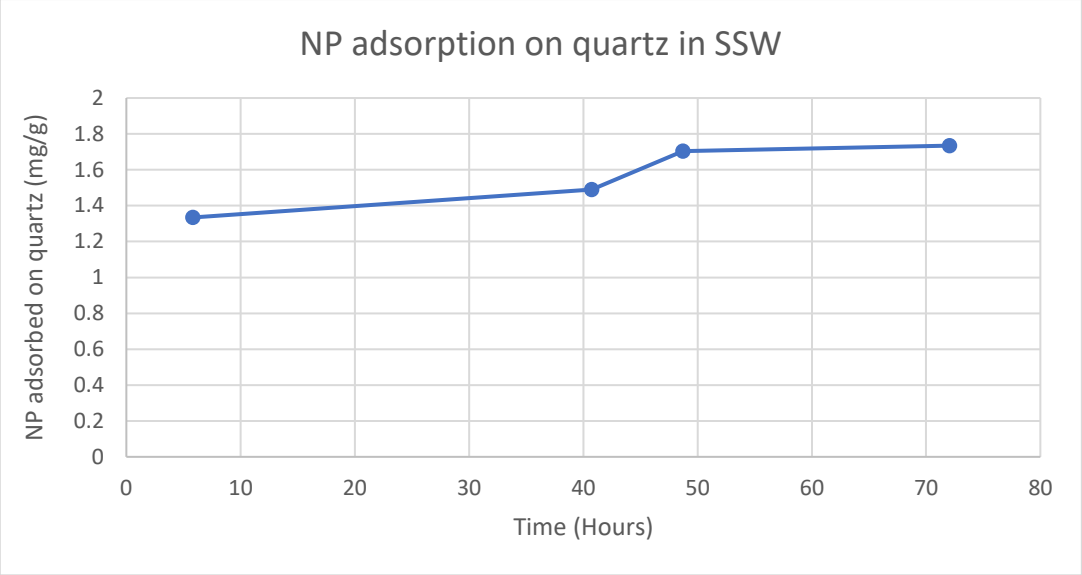

Figure 4.18: NPs adsorption on quartz in SSW.

The results of NP adsorption on quartz in DIW, LSW and SSW are plotted together against the mixing time in Figure 4.19. This figure show that the highest adsorption of NP on quartz is reached in SSW and the lowest in the DIW. This result has the same tendency that observed in the result of NP adsorption on Calcite, but with lower adsorption values for all types of samples as shown in capital 4.1.1. This indicates that increasing the salinity (ionic strength) of the fluid leads to increase the adsorption of nanoparticles on quartz. Increasing the ionic strength of the solution leads to reduce the absolute value of zeta potential for NP and quartz. This happening because increasing the ionic strength leads to compression of the double layer and this leads to reduction of the electrostatic repulsion between the quartz and NP which means that the adsorption of NP on quartz surface is enhanced as showing in Figure 4.19, (Dehghan Monfared et al. 2015; Abdelfatah et al. 2017; Mondragon et al. 2012) have made the same conclusion. The adsorption of NPs on quartz surface is lower than the adsorption on Calcite because of the higher negative zeta potential values measured for quartz than calcite during previous lab work done by (Murzin 2017; Ayoub 2017).

Table 4.6, the detailed information of NPs adsorption on quartz in DIW, LSW and SSW is presented.

Table 4.6: NPs adsorption on quartz in DIW, LSW and SSW.

DIW		LSW		SSW	
Time (Hours)	Adsorption (mg/g)	Time (Hours)	Adsorption (mg/g)	Time (Hours)	Adsorption (mg/g)
6	0.2	1.92	1.18	5.83	1.33
20.17	1.08	24.26	1.38	40.75	1.49
49.22	1.30	40.85	1.39	48.73	1.70
72.28	1.53	48.93	1.47	72.06	1.73

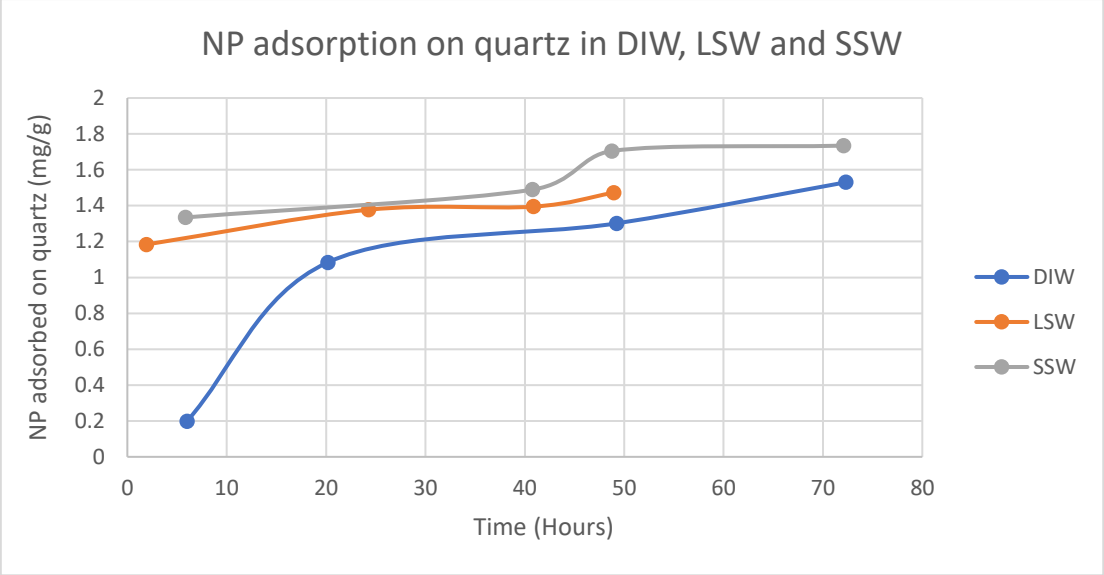

Figure 4.19: NPs adsorption on quartz in DIW, LSW and SSW.

To analyse the kinetic adsorption behaviour of nanoparticles on quartz in DIW, LSW and SSW and its adsorption mechanism, three common kinetic models are investigated. These kinetics models are: pseudo-first order model, pseudo-second order model and Intraparticle diffusion model. The investigation is done in the same way that done for NP adsorption on Calcite.

The first model was investigated to fit the adsorption model of NP with quartz is the pseudo-first order model. As mentioned previously Equation 4.1 is used to plot the adsorption data.

Figure 4.20 shows the description of kinetic adsorption of NPs onto quartz in DIW, LSW and SSW using the pseudo-first order kinetic model. $\ln(q_e(\exp) - q(t))$ is plotted against time for all the three fluids. The q_e (exp) are expected to be 1.6, 1.5, 1.8 (mg/g) for DIW, LSW and SSW respectively, depending on the result presented in Figure 4.19 and Table 4.6. The trendline's equations in Figure 4.20 are used to obtain the K_1 and the q_e (est). K_1 and the q_e (est) are calculated in the same way as done for Calcite experiments and the results are presented together with the correlation coefficient (R^2) in Table 4.7. The best fit is reported for the adsorption of NPs onto quartz in DIW. The constant rate (K_1) show much faster adsorption of NPs on quartz surface in LSW followed by DIW and SSW.

Table 4.7: Estimated parameters of Pseudo-first order kinetic model for quartz.

DIW			LSW			SSW		
K_1 (1/h)	q_e(est) (mg/g)	R^2	K_1 (1/h)	qe(est) (mg/g)	R^2	K_1 (1/h)	q_e(est) (mg/g)	R^2
0.041	1.595	0.9471	0.1149	1.093	0.9025	0.0346	1.459	0.9388

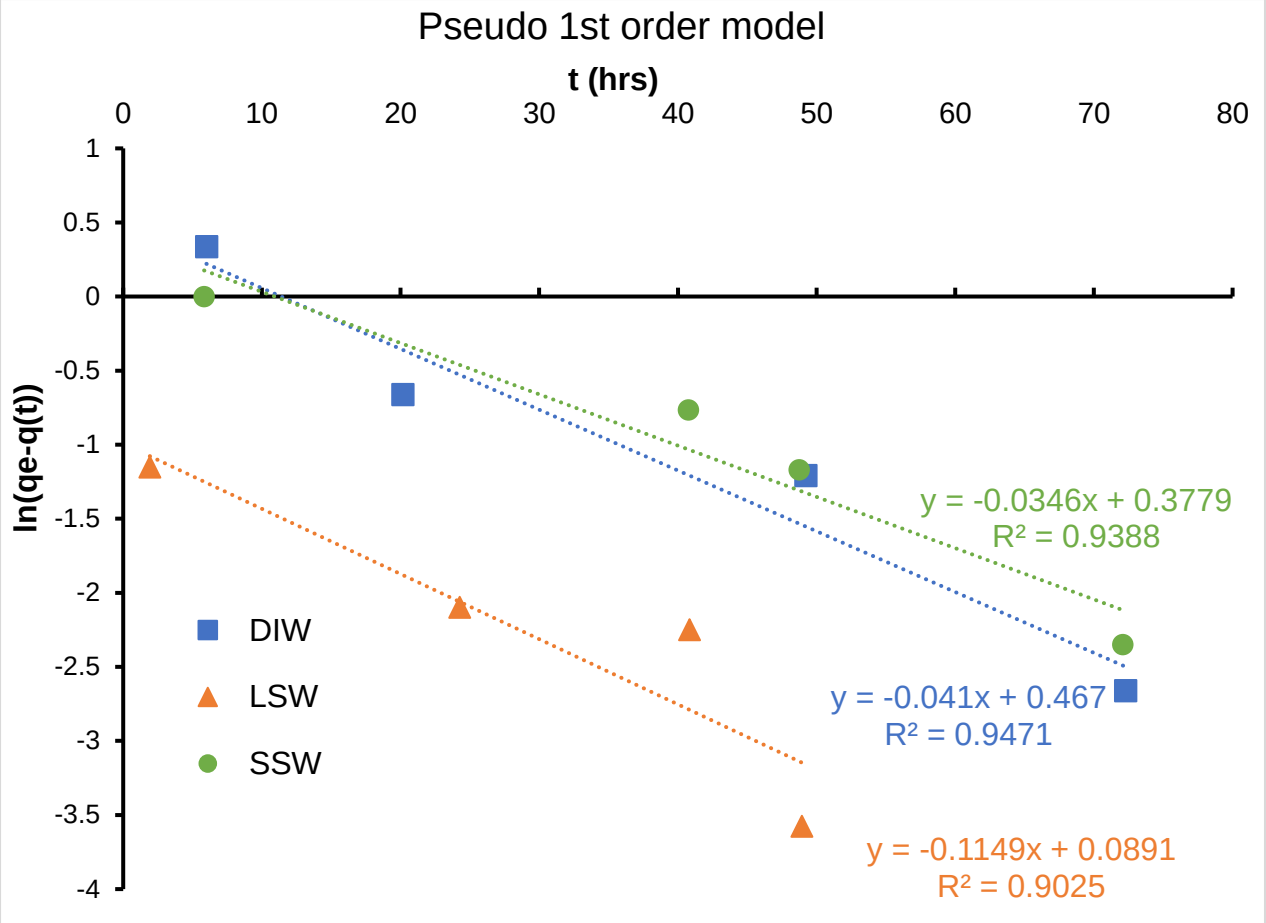

Figure 4.20: Pseudo-first order kinetic model for the adsorption experiments of NPs on quartz in DIW, LSW and SSW.

The second model was investigated to fit the adsorption model of NP with quartz is the pseudo-second order model. As mentioned previously Equation 4.3 is used to plot the adsorption data.

Figure 4.21 shows the description of kinetic adsorption of NPs onto quartz in DIW, LSW and SSW using the pseudo-second order kinetic model. t/q(t) is plotted against time for all the three fluids. The trendline's equations in Figure 4.21 are used to obtain the K_2 and the q_e (est). K_2 and the q_e (est) are calculated in the same way as done for Calcite experiments and the results are presented together with the correlation coefficient (R^2) in Table 4.8. Except for LSW samples, it was impossible to estimate the parameters. The best fit is reported for the adsorption of NPs onto quartz in SSW. The constant rate (K_2) show much faster adsorption of NPs on quartz surface in SSW than DIW.

Table 4.8: Estimated parameters of Pseudo-second order kinetic model for quartz.

DIW			LSW			SSW		
K_2 (g/mg*h)	q_e(est) (mg/g)	R^2	K_2 (g/mg*h)	q_e(est) (mg/g)	R^2	K_2 (g/mg*h)	q_e(est) (mg/g)	R^2
0.0007	57.471	0.782	-	-	-	0.154	1.785	0.9883

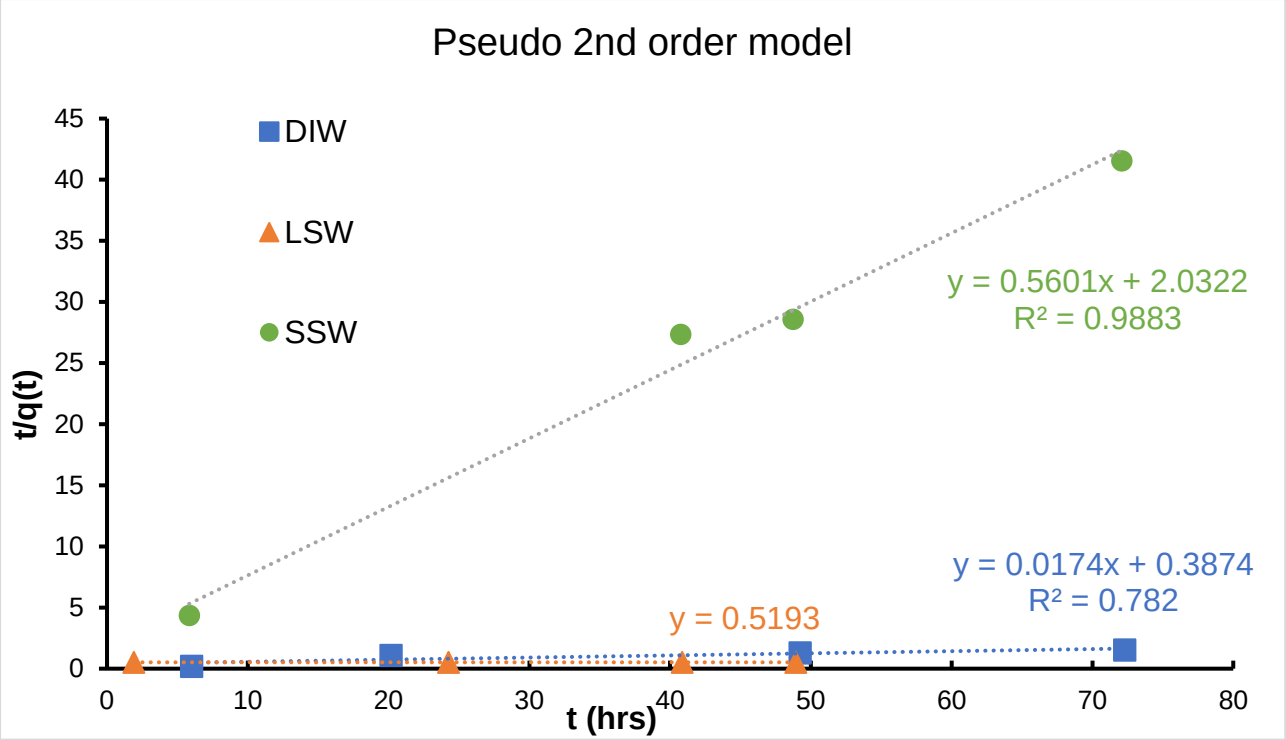

Figure 4.21: Pseudo-second order kinetic model for the adsorption experiments of NPs on quartz in DIW, LSW and SSW.

Table 4.9 shows a comparison between the pseudo first and second order model. It is clear from this table that the NPs adsorption on quartz did not follow the pseudo-second order. According to values presented in Table 4.9, the NPs adsorption on quartz in DIW, LSW and SSW is followed the pseudo-first order kinetic model. Which means pseudo-first order is more suitable model to describe the kinetic behaviour of the adsorption process of NPs on quartz.

Table 4.9: A comparison between Pseudo first and second order model for quartz.

Pseudo-first order						Pseudo-second order					
DIW		LSW		SSW		DIW		LSW		SSW	
R^2	$q_e(exp) - q_e(est)$ (mg/g)	R^2	qe(exp) - qe(est) (mg/g)	R^2	qe(exp) - qe(est) (mg/g)	R^2	qe(exp) - qe(est) (mg/g)	R^2	qe(exp) - qe(est) (mg/g)	R^2	qe(exp) - qe(est) (mg/g)
0.9471	0.005	0.9025	0.407	0.9388	0.341	0.782	-55.87	-	-	0.9883	0.015

According to the pseudo-first order model, the adsorption capacity of quartz or in other word the amount of nanoparticle adsorbed at equilibrium estimated from the model (qe (est)) is highest for the DIW samples followed by SSW and LSW as showing in Table 4.7. The results of adsorption capacity reached by the experiments are different according to Table 4.6. The adsorption experiments show that the adsorption capacity of quartz is highest for SSW followed by DIW and LSW. This could be explained by, although the NP adsorption on quartz are more fit for pseudo-first order, but R^2 and (qe(exp) - qe(est)) values are still not good enough to make this kinetic model an appropriate model to describe the adsorption process. The conclusion is that the both kinetic models (pseudo-first and second order) are not appropriate to describe the kinetic behaviour of the adsorption on quartz in DIW, LSW and SSW.

Finally, the intraparticle diffusion model is used to understand the adsorption mechanism. Equation 4.6 that mentioned previously in Calcite section, is used to describe the adsorption mechanism of NPs on quartz.

To determine the intraparticle diffusion model's parameters (k_i and C_i) for DIW, LSW and SSW, q(t) is plotted against time ($t^{0.5}$) for all these three types of fluids as shown in Figure 4.22. the trendline's equations shown in Figure 4.22 are used to determine the parameters k_i and C_i.

By looking to Figure 4.22 and Table 4.10, the R^2 values for intraparticle diffusion model are relatively high (except for SSW). The best fit is reported for the adsorption of NPs onto quartz in DIW. Table 4.10 shows the values of intraparticle diffusion model's parameters and the values of correlation coefficient (R^2).

As mentioned previously that there are three steps to describe the adsorption mechanisms. These steps are: film diffusion, Intraparticle diffusion and the adsorbate adsorbed at a site on the adsorbent external/internal surface. The Intraparticle diffusion model in Figure 4.22 is used to find the rate controlling mechanism for the adsorption process of NPs onto quartz surface in DIW, LSW and SSW. When the plot is linear and passes through the origin, the intraparticle diffusion is the sole rate controlling mechanism (Ho 2003) . If the plot was only linear and didn't pass through origin, means that the mechanism of intraparticle diffusion is contributed in the adsorption process, but it was not the only the mechanism that contributed in the adsorption process (Dehghan Monfared et al. 2015).

By looking to Figure 4.22, the three plots for DIW, LSW and SSW were linear and didn't pass through the origin. This means that the intraparticle diffusion was not the only rate controlling mechanism and the film (boundary layer) diffusion mechanism had some effect on the adsorption process of NPs onto quartz surface in DIW, LSW and SSW. This is the same observation made for the NPs adsorption onto Calcite surface.

Table 4.10: Estimated parameters and correlation coefficient (R^2) of intraparticle diffusion model for quartz.

DIW			LSW			SSW		
K_i (mg/g*$h^{0.5}$)	Ci (mg/g)	R^2	K_i (mg/g*$h^{0.5}$)	Ci (mg/g)	R^2	K_i (mg/g*$h^{0.5}$)	Ci (mg/g)	R^2
0.1086	0.5808	0.9737	0.0478	1.1215	0.9613	0.0674	1.1569	0.8529

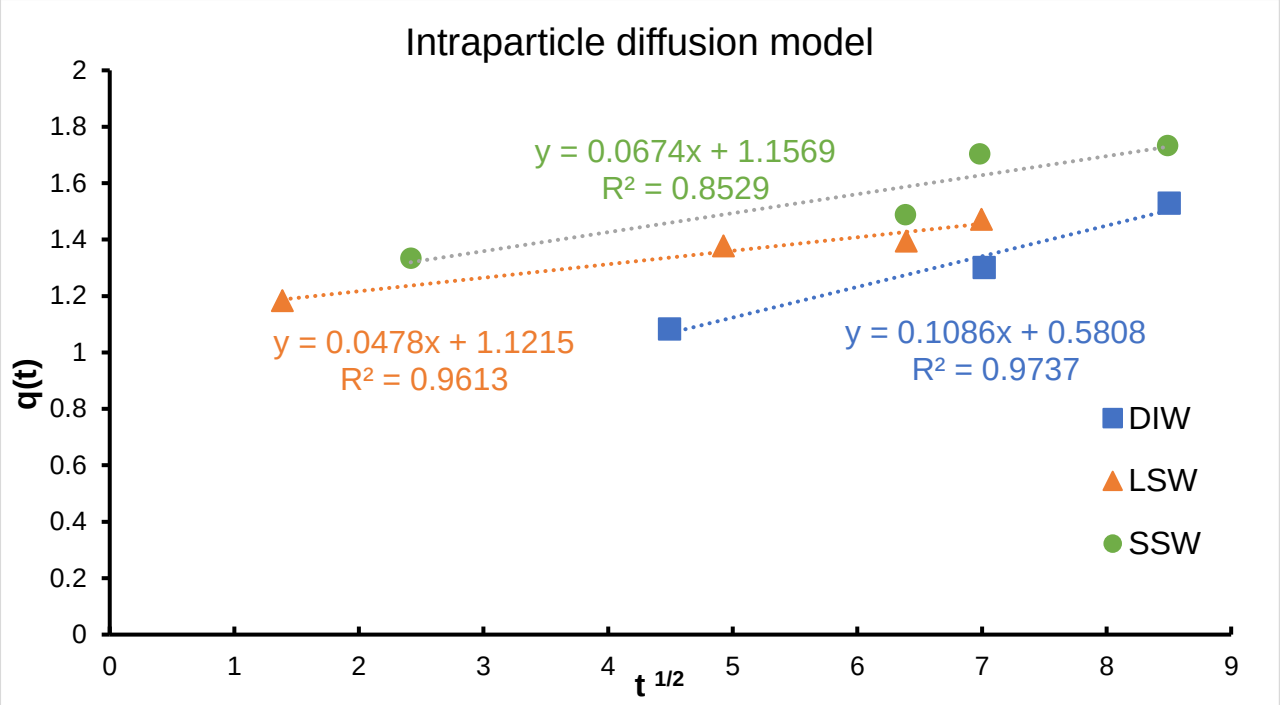

Figure 4.22: Intraparticle diffusion model for the adsorption experiments of NPs on quartz in DIW, LSW and SSW.

4.2. Transport Behaviour of NPs in porous media

In this part of results, the transport behaviour of nanoparticles in Chalk and Berea was investigated by running two core floods, one with Chalk and one with Berea. SSW is injected during the pre-flush and post -flush for both floods. After the pre-flush a nanofluid slug with tracer (1 g/l DP + 0.1M LiCl +SSW) is injected during the Berea and Chalk core floods. As mentioned before DP stands for nanofluid (DP 9711) used during these experiments. Then the absorbance and NPs adsorption on Chalk and Berea surfaces is investigated by using the UV-machine. In addition, the pH and cation concentrations are measured for the effluents collected from the Chalk and Berea floods.

4.2.1. Core flood with Chalk

Chalk core flood experiment is run at injection rate of 10 PV/day or 0.16 ml/min. 7 PV of SSW brine is injected during the pre-flush stage. After that 1.5 PV of nanofluid (DP) slug with tracer (1 g/l DP + 0.1M LiCl +SSW) is injected. Then 7 PV of SSW injected during the post flush stage.

The absorbance (Abs) and pH values of produced effluent samples are measured. The absorbance values are utilized to calculate the NP concentration in the produced effluent samples. Equations (3.11 – 3.15) and the calibration curve shown in Figure 3.3 are used to calculate NP concentration (g/l), total of NPs produced and injected (g) and the amount of NP adsorbed on chalk surface (%) as shown in Table 4.11.

The NP and tracer (Li^+) concentration (g/l) of effluent samples are plotted against pore volume (PV) produced in Figure 4.23. The NP and tracer slug (DP-slug) is injected after PV 7 and stopped at PV 8.5. NP production in the effluent started at PV 8.25 and stopped at PV 9.75. While the production of the unreacted tracer (Li^+) is started at PV 7.5 and stopped at PV 10.75 as shown in Figure 4.23. So, NP production (Breakthrough) is started about 0.75 PV after the Li^+ and stopped about 1 PV before the Li^+. In other words, NP and Li^+ concentration profiles are close to each other.

According to the calculations shown in Table 4.11, only 13.82 % of injected NPs were produced and 86.18 % of injected NPs were adsorbed on the surface of Chalk core. This indicate high adsorption of NPs on Chalk surface in high salinity environments (in SSW). Similar observation was reported previously during the kinetic adsorption experiments in SSW on Calcite. In addition, NP production stopped after the tracer (Li^+) has passed through the core. These observations may indicate that the NPs adsorption on Chalk surface in high salinity environment is a strong irreversible adsorption.

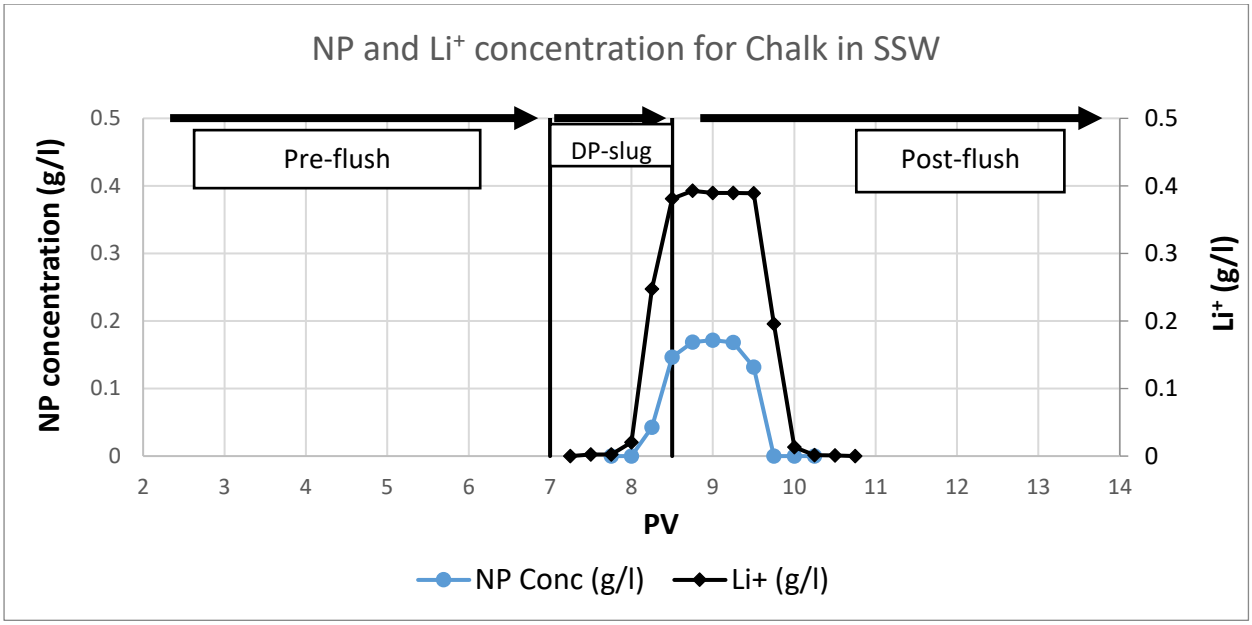

Figure 4.23: NP and Li^+ concentration (g/l) vs. pore volume (PV) produced for Chalk core flood with SSW.

Table 4.11: Calculation of NP concentration, injection production and adsorption based on equations 3.11- 3.15.

PV produced	NP concentration (g/l)	Sample volume (L)	NP produced (g)
8	0	0.00565	0
8.25	0.043	0.00565	0.000241
8.5	0.146	0.00565	0.000827
8.75	0.169	0.00565	0.000955
9	0.172	0.00565	0.00097
9.25	0.168	0.00565	0.00095
9.5	0.132	0.00565	0.000744
9.75	0	0.00565	0
		Total NP produced (g)	0.004687
		Total NP injected (g)	0.033915
		NP adsorbed (%)	86.18
		NP produced (%)	13.82

The pH values of produced effluents and injected fluids are presented in Figure 4.24. The pH values of produced effluent samples are almost constant which indicates that the injected fluid and chalk surface are almost at equilibrium at high salinity environment.

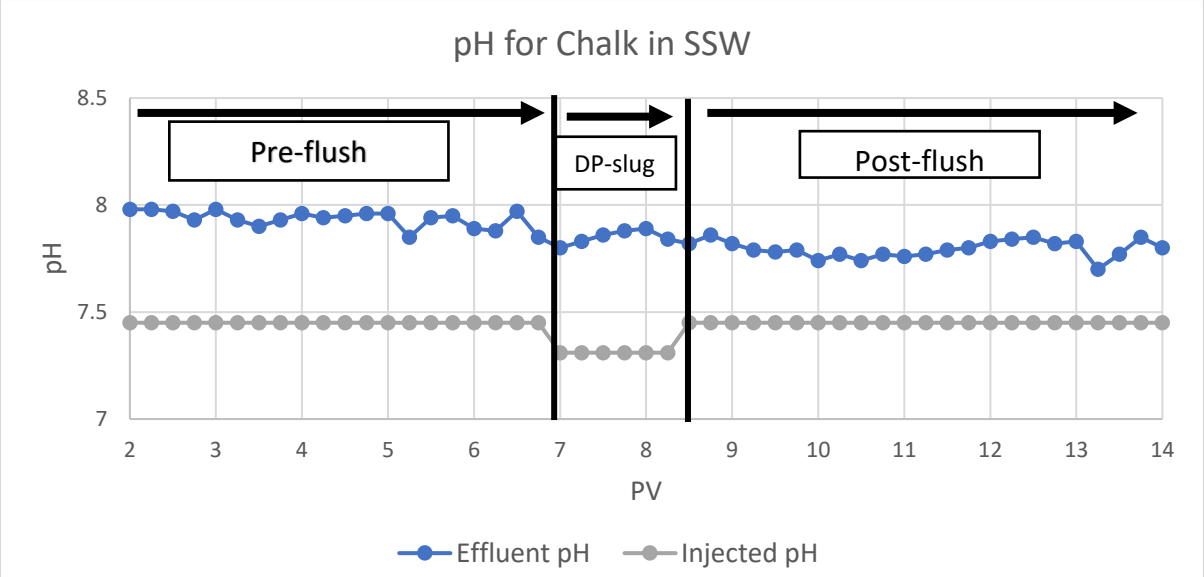

Figure 4.24: The pH values of injected fluid and produced effluents vs. pore volume (PV) produced for Chalk core flood with SSW.

The ion concentration (g/l) of Ca^{2+} and Mg^{2+} in the effluent are plotted against PV in Figure 4.25. The ion concentration (g/l) of Ca^{2+} and Mg^{2+} are almost constant and equal to 0.5 and 1.1 (g/l) respectively, during the whole flooding process. This means that the ion concentration of Ca^{2+} and Mg^{2+} in the produced effluents samples and injected fluid are almost same. This observation is supported by the constant pH values of effluents presented in Figure 4.24. The pH and ion concentration results confirm that there is an equilibrium state between injected fluid and chalk surface in high salinity environments. This leads to have low ionic activity during the flood because of low chemical interaction between the injected fluid and Chalk surface in SSW.

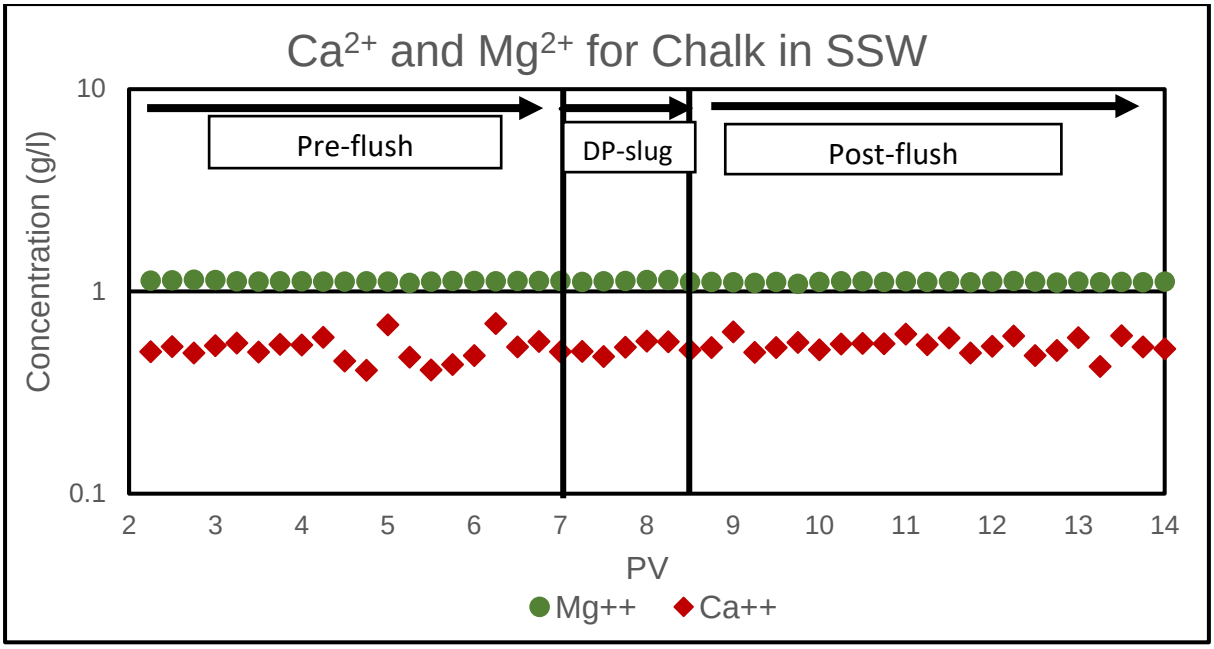

Figure 4.25: Ca^{2+} and Mg^{2+} concentrations (g/l) of produced effluent vs. PV for Chalk core flood with SSW.

The results of Chalk core flood in SSW are compared with the results obtained from previous core flood experiments done on Chalk in LSW. This work is done by (Hamouda, Abhishek, and Ayoub 2018) and its results presented in Figure 4.26,4.27 and 4.28. LSW is injected during the pre and post-flush stages and the nanofluid slug with tracer are prepared in LSW the salinity of LSW are 10 times lower than the salinity of SSW as mentioned before.

By looking to Figure 4.26, the NP production (breakthrough) is started 0.25 PV after the unreacted tracer. The production of NP is continued after the production of the tracer (Li^{+}) is stopped. This production could be explained by the possibility of NPs desorption during the core flood with LSW. only 67.2% of injected NPs are adsorbed on the Chalk surface during the LSW flood (Hamouda, Abhishek, and Ayoub 2018) compared to 86.2% adsorbed during the SSW flood. This result confirms the desorption of NPs in the low salinity environments (LSW). So, reversible adsorption of NPs on Chalk surface observed during the core flood with LSW, while a strong irreversible adsorption observed with SSW. This indicates that the salinity has a strong effect on the NPs adsorption behaviour on Chalk surface.

Figure 4.27 shows the pH for core flood on chalk with LSW. A high variation in pH observed in the effluents during LSW flood experiments compared to SSW flood experiments, where the pH of effluents is almost constant. The desorption of NPs leads to the dissolution of NPs and then a production of a weak acid (silicic acid) (Equation 4.9). The dissolution of the silicic acid (Equation 4.10) reduces the pH of effluents. This describes the slightly reduction in pH after 9 PV, where the production of desorbed NPs starts (Hamouda, Abhishek, and Ayoub 2018). This conclusion confirms the previous proposal of NP desorption/adsorption mechanism.

$$SiO_2\,(s) + 2H_2O \leftrightarrow H_4SiO_4 \tag{4.9}$$

$$H_4SiO_4 \leftrightarrow H_3SiO_4^- + H_3O^+ \tag{4.10}$$

Figure 4.28 presents the concentration of Ca^{2+} and Mg^{2+} in effluents for Chalk core flooding in LSW. A high variation in ion concentration of Ca^{2+} and Mg^{2+} observed in the effluents during LSW flood experiments compared to SSW flood experiments, where the ion concentration of Ca^{2+} and Mg^{2+} in effluents is almost constant. During the pre-flush stage, the concentration of Ca^{2+} is high due to high Calcite dissolution during this stage. During the post-flush stage (after the injection of NP), the concentration of Ca^{2+} is decreased by about 30%. This means that adding that the adsorption of NP on chalk surface reduce the dissolution of calcite. The Mg^{2+} ion concentration is also reduced after the injection of NP. Which means that there is an ion exchange between calcite (Ca^{2+} ions) and magnesium ions (Mg^{2+}) during the chalk flood in LSW. So, the Calcite tends to accommodate the Mg^{2+} ions instead for Ca^{2+} ions in its structure. The same observation made previously for the kinetic adsorption of NP on calcite in LSW. This means that higher ion activity and chemical interaction between Chalk and fluid during the Chalk core flood experiments with LSW compared to Chalk core flood experiments with SSW. So, the ion activity and chemical interaction between Chalk and fluid is higher in the low salinity environments.

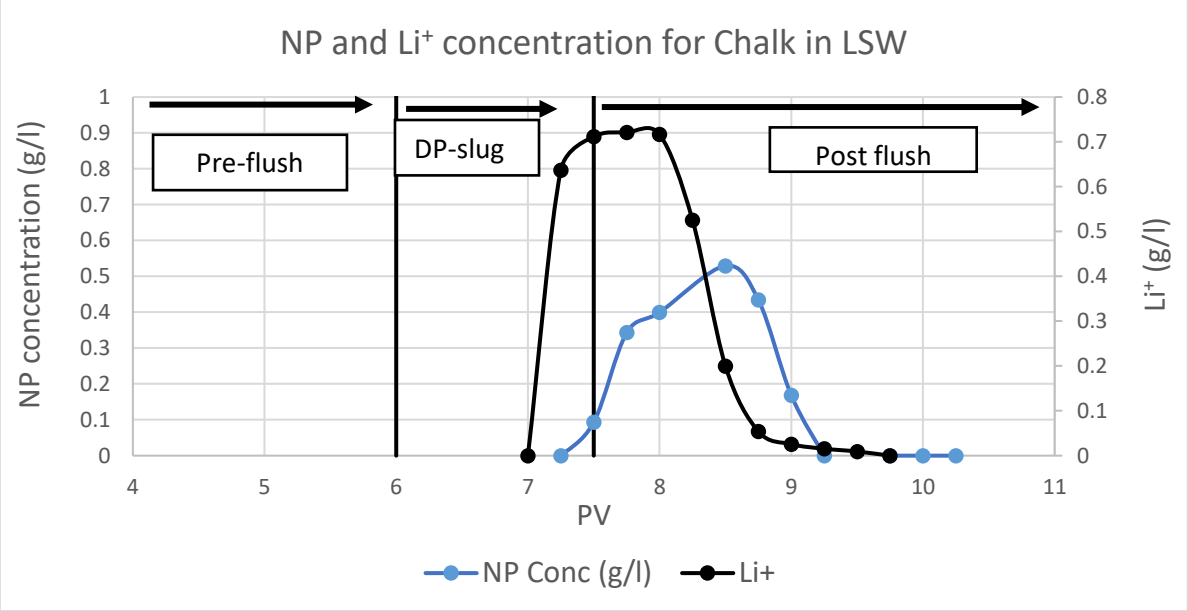

Figure 4.26: NP and Li^+ concentration (g/l) vs. pore volume (PV) produced for Chalk core flood with LSW.

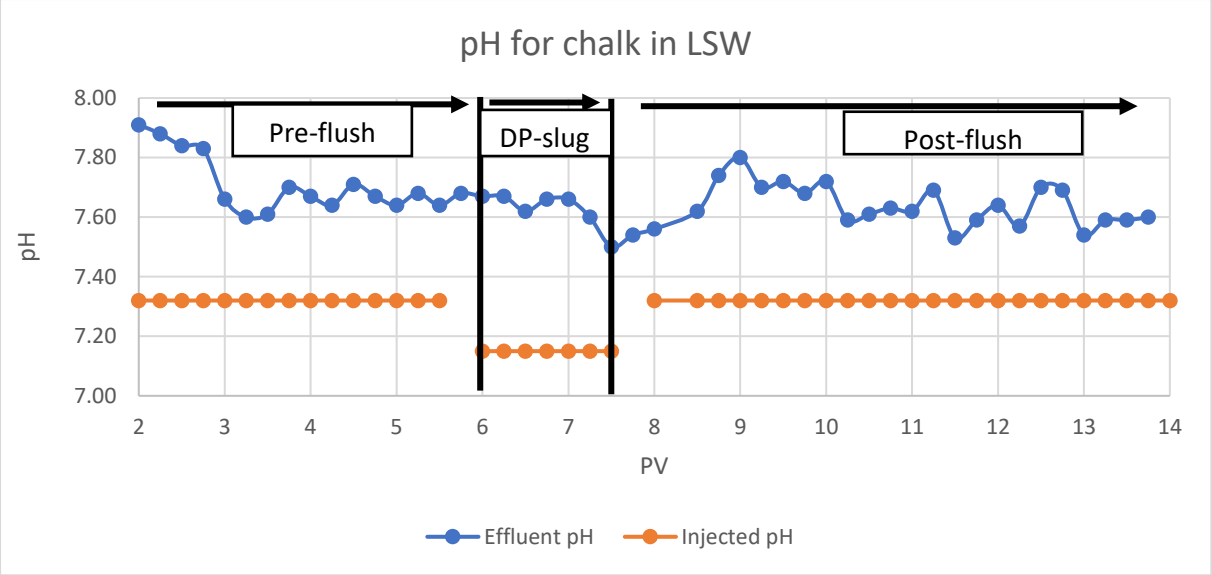

Figure 4.27: The pH values of injected fluid and produced effluents vs. pore volume (PV) produced for Chalk core flood with LSW.

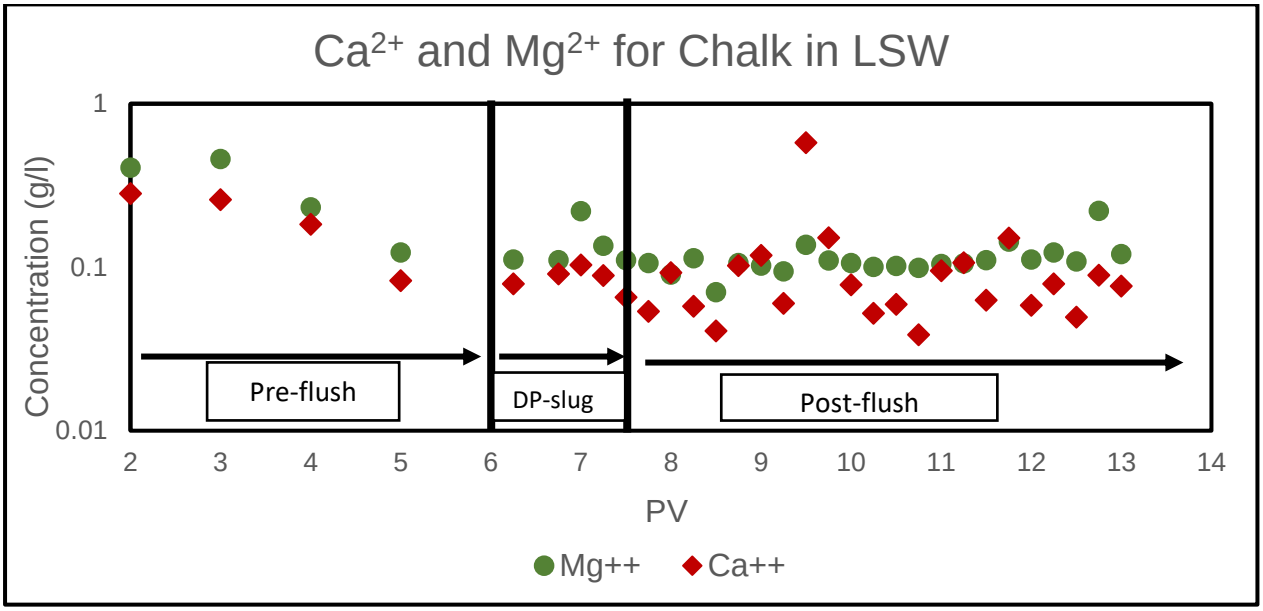

Figure 4.28: Ca^{2+} and Mg^{2+} concentrations (g/l) of produced effluent vs. PV for Chalk core flood with LSW.

The main conclusion from this comparison is that the dynamic adsorption of NPs on Chalk surface leads to decrease the dissolution of Calcite caused by the LSW injection. The same conclusion is made for the kinetic adsorption of NPs on Calcite.

4.2.2. Core flood with Berea

Berea core flood experiment is run at injection rate of 10 PV/day or 0.15 ml/min. 7.75 PV of SSW brine is injected during the pre-flush stage. After that 1.5 PV of nanofluid (DP) slug with tracer (1 g/l DP + 0.1M LiCl +SSW) is injected. Then 5.75 PV of SSW injected during the post flush stage.

The absorbance (Abs) and pH values of produced effluent samples are measured. The absorbance values are utilized to calculate the NP concentration in the produced effluent samples. Equations (3.11 – 3.15) and the calibration curve shown in Figure 3.3 are used to calculate NP concentration (g/l), total of NPs produced and injected (g) and NP adsorbed on Berea surface (%) as shown in Table 4.12.

The NP and tracer (Li^+) concentration (g/l) of effluent samples are plotted against pore volume (PV) produced in Figure 4.29. The NP and tracer slug (DP-slug) is started to inject at PV 8 and stopped at PV 9.5. NP production is started at PV 9.25 and stopped at PV 11. The production of the unreacted tracer (Li^+) is started also at PV 9.25 and stopped at PV 11.25 as shown in Figure 4.29. So, breakthrough of NP and tracer is happened at the same time, but the NP production is stopped about 0.25 PV before the Li^+. In other words, NP and Li^+ concentration profiles are very close to each other.

According to the calculations shown in Table 4.12, only 18.33 % of injected NPs were produced and 81.67 % of Injected NPs were adsorbed on the surface of Berea core. This indicates high adsorption of NPs on Berea surface in high salinity environments (in SSW). Same observation reported previously during the kinetic adsorption experiments in SSW on quartz (94% of Berea is quartz (Table 3.4)). In addition, NP production is stopped after the tracer (Li^+) has passed through the core. These observations may indicate that the NPs adsorption on Berea surface in high salinity environment is a strong irreversible adsorption. The same conclusion made during the Chalk core flooding in SSW.

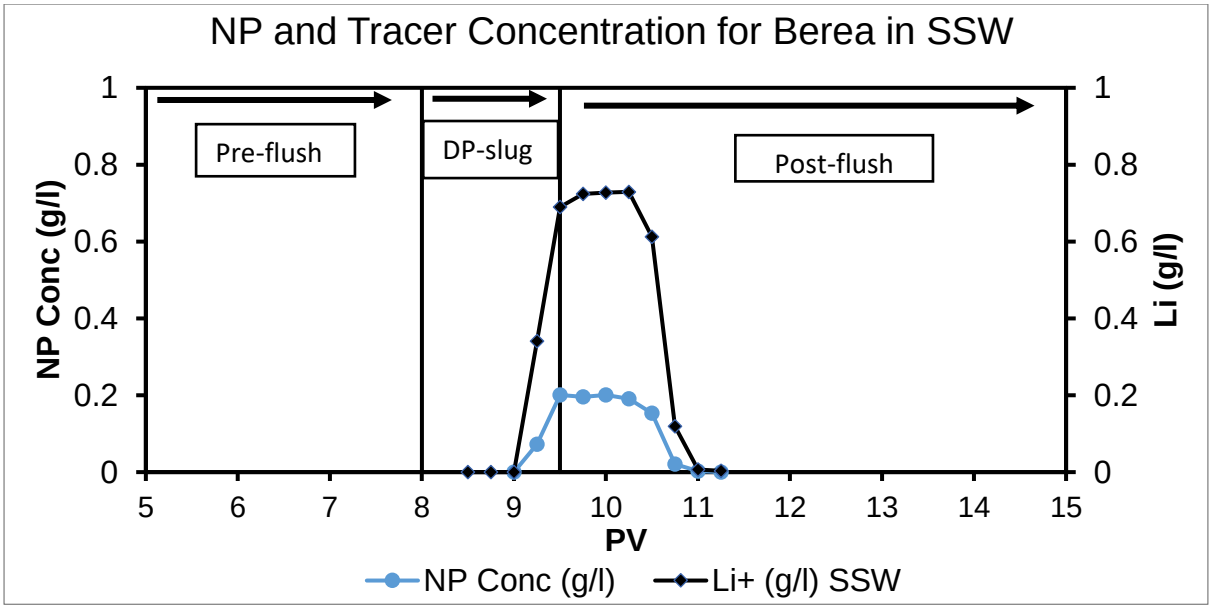

Figure 4.29: NP and Li^+ concentration (g/l) vs. pore volume (PV) produced for Berea core flood with SSW.

Table 4.12: Calculation of NP concentration, injection production and adsorption for Berea core flood based on equations 3.11- 3.15.

PV produced	NP concentration (g/l)	Sample volume (L)	NP produced (g)
9	0	0.00534	0
9.25	0.073	0.00534	0.000411
9.5	0.201	0.00534	0.001135
9.75	0.196	0.00534	0.001109
10	0.201	0.00534	0.001135
10.25	0.191	0.00534	0.001078
10.5	0.153	0.00534	0.000868
10.75	0.021	0.00534	0.000118
11	0.003	0.00534	0.0000154
11.25	0	0.00534	0
		Total NP produced (g)	0.005868
		Total NP injected (g)	0.03201
		NP adsorbed (%)	81.67
		NP produced (%)	18.33

The pH values of produced effluents and injected fluids are plotted against PV in Figure 4.30. In general, the pH values of produced effluent samples are almost constant which indicates that the injected fluid and Berea surface are almost at equilibrium at high salinity environment.

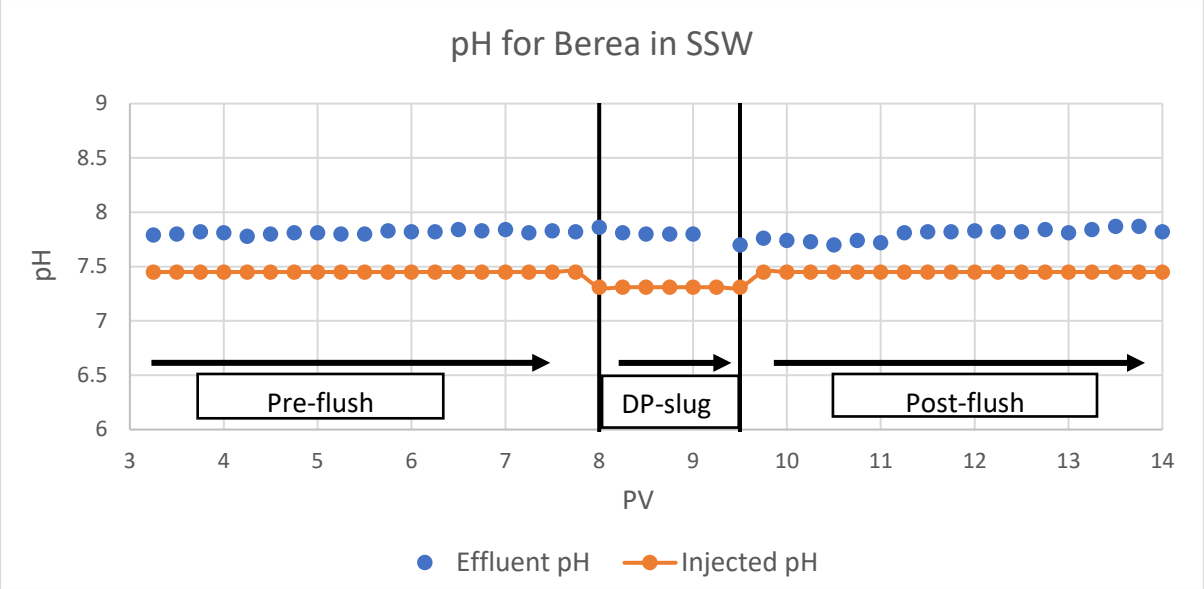

Figure 4.30: The pH values of injected fluid and produced effluents vs. pore volume (PV) produced for Berea core flood with SSW.

The ion concentration of Na^+ and K^+ in the effluent are plotted against PV in Figure 4.31. The ion concentration (g/l) of Na^+ and K^+ are almost constant and equal to around 0.4 and 10.4 (g/l) respectively, during the whole flooding process. This means that the ion concentration of Na^+ and K^+ in the produced effluents samples and injected fluid are almost same. This observation is supported by the stable pH values of effluents presented in Figure 4.30. The pH and ion concentration results confirm that there is an equilibrium state between injected fluid and Berea surface in high salinity environments. This leads to have low ionic activity during the flood because of low chemical interaction between the injected fluid and Berea surface in SSW. The same conclusion made during the Chalk core flooding with SSW.

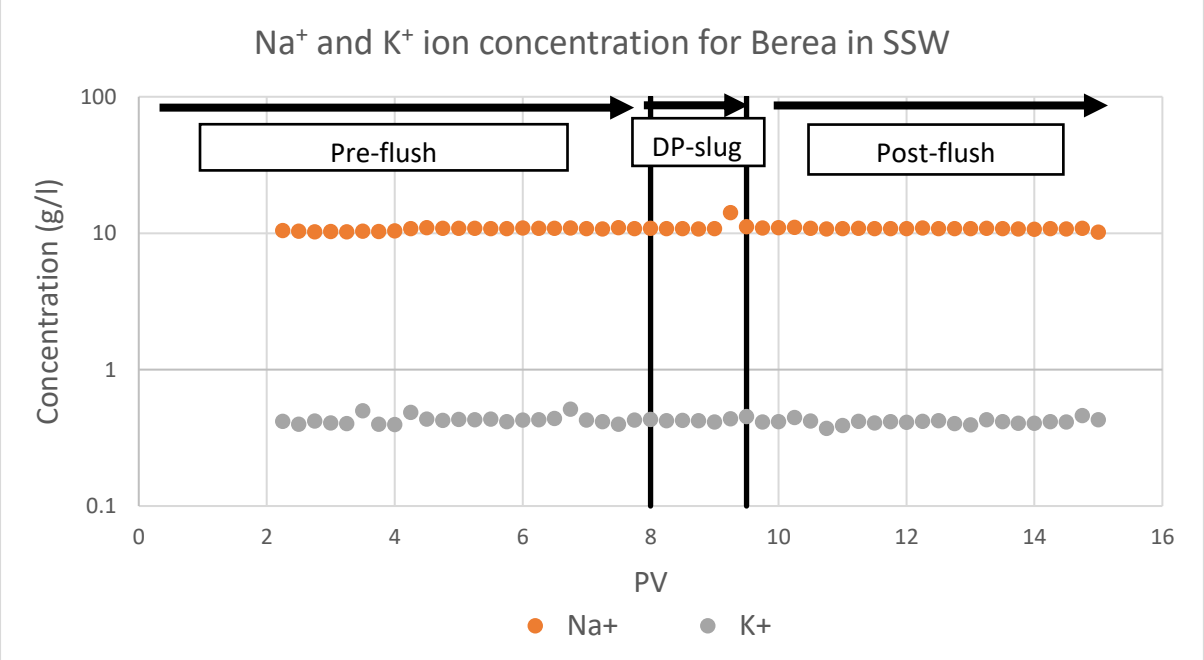

Figure 4.31: Na^+ and K^+ concentrations (g/l) in produced effluent vs. PV for Berea core flood with SSW.

The results of Berea core flood in SSW are compared with the results obtained from previous core flood experiments done on Berea in LSW. This work is done by (Abhishek, Hamouda, and Murzin 2018) and its results presented in Figure 4.32,4.33 and 4.34. LSW is injected during the pre and post-flush stages and the nanofluid slug with tracer are prepared in LSW. The salinity of LSW are 10 times lower than the salinity of SSW as mentioned before.

By looking to Figure 4.32, the NP production (breakthrough) is occurred almost at the same time with the unreacted tracer (Li^+) breakthrough. The production of NP is continued after the production of the tracer (Li^+) is stopped. This production could be explained by the possibility of NPs desorption during the core flood with LSW. Only 35.36% of injected NPs are adsorbed on the Berea surface (irreversible adsorption) during the LSW flood (Abhishek, Hamouda, and Murzin 2018) compared to 81.67% adsorbed (irreversible adsorption) during the SSW flood. This result shows the desorption of NPs in the low salinity environments (LSW). So, reversible adsorption desorption of NPs on Berea surface observed during the core flood with LSW, while a strong irreversible adsorption observed with SSW. This indicates that the salinity has a strong effect on the NPs adsorption behaviour on Berea surface.

Figure 4.33 shows the pH in effluents together with NP concentration (g/l) for core flood on Berea with LSW. Higher variation in pH observed in the effluents during LSW flood experiments compared to SSW flood experiments. At the start, the pH value was stable around 7 and then it is stared to increase due to the dissolution of mineral presented in Equation 4.11. During the desorption (dissolution) of NPs, production of a weak acid (silicic acid) (Equation 4.9) occurs. The silicic acid further follows Equation 4.10 and reduces the pH of effluents. This describes the reduction in pH after 10 PV, where the production of desorbed NPs starts (Abhishek, Hamouda, and Murzin 2018). This result confirms the adsorption/desorption mechanism of NPs on Berea surface mentioned previously during Berea core flooding in LSW and SSW.

$$4\mathrm{KAlSi_3O_8(s)(orthoclase)} + 22\mathrm{H_20(aq)} \rightarrow \mathrm{Al_4Si_4O_{10}(s)(kaolinite)} + 8\mathrm{H_4SiO_4(aq)} + 4\mathrm{K^+(aq)} + 4\mathrm{OH^-(aq)} \ldots \quad (4.11)$$

Figure 4.34 presents the concentration of Na^+ and K^+ in effluents for Berea core flooding in LSW. A high variation in ion concentration of Na^+ and K^+ observed in the effluents during LSW flood experiments compared to SSW flood experiments, where the ion concentration of Na^+ and K^+ in effluents is same as the injected fluid. During the pre-flush stage, the concentration of K^+ is high due to high mineral (K-feldspar) dissolution (Equation 4.11) suggest during this stage. During the post-flush stage (after the injection of NP), the concentration of K^+ is decreased. This means that the adsorption of NPs on Berea surface could reduce the dissolution of K-feldspar mineral in low salinity environment. This can reduce formation damage in sandstone reservoirs. The ion concentration of Na^+ before and after the injection of NP (DP-slug) indicates that there is an ion exchange between K-feldspar mineral (K^+ ions) and Sodium ions (Na^+) during the Berea flood in LSW as shown in Equation 4.12 (Hamouda et al. 2014; Abhishek, Hamouda, and Murzin 2018).

$$4\mathrm{KAlSi_3O_8(s)(orthoclase)} + Na^+(aq) \rightarrow K^+ + NaAlSi_3O_8(s)(albite) \ldots \quad (4.12)$$

This means that the adsorption of NPs on Berea surface during LSW flooding affect the interactions between the injected fluid and the Berea surface. This observation did not detect during the Berea SSW flooding. This means that higher ion activity and chemical interaction between Berea surface and fluid in low salinity environments than high salinity environments.

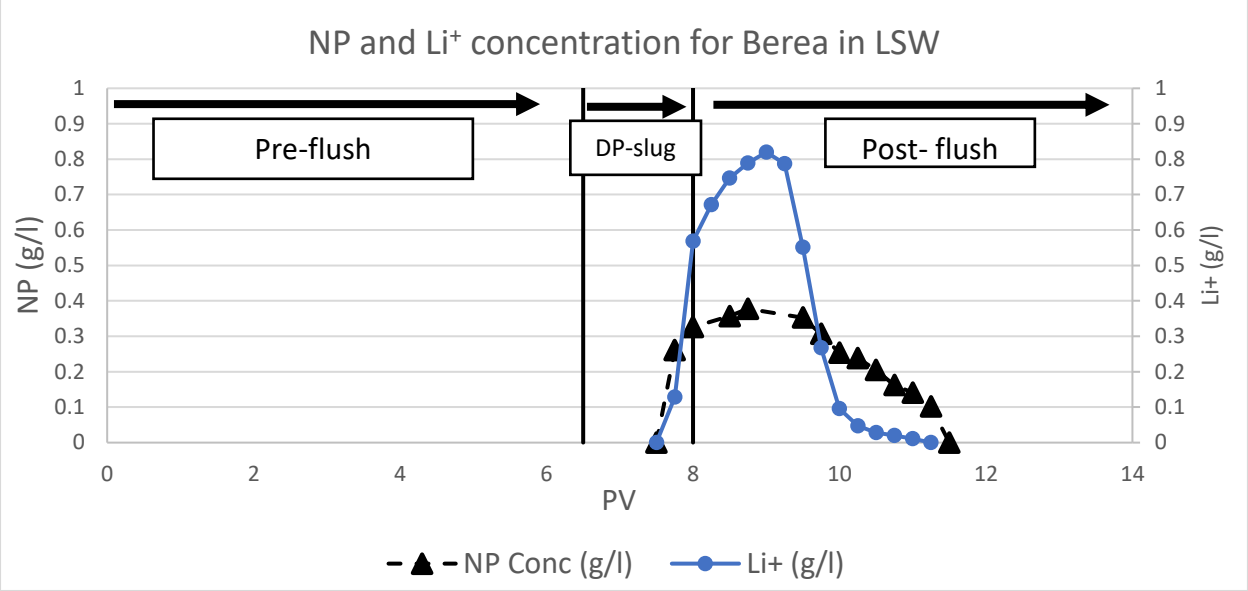

Figure 4.32: NP and Li^+ concentration (g/l) vs. pore volume (PV) produced for Berea core flood with LSW.

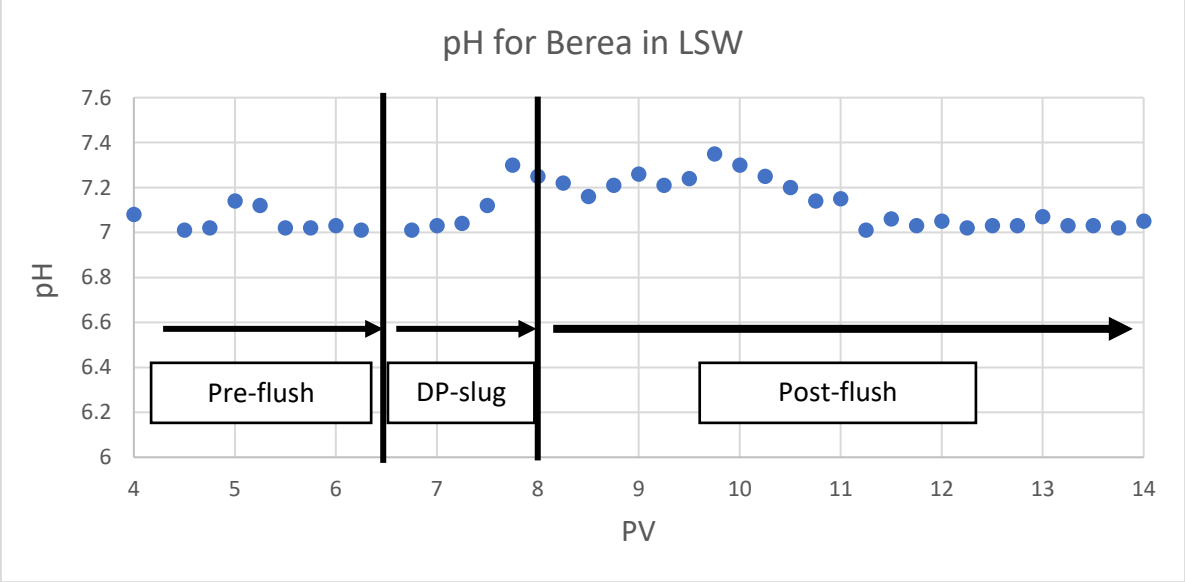

Figure 4.33: The pH values of produced effluents vs. pore volume (PV) produced for Berea core flood with LSW.

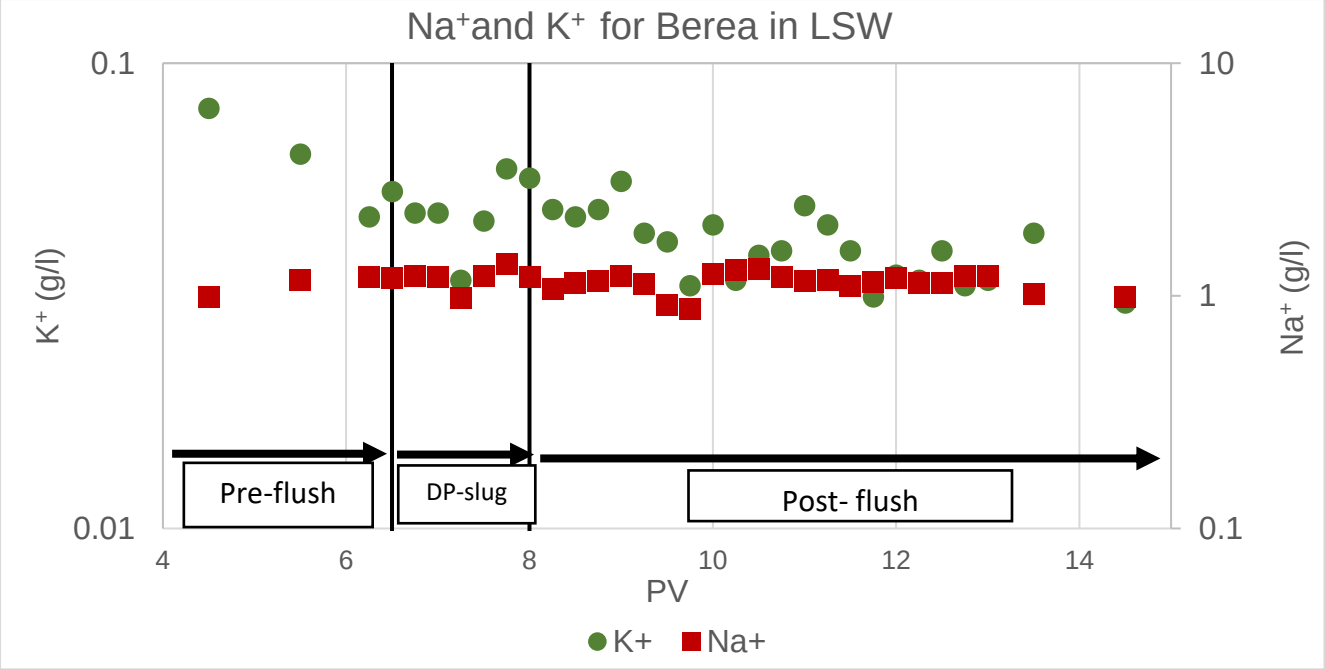

Figure 4.34: Na^+ and K^+ concentrations (g/l) in produced effluent vs. PV for Berea core flood with LSW.

In summary, from the experimental work presented in this thesis, (1) NP adsorption can reduce the calcite dissolution induced by low salinity flooding in chalk reservoirs and (2) NP adsorption can reduced formation damage in sandstone reservoirs. This suggests a synergy between silica nanofluid and low salinity flooding techniques.

5. Conclusions

Based on the kinetic and dynamic adsorption results of NP obtained in this thesis, the following conclusions can be made:

1. The highest NP adsorption was observed in SSW for calcite and quartz during the kinetic adsorption experiments.
2. Increasing the salinity leads to increased adsorption of NP on both mineral surfaces (calcite and quartz).
3. The adsorption of NP on calcite higher than that on quartz according to the results obtained from the kinetic adsorption experiments in DIW, LSW and SSW.
4. The pH and IC results of kinetic adsorption experiments suggest that adding NP to DIW, LSW and SSW leads to reduction in calcite dissolution due to NP adsorption.
5. Ion exchange between Ca^{2+} and Mg^{2+} was observed during the kinetic adsorption of NP on calcite in LSW, but it was not clear for SSW. The ion exchange between Ca^{2+} and Mg^{2+} during kinetic adsorption of NP on calcite in high salinity condition needs more investigation.
6. The adsorption of NP on calcite followed pseudo-second order kinetic model.
7. The both kinetic models (pseudo-first and second order kinetic model) did not give good fits to describe the kinetic behaviour of the NP adsorption on quartz.
8. Higher adsorption rate of NP on calcite in SSW followed by DIW and LSW.
9. The kinetic adsorption mechanism of NP on calcite and quartz surfaces was controlled by intraparticle diffusion and film diffusion mechanisms.
10. 86% of injected NP adsorbed on Chalk surface during Chalk core flood experiments with SSW.
11. 81% of injected NP adsorbed on Berea surface during Berea core flood experiments
12. Irreversible adsorption of NP on Chalk and Berea surfaces observed during the core flooding experiments with SSW.
13. Increasing the Salinity increases the dynamic adsorption of NP on Berea and Chalk surface. This is supported by the observations made during by kinetic adsorption of NP on calcite and quartz.
14. The pH and (IC) results of core flooding experiments suggest low ion activity and interaction between Chalk/Berea and injected fluid in high salinity condition.
15. The reduction in mineral dissolution and the ion exchange were not clear during SSW flooding.
16. Comparing the results from this thesis to work previously done in our lab showed that: (1) NP adsorption can reduce the calcite dissolution induced by low salinity flooding in chalk reservoirs and (2) NP adsorption can reduce formation damage in sandstone reservoirs. This observation suggests a synergy between silica nanofluid and low salinity flooding techniques.

6. References

1. Abdelfatah, E. R., K. Kang, M. Pournik, B. Shiau, J. Harwell, M. R. Haroun, and M. M. Rahman. 2017. Study of Nanoparticle Adsorption and Release in Porous Media Based on the DLVO Theory. In *SPE Latin America and Caribbean Petroleum Engineering Conference*. Buenos Aires, Argentina: Society of Petroleum Engineers.
2. Abhishek, R., G. Suresh Kumar, and R. K. Sapru. 2015. Wettability Alteration in Carbonate Reservoirs Using Nanofluids. *Petroleum Science and Technology* 33 (7):794-801.
3. Abhishek, Rockey, Nikhil Bagalkot, and G. Suresh Kumar. 2016. Effect of transverse forces on velocity of nanoparticles through a single fracture in a fractured petroleum reservoir. *International Journal of Oil, Gas and Coal Technology* 12 (4):379-395.
4. Abhishek, Rockey, and Aly A. Hamouda. 2017. Effect of Various Silica Nanofluids: Reduction of Fines Migrations and Surface Modification of Berea Sandstone. *Applied Sciences* 7 (12):1216.
5. Abhishek, Rockey, Aly. A. Hamouda, and Ivan Murzin. 2018. Adsorption of Silica Nanoparticles and its synergistic effect on fluid/rock interactions during Low Salinity flooding in Sandstones.
6. Arab, Danial, and Peyman Pourafshary. 2013. Nanoparticles-assisted surface charge modification of the porous medium to treat colloidal particles migration induced by low salinity water flooding. *Colloids and Surfaces A: Physicochemical and Engineering Aspects* 436:803-814.
7. Assef, Yasaman, Danial Arab, and Peyman Pourafshary. 2014. Application of nanofluid to control fines migration to improve the performance of low salinity water flooding and alkaline flooding. *Journal of Petroleum Science and Engineering* 124:331-340.
8. Ayoub, Amr. 2017. Transport Behavior of Nanoparticles (NP) in Stevns Klint Chalk Rock and EOR potential. Master's Thesis, University of Stavanger.
9. Bera, Achinta, and Hadi Belhaj. 2016. Application of nanotechnology by means of nanoparticles and nanodispersions in oil recovery - A comprehensive review. *Journal of Natural Gas Science and Engineering* 34:1284-1309.
10. Coletti, Dario. 2018. *UV-1700 Spectrophotometer From Shimadzu*. Biocompare 2007 [cited 29.04.2018 2018]. Available from https://www.biocompare.com/Product-Reviews/40948-UV-1700-Spectrophotometer-From-Shimadzu/.
11. Dehghan Monfared, A., M. H. Ghazanfari, M. Jamialahmadi, and A. Helalizadeh. 2015. Adsorption of silica nanoparticles onto calcite: Equilibrium, kinetic, thermodynamic and DLVO analysis. *Chemical Engineering Journal* 281:334-344.
12. Habibi, A., M. Ahmadi, P. Pourafshary, S. Ayatollahi, and Y. Al-Wahaibi. 2012. Reduction of fines migration by nanofluids injection: an experimental study. *SPE J.* 18:309-318.
13. Hamouda, A. A., O. M. Valderhaug, R. Munaev, and H. Stangeland. 2014. Possible Mechanisms for Oil Recovery from Chalk and Sandstone Rocks by Low Salinity Water (LSW): Society of Petroleum Engineers.
14. Hamouda, Aly. A., Rockey Abhishek, and Amr Ayoub. 2018. Investigating the synergy between silica nanofluid and low salinity water for potential oil recovery from chalk reservoirs.
15. Hendraningrat, Luky, Shidong Li, and Ole Torsæter. 2013. A coreflood investigation of nanofluid enhanced oil recovery. *Journal of Petroleum Science and Engineering* 111:128-138.
16. Hendraningrat, Luky, and Ole Torsæter. 2014. Metal oxide-based nanoparticles: revealing their potential to enhance oil recovery in different wettability systems. *Applied Nanoscience* 5 (2):181-199.
17. Ho, Y. S., and G. McKay. 1999. Pseudo-second order model for sorption processes. *Process Biochemistry* 34 (5):451-465.

18. Ho, Yuh-Shan. 2003. Removal of copper ions from aqueous solution by tree fern. *Water Research* 37 (10):2323-2330.
19. Li, Hui, Hui-gang Xiao, Jie Yuan, and Jinping Ou. 2004. Microstructure of cement mortar with nano-particles. *Composites Part B: Engineering* 35 (2):185-189.
20. Li, Shidong, and Ole Torsæter. 2015. Experimental Investigation of the Influence of Nanoparticles Adsorption and Transport on Wettability Alteration for Oil Wet Berea Sandstone: Society of Petroleum Engineers.
21. Metin, C. O., J. R. Baran, Jr., and Q. P. Nguyen. 2012. Adsorption of surface functionalized silica nanoparticles onto mineral surfaces and decane/water interface. *J Nanopart Res* 14 (11):1246.
22. Mondragon, Rosa, J. Enrique Julia, Antonio Barba, and Juan Carlos Jarque. 2012. Characterization of silica–water nanofluids dispersed with an ultrasound probe: A study of their physical properties and stability. *Powder Technology* 224:138-146.
23. Murzin, Ivan. 2017. Transport behavior of nanoparticles (NP) in Berea sandstone rock and the determining the EOR potential. Master's thesis in Petroleum engineering, University of Stavanger, Norway.
24. NYACOL. 2018. *DATA SHEET NYACOL® DP9711* NYACOL® Nano Technologies Inc [cited 2018]. Available from http://www.nyacol.com/app/uploads/2015/04/DP9711-Data-Sheet-20130812.pdf.
25. Petrovich, R, and A Hamouda. 1998. Dolomitization of Ekofisk Oil Field reservoir chalk by injected seawate. In *International symposium; 9th, Water-rock interaction.* Taupo; New Zealand: A A Balkemia.
26. Prodanovic, Masa, Seungyup Ryoo, Amir Reza Rahmani, Roman V. Kuranov, Csaba Kotsmar, Thomas E. Milner, Keith P. Johnston, Steven Lawrence Bryant, and Chun Huh. 2010. Effects of Magnetic Field on the Motion of Multiphase Fluids Containing Paramagnetic Nanoparticles in Porous Media. In *SPE Improved Oil Recovery Symposium*. Tulsa, Oklahoma, USA: Society of Petroleum Engineers.
27. Shimadzu. 2018. *The Structure of a Spectrophotometer of UV-Vis-NIR*
28. *Spectroscopy*. Shimadzu Corporation 2018 [cited 29.04.2018 2018]. Available from https://www.shimadzu.com/an/uv/support/fundamentals/structure.html#1.
29. Stumm, W. Eidgenoessische Technische Hochschule, Zurich Switzerland, and J. J. Morgan. 1970. *Aquatic chemistry: An introduction emphasizing chemical equilibria in natural waters*. Vol. 139.
30. Suleimanov, B. A., F. S. Ismailov, and E. F. Veliyev. 2011. Nanofluid for enhanced oil recovery. *Journal of Petroleum Science and Engineering* 78 (2):431-437.
31. Suriyanon, Nakorn, Patiparn Punyapalakul, and Chawalit Ngamcharussrivichai. 2013. Mechanistic study of diclofenac and carbamazepine adsorption on functionalized silica-based porous materials. *Chemical Engineering Journal* 214:208-218.
32. Wang, Wendong, Bin Yuan, Yuliang Su, Kai Wang, Miaolun Jiang, Rouzbeh Ghanbarnezhad Moghanloo, and Zhenhua Rui. 2016. Nanoparticles Adsorption, Straining and Detachment Behavior and its Effects on Permeability of Berea Cores: Analytical Model and Lab Experiments. Dubai, UAE: Society of Petroleum Engineers.
33. Wasan, Darsh T., and Alex D. Nikolov. 2003. Spreading of nanofluids on solids. *Nature* 423:156.
34. William, Jay Karen Maria, Swaminathan Ponmani, Robello Samuel, R. Nagarajan, and Jitendra S. Sangwai. 2014. Effect of CuO and ZnO nanofluids in xanthan gum on thermal, electrical and high pressure rheology of water-based drilling fluids. *Journal of Petroleum Science and Engineering* 117:15-27.
35. Yuan, Bin, Rouzbeh Ghanbarnezhad Moghanloo, and Da Zheng. 2016. Analytical Evaluation of Nanoparticle Application To Mitigate Fines Migration in Porous Media. *Society of Petroleum Engineers*.

36. Yuh-Shan, Ho. 2004. Citation review of Lagergren kinetic rate equation on adsorption reactions. *Scientometrics* 59 (1):171-177.
37. Zhang, Hua, Alex Nikolov, and Darsh Wasan. 2014. Enhanced Oil Recovery (EOR) Using Nanoparticle Dispersions: Underlying Mechanism and Imbibition Experiments. *Energy & Fuels* 28 (5):3002-3009.
38. Zhang, Tiantian, Michael Murphy, Haiyang Yu, Hitesh G. Bagaria, Ki Youl Yoon, Bethany M. Nielson, Christopher W. Bielawski, Keith P. Johnston, Chun Huh, and Steven Lawrence Bryant. Investigation of Nanoparticle Adsorption During Transport in Porous Media: Society of Petroleum Engineers.